A Propeller Analysis and Sizing Method in Takeoff Conditions

MSc Thesis

F.S. Heeres

Technische Universiteit Delft

TU Delft

Cover image: Wubben, A. https://unsplash.com/photos/pFUEpJUSyyE

A Propeller Analysis and Sizing Method in Takeoff Conditions

Master Thesis

by

F.S. Heeres

in partial fulfillment of the requirements for the degree of

Master of Science
in Aerospace Engineering

at the Delft University of Technology,
to be defended publicly on Wednesday February 3, 2021 at 12:30.

Student number:	4230779	
Supervisor: Thesis committee:	Dr. ir. R. Vos	TU Delft, supervisor
	Prof. dr. ir. L.L.M. Veldhuis,	TU Delft, chairman
	Ir. T.J. Mulder,	TU Delft

TU Delft Delft University of Technology

SUMMARY

In the current era, propulsion systems have become more advanced and diverse, capable of taking hundreds of people into the air. The propulsion systems have become an integral part of the aircraft design to be taken into account during the design phase. Despite all the technological advancements that have been made over the years, the methods used in the preliminary design phase to determine the aircraft wing and engine size still depend on empirical methods based on data from historical aircraft. Furthermore, it is found to be difficult to design for propellers and turbofans in the same design cycle.

While a lot of knowledge is available on propeller performance, thrust and power, in cruise, on-design, conditions, less is known in the area of propeller performance in takeoff, off-design, conditions. The aircraft takeoff performance is often a critical constraint and being able to solve this constraint accurately and analytically in early design stages would increase knowledge and design certainty further in the aircraft design process.

The aim of this research is to create a better understanding of propeller performance, specifically the thrust and power relation, in takeoff conditions for future researchers and aircraft designers. The objective of this research is to develop a propeller sizing method at takeoff conditions, taking into account the low speed aerodynamic effects and the resulting effect on the takeoff performance.

A methodology has been developed to be able to perform propeller sizing and analysis in the preliminary design stage. The goal is to generate a analytical solution of the takeoff distance requirement in the wing and power loading diagram and consequently an analytical solution for the aircraft design point.

The aircraft preliminary sizing tool (PST) by de Vries[1] is used as a basis on which the propeller sizing tool is build. The PST performs an initial aircraft sizing, generating a preliminary aircraft sizing. Following the initial sizing by PST, a takeoff performance analysis sequence (TOPAS) is performed. Using the equilibrium flight conditions in cruise a propeller could be generated that satisfies minimum induced loss conditions in cruise flight using a inverse propeller design sequence of XROTOR[2]. Thereafter, the generated propeller geometry is analysed using the Blade Element Momentum method. Using the propeller performance and the initial aircraft sizing an aircraft takeoff analysis is performed, of which the results could be compared to the takeoff distance mission requirement.

To accurately model propeller performance during the takeoff procedure two types of corrections were used to modify the 2D airfoil polars created by XFOIL[3]. First of all, a post-stall correction developed by Traub matching the airfoil polars at high angles of attack to flat plate polars. Secondly, two different 3D rotation corrections by Snel[4, 5] and Corrigan & Schillings[4, 5] were implemented.

Combining the modules, creating the propeller sizing method, it is possible to analyse the propeller performance during takeoff. Furthermore, the aircraft and propeller are being sized by an analytical calculation process in the preliminary design phase.

The modules are verified and validated using experimental results. The combination of 2D to 3D corrected airfoil polars and the Blade Element Moment method showed good correspondence with reality. Calculating the thrust coefficient within 5% accuracy and within 5-15% accuracy for power coefficient. The errors with respect to power were on the low end for the low advance ratios that are encountered during takeoff.

Validation of the aircraft takeoff performance using a Boeing 737-200 as reference provided good results and an error within 5%. However, it was shown that the calculation of the takeoff distance was sensitive to the input parameters, of which a number were assumed or determined using engineering equations and prediction methods.

The developed propeller sizing method is used to analyse the design solution based on the mission requirements of the De Havilland Q400 Dash 8 and the ATR72-600. The generated cruise speed and takeoff distance constraint curves in the wing and power loading diagram match the shape of the empirically calculated curves.

The calculated wing loading values are matched within 0.5% error to the reference data due to selection of $C_{L_{max,clean}}$. More interesting are the power loadings, which show only 4% error for the TOPAS results with respect to the Q400 reference data. However, in the case of the ATR72-600 the discrepancy is a significant 35%. The TOPAS generated power loading values are consistently below the values predicted using the empirical methods.

Additionally, the uncertainty in a number of other parameters and used simplifications could result in relatively large inaccuracies, which are difficult to quantify using the currently available data and at this stage in the aircraft design process.

With respect to the propeller design solutions that have been generated it could be seen that the propeller designs followed expected trends. Increasing the wing loading requires a larger propeller to generate higher static thrust values at the cost of higher required maximum power.

Two relations propeller performance and propeller geometry were found. Firstly, a relation between static thrust and total activity factor (T_0/TAF) which showed to be constant for propellers with an equal amount of blades, increasing the static thrust proportional to the propeller activity factor. Secondly, the relation of maximum required takeoff power and chord ratio factor (P_{max}/CRf) showing that for propellers with an equal amount of blades, increasing the chord ratio factor proportionally increases the required maximum takeoff power.

To conclude, this study shows that it is possible to develop a propeller sizing method in the preliminary aircraft design phase which is able to analytically calculate propeller takeoff performance. However, due to contradiction results and lack of matching realistic input parameters, no conclusive verdict on the effectiveness of the developed propeller sizing method could be made.

PREFACE

This Master thesis will be the final deliverable in my studies of becoming an Aerospace Engineer. Finishing this thesis has been a long road with ups and downs. I am glad to say that as I write this, it has been almost completed. Due to the Covid-19 pandemic and the current lockdown measures there will be no big celebration, however I will be happy to celebrate this achievement with my friends and family in small over the period to come.

I have received a lot of support during the research of this Master thesis and I would like to thank the people that have supported me along the way. First of all, I would like to thank my family, your relentless support and encouragement during this project have been invaluable. I would like to thank the many friends I have made during my studies, who have stood by my side and made the whole journey one to cherish and remember. I would especially like to note the members of the 2.44 and FPP study rooms with whom I have shared many relaxing lunch, beers in 'the Atmosfeer' and uplifting conversations. Liv and Julia for always being there to have a cup of tea and put a smile on my face. Chenoa, I am happy to have met you, thank you for your puzzling and moral support. Mathieu, we have known each other for a long time and soon we will be able to enjoy the end of this journey together also, thank you for all the great moments we have shared. I would like to thank Rick, your decision to become a pilot, fly the Boeing 737 and be able to spar with me on the takeoff characteristics and procedures from a pilot's perspective was both very helpful and enjoyable.

From the TU Delft, I would first like to thank Roelof Vos for giving me the possibility to work on this novel research project. Thank you for your guidance and feedback for the complete duration of this thesis. Also, thank you Thomas Sinnige for helping me out when I got stuck on some of the particulars of rotor aerodynamics. Thank you Reynard de Vries and Maurice Hoogreef for assisting me in setting up, as I so call it, the *Preliminary Sizing Tool*.

F.S. Heeres
Delft, January 2021

If I have seen further than others,
it is by standing upon the shoulders of giants.
Isaac Newton

Contents

List of Figures

List of Tables

NOMENCLATURE

ALPHABETICAL

A	=	Surface area [m/s]
A	=	Aspect ratio [-]
BAF	=	Blade activity factor [-]
c	=	Chord length [m]
C_D	=	Drag coefficient [-]
C_L	=	Lift coefficient [-]
C_P	=	Power coefficient [-]
C_T	=	Thrust coefficient [-]
CRf	=	Chord ratio factor [-]
D	=	Diameter [m]
D	=	Aerodynamic drag [N]
e	=	Elliptical lift distribution [-]
F_r	=	Rolling friction [N]
FOM	=	Figure of merit [-]
g	=	Gravity [m/s^2]
J	=	Advance ratio [-]
n	=	Rotational blade frequency - speed [1/min]
P	=	Power [W]
r	=	Local blade span [m]
R	=	Radius [m]
S	=	Wing surface area [m^2]
t	=	Time [s]
T_0	=	Static thrust [N]
TAF	=	Total activity factor [-]
U	=	Total velocity at the blade section [m/s]
V	=	Velocity [m/s]
V_∞	=	Free stream velocity [m/s]
V_1	=	Decision speed [m/s]
V_2	=	Obstacle clear speed [m/s]
V_EF	=	Engine failure speed [m/s]
V_LOF	=	Lift-off speed [m/s]
V_R	=	Rotation speed [m/s]
V_S	=	Stall speed [m/s]
W	=	Weight [N]
W/P	=	Power loading [N/W]
W/S	=	Wing loading [N/m^2]

GREEK

SUBSCRIPTS

α	=	Angle of attack [°]
ΔV	=	Velocity increment [m/s]
η	=	Efficiency [-]
γ	=	Aircraft pitch angle [°]
μ_r	=	Friction coefficient [-]
ω	=	Rotational velocity [m/s]
ϕ	=	Local inflow angle [°]
ρ	=	Density [kg/m^3]
σ	=	Density ratio between takeoff and ISA sea level conditions [-]

0	=	Zero lift
clean	=	Clean wing configuration
CR	=	Cruise condition
max	=	Maximum
min	=	Minimum
p	=	Propeller
TO	=	Takeoff condition
ρ	=	Density

1

INTRODUCTION

Every day more than 100.000 flights take off and land, carrying millions of passengers around the globe. Most of these passengers have no idea how an aircraft is built or even how it is able to fly while being heavier than air. Aeronautical engineers have been improving aircraft ever since the Wright Flyer took the Wright Brothers into the air for not even a minute at a time. To power this aircraft the Wright Brothers designed a propulsion system of which the most innovative feature was the propeller. The propellers were designed as rotary wings, producing a horizontal lift force, in other words thrust.[1] In the current era, propulsion systems have become more advanced and diverse, capable of taking hundreds of people into the air. The propulsion systems have become an integral part of the aircraft design to be taken into account during the design phase. Step one of flying an aircraft is taking it into the air, therefore designing an aircraft for takeoff is essential and an important factor in the aircraft design phase.

In the current economic situation and global search for more sustainable developments, aircraft designers have gained a renewed interest in propeller powered aircraft. Propellers engines provide an inherently higher propulsive efficiency with respect to turbofan and turbojet engines, as can be explained by eq. (1.1). Propellers accelerate a relatively large mass flow of air with a small velocity increment, where jet engines accelerate a relatively small mass flow of air with a large velocity increment.

$$\eta = \frac{2}{1 + \frac{\Delta V}{V_\infty}} \tag{1.1}$$

Despite all the technological advancements that have been made over the years, the methods used in the preliminary design phase to determine the aircraft wing and engine size still depend on empirical methods based on data from historical aircraft[7–10]. Furthermore, it is found to be difficult to design for propellers and turbofans in the same design cycle since the governing equations are too different, propellers are power rated and jets/turbofans are thrust rated. Therefore, engine design studies focus mostly on a single propulsion type[11–14]. Consequently, aircraft design studies considering different engine types[15, 16] are limited to "Class-I" empirical methods.

While a lot of knowledge is available on propeller performance, thrust and power, in cruise, on-design, conditions, less is known in the area of propeller performance in takeoff, off-design, conditions. The aircraft takeoff performance is often a critical constraint and being able to solve this constraint accurately in early design stages would increase knowledge and design certainty further in the aircraft design process.

Enhancing the design capability and freedom to analyse multiple different aircraft architectures and propulsion types would open up the ability to better compare novel aircraft types. A step to be taken is increasing knowledge on the propeller takeoff, off-design, performance to better understand thrust and power relations. To be able to better compare propellers with jets and fans in the future.

[1] 1903 Wright Flyer - Smithsonian National Air and Space Museum https://airandspace.si.edu/collection-objects/1903-wright-flyer

1.1. RESEARCH OBJECTIVES

The aim of this research is to create a better understanding of propeller performance, specifically the thrust and power relation, in takeoff conditions for future researchers and aircraft designers. The objective of this research is *to develop a propeller sizing method at takeoff conditions, taking into account the low speed aerodynamic effects and the resulting effect on the takeoff performance.*

The method will output typical propeller sizing parameters such as the diameter and number of blades. To verify the method, trade studies will be performed to demonstrate the impact of the developed sizing method on overall aircraft performance and weight. The proposed method could enable a physics based model for propeller design and sizing providing both power and thrust. Consequently, this enables more accurate propeller sizing with respect to current sizing methods, increased applicability to novel aircraft configurations and better comparison to turbofan powered aircraft in the conceptual design phase.

The research is split into two parts; the development of a propeller sizing method and the evaluation of the developed method. The two parts have a separate research question with a number of sub-questions, which are the following:

1. **How can the propeller performance in takeoff conditions be determined in the conceptual design phase?**
   (a) How is propeller thrust related to shaft power in takeoff conditions?
   (b) How should the propeller and engine be sized to meet the requirements of performance at all operating conditions?
2. **What is the impact of a new design method, determining propeller performance in static conditions, on the conceptual design of turboprop aircraft?**
   (a) What is the impact of a new design method, determining propeller performance in static conditions, on the resulting propeller design and engine size?
   (b) What is the impact of a new design method using static propeller performance in a point mass analysis on the power/thrust loading constraint?
   (c) What is the impact of a new design method, determining propeller performance in static conditions, on the conceptual design cycle solution, such as weight and geometry parameters?

1.2. THESIS OUTLINE

First of all, this thesis will discuss the methodology used to create a new propeller sizing method for takeoff in chapter 3. The different modules that together make up the sizing method and how they are integrated together are discussed. Chapter 4 will elaborate on the verification and validation process of the various tools to ensure the validity and accuracy of the overall created propeller sizing method. The results of the propeller sizing method are discussed in chapter 5. The thesis is concluded in chapter 6 after which a set of recommendations for future research is presented in chapter 7.

2

BACKGROUND

The objective of this thesis is to develop a propeller sizing method to be used in the preliminary aircraft design phase. Therefore, it is important to first understand the background of aircraft preliminary design which will be elaborated in section 2.1. Secondly, the background of propeller performance is discussed in section 2.2.

2.1. PRELIMINARY AIRCRAFT DESIGN

In the preliminary aircraft design phase a study is performed to investigate whether it is possible to design an aircraft according to a set of mission requirements. Many aircraft design methods have been created by for example Roskam[7], Torenbeek[10, 17] and Raymer[9]. These methods provide the engineering and empirical methods required to translate the mission requirements into actual aircraft parameters such as weight, wing surface area and required propulsive power. With a limited number of known and available requirements, parameters and resources the initial sizing of an aircraft is created which would be used in the full scale development of an aircraft.

A useful tool aircraft designers use in the preliminary design stage is the wing and power loading diagram. A wing and power loading diagram is a way to visualise the available design space of different aircraft mission requirements with respect to the required wing and power loading. For example the maximum takeoff distance requirement and mission cruise speed could be evaluated in takeoff and cruise constraints.

An example of a wing and power loading diagram is shown in fig. 2.1. Where an aircraft with values of wing and power loading in the red feasible design space satisfies the cruise speed, takeoff distance and stall speed requirements present in the figure.

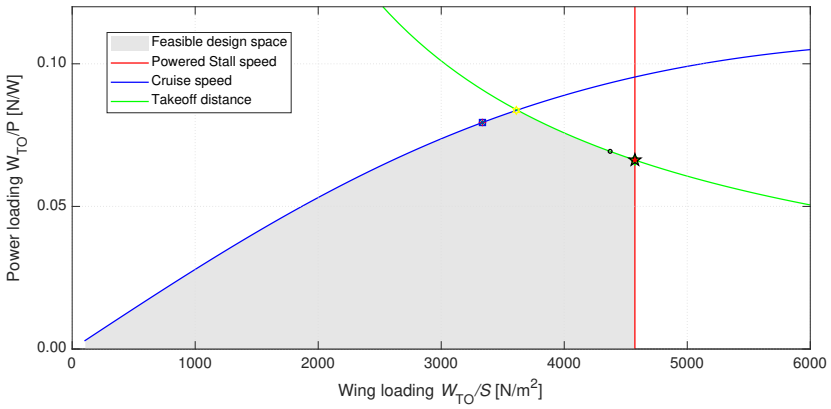

Figure 2.1: Example wing and power loading diagram

The takeoff distance constraint is in current preliminary design methods[7–10] is based on a empirical method

using historical aircraft takeoff data. The method uses the so called takeoff parameter (TOP) to relate the required takeoff distance to wing and power loading according to eq. (2.1). Where σ is the density ratio between takeoff and ISA sea level conditions, $C_{L_{TO}}$ is the lift coefficient in takeoff configuration and W/S and P/W respectively the wing loading and inverse power loading.

$$TOP = \frac{W/S}{\sigma C_{L_{TO}} P/W} \tag{2.1}$$

The historical power and takeoff data of aircraft taking their first flight as early as 1955 and up to 1970 are used by Loftin[8] and subsequently Raymer[9]. The relation between takeoff parameter and takeoff distance is shown in fig. 2.2.

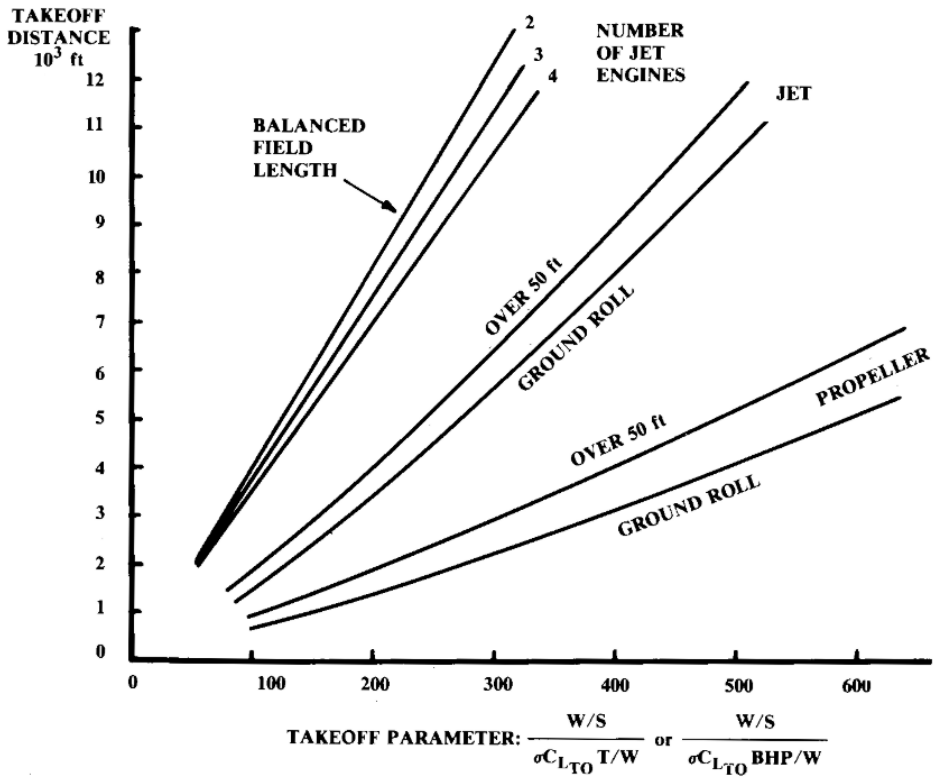

Figure 2.2: Takeoff distance as a function of TOP [9]

The, as it will be called in this thesis, Preliminary Sizing Tool[1] (PST) is a matlab script created by Reynard de Vries at the TU Delft faculty of Aerospace Engineering. The PST combines the wing and power loading diagrams with a mission analysis to complete a "Class-1.5" preliminary aircraft sizing. Originally the script was created to research benefits of hybrid-electric aircraft, it is also able to perform the preliminary sizing for conventional turbo(prop) engines. The empirical takeoff distance relation of Raymer[9] is used to determine the takeoff distance constraint.

2.2. PROPELLER PERFORMANCE

The propeller performance will be discussed on three levels. Firstly, the basic propeller theory is addressed in section 2.2.1. During the aircraft takeoff a propeller is in the so called off-design condition which results in important differences to the on-design cruise condition, of which the effects are discussed in section 2.2.2. Finally, in section 2.2.3 the available tools and methods to calculate propeller performance are discussed.

2.2.1. BASIC PROPELLER THEORY

Propellers are a type of rotating blades that are used since the beginning of aviation. The propeller is a device used on an aircraft to transfer shaft power generated by an engine into a velocity increment of the captured air. The blades of a propeller could be seen as rotating wings, creating lift the same way as a wing, however instead of upward lift, the lift is translated forward and called thrust. When rotating a propeller the combination of lift and drag forces on the blade could be broken down into 2 traditional propeller force components; the axial, thrust, component and the tangential, torque, component.

The propeller force and flow components are shown in fig. 2.3. Where α is the angle of attack, θ the pitch angle and ϕ the local inflow angle. Furthermore, the axial and tangential velocity components are denoted by W_a and W_t. Which together with the free stream velocity, V, and rotational velocity, $\omega \cdot r$ they form the total velocity at the blade section, U.

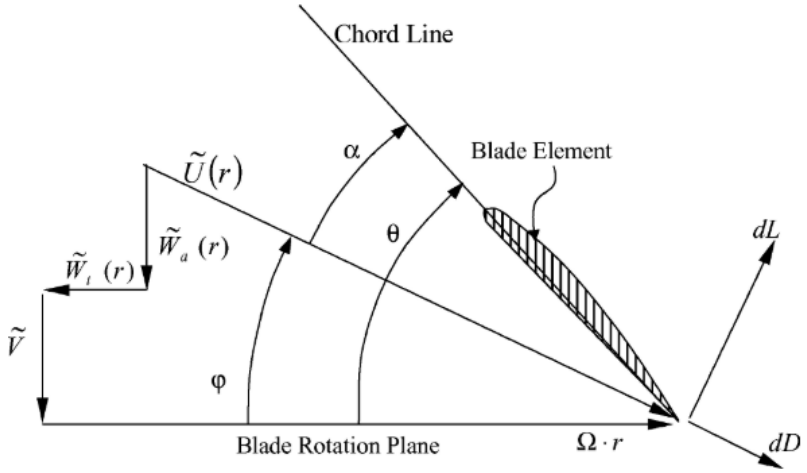

Figure 2.3: Propeller blade airfoil cross-section including angles due to induced velocities [6]

To move forward a propeller has to provide thrust, which is the result from the axial force components due to blade rotation. Keeping the blade rotating and producing thrust is resisted by the tangential forces, the required torque and over time required power. Thrust and power coefficients can be useful for non-dimensional comparisons and efficiency computation. The thrust and power coefficients are calculated using eq. (2.2) and eq. (2.3). In these equations the air density is denoted by ρ, the blade frequency of rotation by n and the propeller blade diameter is D.

$$C_T = \frac{T}{\rho n^2 D^4} \tag{2.2}$$

$$C_P = \frac{P}{\rho n^3 D^5} \tag{2.3}$$

The propeller efficiency is calculated as a function of the thrust and power coefficients using eq. (2.4). Where J is the advance ratio, a non-dimensional ratio of the free stream velocity, V_∞, and rotational velocity nD. The advance ratio is a useful parameter in propeller design since propellers will experience the same angle of attack on every blade airfoil section at the same advance ratio regardless of actual forward speed. Thus, the advance ratio is an indication of the propeller operating condition. Where an advance ratio of $J = 0$, where no free stream velocity is present, is called the static condition, since the free stream are is stationary. The propeller performance is calculated over a range of advance ratios and pitch angles for each propeller design, to cover the complete envelope of the propeller performance, such an example is shown in fig. 2.4.

$$\eta = J\frac{C_T}{C_P} = \frac{V_\infty}{nD}\frac{C_T}{C_P} \tag{2.4}$$

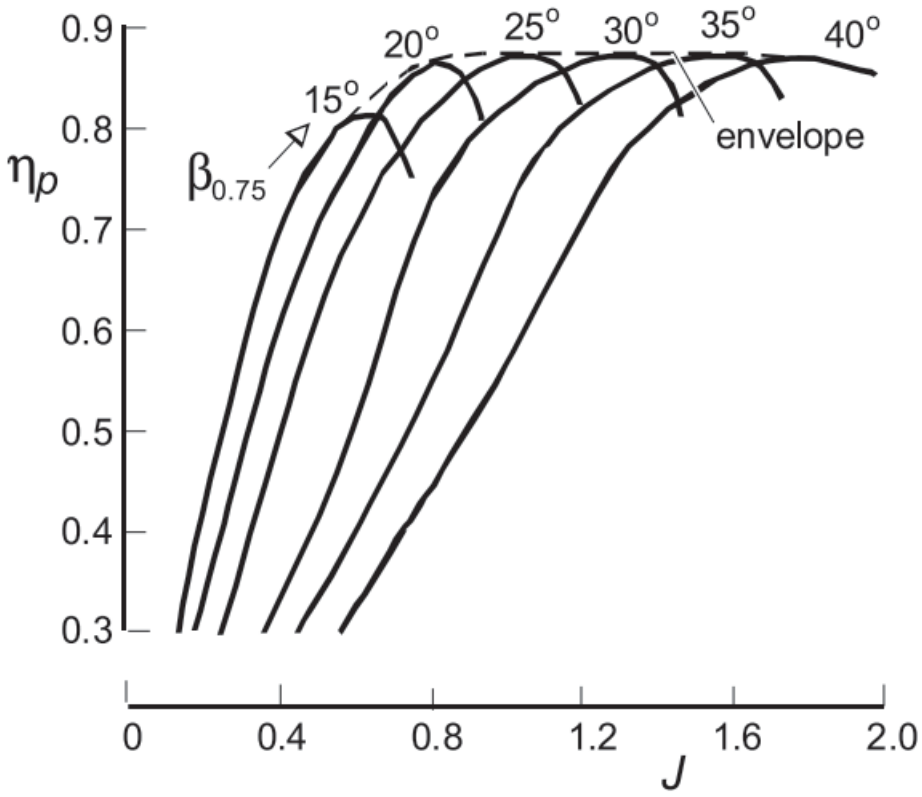

Figure 2.4: Example of propeller efficiency as a function of advance ratio [18]

2.2.2. PROPELLERS IN TAKEOFF

During takeoff, propellers have to accelerate air in order to produce thrust and accelerate the aircraft. However, accelerating a static volume of air is very different from (further) accelerating a volume air that is already moving in the direction of acceleration. In case of static operation, the propeller has to create its own inflow velocity. The propeller is basically sucking the air in, while the free stream velocity of the air is zero, the actual velocity of the air at the propeller disk would be non-zero. The propeller has already induced a velocity on the air and this induced velocity is relatively large with respect to the induced velocity added in cruise. The streamlines of this inflow air vary greatly in the radial direction as could be seen from fig. 2.5. The area of the incoming stream tube is very large and inflow of air is not uniform over the radius of the blade. Adding to the difficulty in accurately modelling the flow regime across the propeller.

The velocity of the rotating propeller blades relative to the static air is very high and consequently the advance ratios are very low, approaching zero. This results in large differences in angle of incidence over the radius of the propeller blade. Consequently, resulting in sections of the blade encountering very high angles of attack. Angles of attack that are outside of the normal operating range of the airfoil and being in the stall and post-stall regimes. Stall behaviour is difficult to be modelled by most analysis methods and therefore results in discrepancies with reality when it occurs. Resulting in under-predictions of the thrust and power coefficients of the propeller.

Gur et al.[6] show that for blades with a 75% radius pitch angle over 30°, already at an advance ratio of 0.3, 45% of the blade area operates at an angle of attack higher than 8°, which is in the stall domain. They also show that a propeller with a 75% radius pitch angle of 40 has 47% of it's disk area operating at an angle of attack higher than 25° which is in the post-stall domain. Large portions of the blade area operate at (very) high angles of attack and in the stall and post-stall flow regimes.Therefore, only having data of the linear operating range of an airfoil is no longer sufficient and accurate airfoil polars up to high angles of attack are necessary.

The flow regimes to be modelled are those from the fully attached, partially attached and separated flow.[19] Where in conventional wing aerodynamics the lift and drag curves go up to the stall, up to an angle of attack

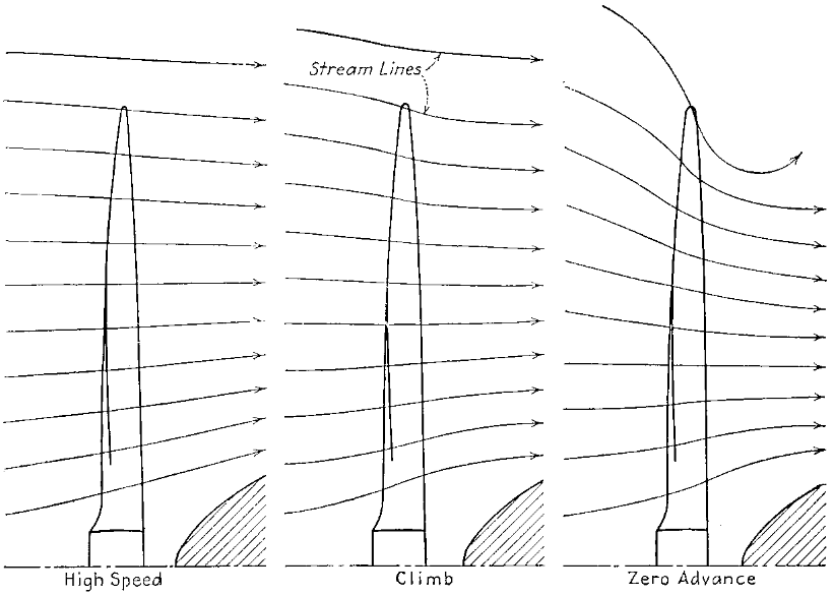

Figure 2.5: Propeller radial inflow velocity for different flight conditions

of 15-20°. In propeller static conditions the angles of attack experienced by the blade section could be much higher. Thus, lift and drag data needs to be available for the complete range of angles of attack. The lift polars of the NACA 0012 and 4415 airfoils could be seen in figs. 2.6a and 2.6b. One could clearly see that in the linear range, with fully and partially attached flow, both airfoils have significantly different characteristics. In fully separated regime, from an angle of attack of 30° onwards, the lift polars are almost identical. This is due to the fact that at these high angles of attack the airfoil is completely stalled and it's shape only has marginal effects on the flow, basically reducing to the effectiveness of a flat plate. The lift and drag polars of a flat plate are presented in fig. 2.7.

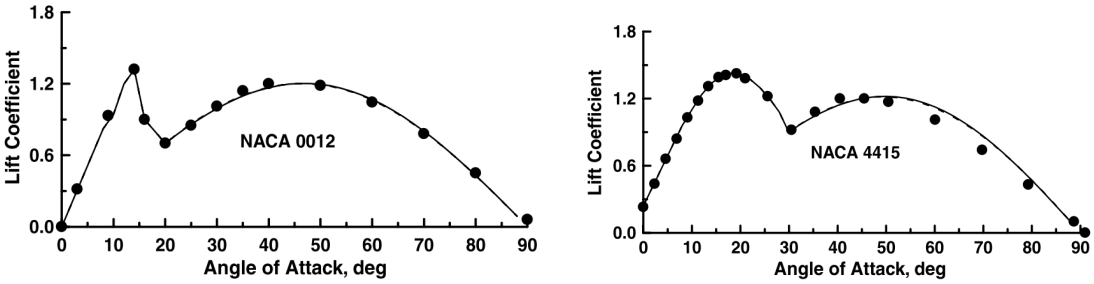

(a) (b)

Figure 2.6: Lift polar from 0-90° of (a) NACA0012 and (b) NACA4415 airfoils[19]

During experiments it was noticed that on a rotating blade the lift coefficients would go as high as three near the hub. Stall behaviour of an airfoil changes when an airfoil is rotating, most dominantly on hub sections of highly loaded rotors.[6, 20] This effect is called 'centrifugal pumping' and gives an additional negative pressure on the airfoil surface, which is favourable for the stability of the boundary layer.[4] Due to this effect, stall on a rotating airfoil is delayed and 2D airfoil lift polars are altered, becoming 3D lift polars. fig. 2.8 shows the increase in lift due to the blade rotation as found by research of Bosscher et al.[20].

Research of Gur et al.[6], Traub[19, 21], Morgado et al.[22, 23], Tangler[24], Lindenberg[4] and Breton[5] describe and evaluate methods to correct the airfoil characteristics for stall/post-stall behaviour and the effects of blade rotation. The methods use different types of corrections to make a prediction on the airfoil behaviour. A common theme between the methods is the use of 2D airfoil data as a basis, and using an adaptation of the

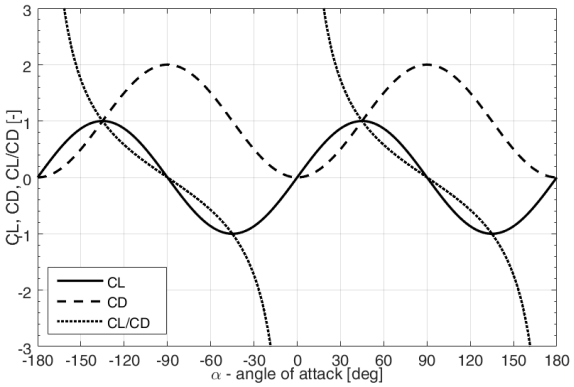

Figure 2.7: Lift, drag and lift-over-drag polars according to flat plate theory

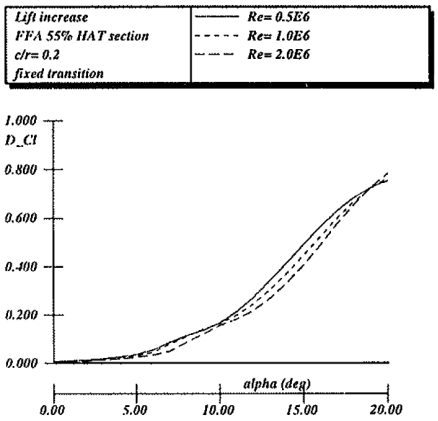

Figure 2.8: Calculated increase in lift coefficient due to blade rotation[20]

inviscid lift coefficient to adapt the lift polars. The drag polars are not affected by the 3D rotation correction methods.

2.2.3. PROPELLER PERFORMANCE ANALYSIS METHODS

It is possible to model the performance of a propeller using various methods. Methods ranging from being very basic to very elaborate and expensive. Important in selecting the right analysis method is the trade-off between accuracy, computational time and required input data. Since the propeller sizing tool is to be used in the preliminary design phase, the analysis should not be too computationally expensive, as well as require elaborate input data which is not yet available at that stage.

ACTUATOR DISK THEORY

Actuator disk theory uses a very simplified model of a rotor, the actuator disk, to connect thrust, velocity and power for predicting the performance of a rotating blade row, e.g. a fan, propeller or helicopter rotor. [25] The classical Actuator Disk model only takes into account forces in axial direction, it is an one-directional model. From actuator disk theory an equation could be derived for the ideal static thrust, which is shown in eq. (2.5). Where T_0 is the ideal static thrust, P the propeller power, ρ the air density and A_1 the surface area of the propeller disk. The actuator disk theory is only able to take into account the propeller diameter as a propeller sizing parameter. Although, diameter is an important propeller sizing parameter, it offers only limited insight.

$$T_0 = \sqrt[3]{P^2\ \rho\ A_1} \tag{2.5}$$

BLADE ELEMENT MOMENTUM METHOD

To more closely model real rotors and the radial distributions of velocity and load, the actuator disk concept has been adapted by many to make it useful for rotors with a finite number of blades. Glauert (1935) coupled disc loads to blade loads and introduced the torque in the momentum theory, resulting in the Blade Element Momentum method (BEM).[25]

BEM in it's basic form is best explained with fig. 2.9 in mind. BEM, as the name suggests, is a combination of a momentum part and a blade element part. Momentum theory is used to find the induction at the rotor. However, unlike in Actuator Disk Theory it is not done for the entire rotor disc but for each radial element, Δr , of the rotor blades. The momentum part requires the blade loads as input. Here the blade element part is used, 2D airfoil properties provide the C_L and C_D for a given induced angle of attack. The momentum and blade element parts are solved iteratively.[25] Once solved, the blade loads in axial, radial and transversal direction are known and used to calculate the blade thrust and torque.

The possibility for propeller performance analysis at low advance ratios and static conditions is important for this literature study. At low advance ratios large portions of the blades' cross sections operate at stall

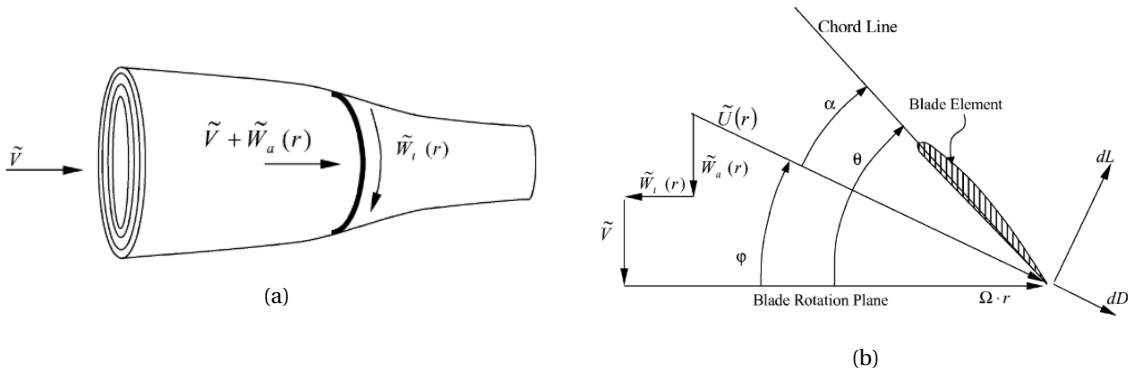

Figure 2.9: Visual representation of BEM. In (a) the control volume of the momentum model and in (b) the blade cross section as used by the blade-element model [6]

conditions. Stall is difficult to model due to its stochastic nature and therefore many BEM models or implementations in design routines don't show results below an advance ratio of 0.2. To be able to calculate the propeller performance in static conditions the BEM model needs to be adapted to incorporate stall phenomena.

The BEM method is a very efficient method for calculating the propeller's aerodynamic performance. In comparison to detailed vortex models or CFD models it requires very small computational resources. This computational efficiency comes at the price of having to know the 2D airfoil data, the C_L and C_D, for a large range of angles of attack, Mach numbers and Reynolds numbers. Maintaining a database of this wide range of angles of attack, Mach numbers and Reynolds numbers is the main difficulty of this method.[6]

COMPUTATIONAL FLUID DYNAMICS

Computational Fluid Dynamics (CFD) refers to computational algorithms which solve the Euler and Navier-Stokes equations of fluid flows, in this case air flows. It is a high fidelity method which when used correctly would provide highly accurate results. However, this comes at great computational cost and thus time, especially in the analysis of unsteady flow around rotating rotor blades. Furthermore, to perform a proper CFD analysis the propeller geometry has to be known in detail, which is not the case in the preliminary design stage.

3

METHODOLOGY

This chapter will describe the methodology used to create a propeller sizing method for propellers in takeoff conditions to be used in the preliminary design phase. The methodology will, at first, be elaborated on in anti-chronological order, starting off with providing an overview of the developed propeller sizing method in section 3.1. As such, the perspective is provided in which the content of the propeller sizing method is thought to be more easily understood. The propeller sizing method combines a significant number of different modules to be able to perform its analysis using only parameters that would be available during the preliminary design stage. Having provided an overview, it is well possible that not all information is provided to understand the workings of the developed propeller sizing method. The details of the various used modules will be provided subsequently.

The aircraft preliminary design basis of the Preliminary Sizing Tool will be discussed in section 3.2. Section 3.3 elaborates on the 2D airfoil polar analysis which is performed by XFOIL. Subsequently, in section 3.4 the inverse propeller design tool XROTOR is discussed that generates an initial propeller geometry from the scarcely available preliminary input parameters. The effects of rotation on the 2D airfoil polars is corrected using methods explained in section 3.5. The propeller performance analysis module uses the Blade Element Method (BEM) to calculate propeller performance and is discussed in section 3.6. Subsequently, the takeoff module (TOM) that calculates the aircraft takeoff performance is addressed in section 3.7. Finally, section 3.8 discusses the creation of the analytical takeoff and cruise constraints.

3.1. PROPELLER SIZING METHOD OVERVIEW

The background of aircraft preliminary design and analysis of propeller performance has been discussed in chapter 2. Using this the propeller and sizing method has been developed to implement the Take Off Performance Analysis Sequence (TOPAS) into the 'Preliminary Sizing Tool'[1], an overview flow chart could be seen in fig. 3.1, which will be further elaborated on below the figure. Furthermore, a design structure matrix in the form of a N^2 chart is presented in fig. 3.2. Analytical takeoff and cruise constraint curves will be generated and added to the wing and power loading diagram. Consequently, providing an analytical basis for the aircraft design point.

The 'Preliminary Sizing Tool' (PST) by Reynard de Vries will be used as a basis that performs the "Class 1-1.5" aircraft design cycle, which will be further discussed in section 3.2. The PST is able to create a wing and power loading diagram based on empirical relations to provide an initial aircraft design point. Thereafter, performing a mission analysis which provides a takeoff weight with which other relevant parameters such as wing surface area and eventually cruise drag could be calculated. This cruise drag is important, since it enables a means to size an initial propeller.

From the equilibrium of forces in cruise flight, it is known that thrust equals drag, T=D. Therefore, a required thrust in cruise conditions is known which together with the cruise mission requirements could be used to size a propeller. A propeller could be generated that satisfies minimum induced loss conditions in cruise flight using a inverse propeller design sequence, this is further elaborated on in section 3.4. The propeller geometry that is generated consists of spanwise chord and twist distributions, which is sufficient to be used in a propeller analysis using the Blade Element Momentum method (BEM). A propeller should be most

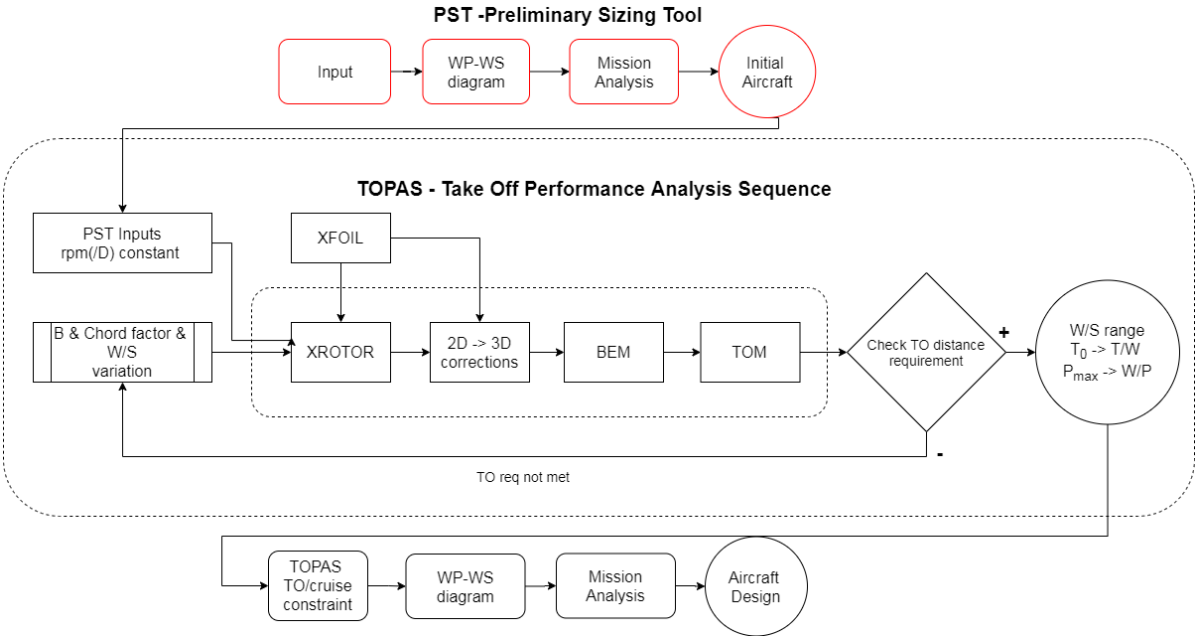

Figure 3.1: Flow chart of the created Take Off Performance Analysis Sequence (TOPAS) implementation in the Preliminary Sizing Tool (PST)

efficient during cruise flight since this is the flight condition an aircraft operates most of it time in, therefore an propeller with minimum induced loss in cruise is an extra benefit.

Unfortunately, it was found that sizing a propeller for cruise conditions results in a propeller geometry that is generally too small to provide sufficient thrust to meet the takeoff distance requirement. Wherein too small means that the propeller chord length was too short and the available propeller surface area, or activity factor, was insufficient to provide sufficient takeoff thrust at any pitch angle. It was found that the most straightforward way to scale up the propeller geometry was to multiply the resulting chord length along the blade length. Resulting in the introduction of the chord ratio factor, CRf, a factor that indicates the ratio by which the initial propeller chord length is multiplied. An iterative process is required to determine what value of CRf creates a propeller that is able to satisfy the takeoff distance requirement. This could be seen as the start of the inner TOPAS loop in fig. 3.1.

Besides, an iterative process to find CRf, the number of blades B and wing loading W/S are varied. The number of blades is varied to enable design freedom and gain insight into the impact of an important propeller sizing parameter. The wing loading is varied to generate power loading points from the propeller sizing method along different wing loading points in order to fit a complete performance constraint curve.

The actual propeller sizing, analysis and evaluation with respect to the takeoff distance and cruise speed constraints is performed in the Take Off Performance Analysis Sequence, abbreviated to TOPAS. TOPAS is able to create a propeller geometry using the inverse propeller design function of XROTOR, further elaborate on in section 3.4. Which uses 2D airfoil data generated by XFOIL, further explained in section 3.3. Thereafter, the 2D airfoil data is corrected for 3D rotation effects, which are described in section 3.5. Using the generated propeller geometry and the 3D airfoil polars a Blade Element Moment method propeller analysis is performed, detailed in section 3.6. The propeller performance, specifically the thrust lapse, is used to simulate and analyse the aircraft takeoff performance in the takeoff model (TOM), which section 3.7 describes in more detail. Resulting in a minimum required takeoff distance for a combination of aircraft and propeller design solutions, which is to be checked with the mission requirement of the takeoff distance. If the calculated takeoff distance is within the set margins, the data point is saved and used in creation of the wing and power loading constraint curves. Otherwise, the sequence is performed again using a different CRf to scale the propeller geometry and consequently the available propeller thrust.

In addition to the overview flow chart of the developed propeller sizing tool, a design structure matrix in the form of a N^2 chart is shown in fig. 3.2. The main variable structures used in the propeller sizing tool and N^2

chart are described in table 3.1. A list of relevant input parameters used to run the PST and TOPAS functions could be found in appendix A. The design structure matrix helps in understanding the flow of variables between the modules that, when combined, form the propeller sizing method. The takeoff performance analysis sequence (TOPAS) is indicated by the blue bordered box and the iterative process determining the CRf that matches propeller size to the takeoff distance requirement is depicted by the red bordered box.

Start	Case input file, XFOIL data							XFOIL data	XFOILdata							
	Input	*a, m, p, c, s, f, TOPASin*	*MA_in, c, s, f*	*TOPASin, a, m, p, c, s, f*			TO distance, TO distance margin					TO distance, TO distance margin				
		Wing-Power-loading diagram	*WS, WP, AERODes, a, m , p*	WS.Landing												
			Mission Analysis	aircraft.TOM				aircraft.TOM			aircraft.TOM					
				TOPAS_start	TOPASin. Brange	TOPASin. WSrange	TO distance error	TOPASin.CRf	*TOPASin*	*TOPASin*	*TOPASin*	TOPASin.CRf	*TOPASin*			
					Blade number loop	TOPASin.B		TOPASin.B	TOPASin.B	TOPASin.B	TOPASin.B					
						WS loop		TOPASin.WS			TOPASin.WS					
							Prop - TO distance matching									
								XROTOR	*XROTORout*	*XROTORout.*			*XROTORout*			
									3D Airfoil Corrections	*CORRout*			*CORRout*			
										BEM	*BEMout*	TOPASout. BFL	BEMout			
							TOMout.BFL				**TakeOff Model**		*TOMout*			
							TOPASout. CRf, TO distance	TOPASout. CRf				**Chord ratio factor optimisation**	TOPASout. CRf			
													Save TOPAS datapoint output	*TOPASsave*	*TOPASsave*	*TOPASsave*
														Wing-Power-loading diagram	*WS, WP, AERODes, a, m , p*	WS, WP
															Mission Analysis	*aircraft*
																Save data

Figure 3.2: Design structure matrix of the propeller sizing method

3.2. PRELIMINARY SIZING TOOL

The Preliminary Sizing Tool[1] (PST) is a matlab script that combines wing-loading and power-loading diagrams and a mission analysis to complete a "Class-1.5" preliminary aircraft sizing. Originally created to research benefits of hybrid-electric aircraft it is also able to perform the preliminary sizing for conventional turbo(prop) engines. A list of relevant input parameters used to run the PST could be found in appendix A.

Currently the cruise and takeoff constraints in PST's wing and power loading diagram are created using an empirical relation from Roskam[7]. The empirical method uses the so called takeoff parameter (TOP) to relate the required takeoff distance to wing and power loading as described in section 2.1.
As visualised in section 3.1 the main modules from PST are the module that creates the wing and power loading and the mission analysis module. Both have been kept mostly unchanged besides the extra code required to create the TOPAS cruise and takeoff constraints and accommodate the extra variables. Different wing and power loading diagrams are created for different types of engine components, such as gas turbine power

Table 3.1: Variable structure description of the design structure matrix

Variable structure name	Description
a	Aerodynamic/geometric airframe properties
AERODes	Aerodynamic and operational aircraft properties per flight condition
aircraft	Basic top-level aircraft results
BEMout	BEM propeller performance outputs
c	Constants
CORRout	3D correction airfoil polar outputs
f	Functions and dependencies
m	Mission/operational requirements
MA_in	Mission Analysis input
p	Propulsion system properties
s	PST program settings
TOMout	TOM takeoff performance outputs
TOPASin	TOPAS program settings and design parameters
TOPASsave	TOPAS collection of results
WP	Power loading values for each constraint
WS	Wing loading values for each constraint
XFOIL data	XFOIL 2D airfoil polars
XROTORout	XROTOR propeller geometry outputs

(which in a conventional turbo engine is equal to the shaft power), sea level corrected gas turbine power and propulsive power, which is the effective power that is transferred to the air. In a conventional turboprop configuration the sea level corrected gas turbine power is used to size the engine and aircraft. Therefore, the wing and power loading diagrams shown in this thesis will be with respect to the sea level corrected gas turbine power. Using the sea level corrected gas turbine power mainly affects the cruise and other high altitude constraints, since takeoff already takes place at sea level conditions.

Using the empirical methods to generate the performance constraints, the types of power used in the power loading are derived from the thrust-power relation $P = T \cdot V$, which is an approximation of the power. In equilibrium cruise conditions this approximation is close to reality since the thrust and velocity are constant, however, in takeoff conditions the thrust and velocity change continuously and the approximation is loses validity and accuracy.

The added cruise speed and takeoff constraint curves that are computed analytically using TOPAS use the calculated propeller shaft power. The used propeller power is the maximum required power in the specific performance case, which in case of takeoff is the maximum power required during the takeoff run and is found to correspond to power at the maximum velocity encountered during takeoff.

3.3. AIRFOIL ANALYSIS MODULE

The propeller performance analysis require a set of airfoil polars over a range of Reynolds numbers. Experimental data of 2D airfoil polars is available, however these polars are difficult to extract from literature and do not cover the required Reynolds number and angle of attack ranges. Therefore, the design and analysis program XFOIL[3] created by M. Drela is used to numerically calculate airfoil performance.

XFOIL is used to create a 2D airfoil polar database for a range of Reynolds numbers that could be used in the propeller analysis. A database is created for the ARA-D, CLARK Y, NACA0012 and NACA4415 airfoils for a Reynolds number from $1e5 - 1e7$, which is the typical range of Reynolds numbers for turboprop propellers. The calculated angle of attack range is between -7° to 35°, to capture the lift loss due stall effects.

The ARA-D airfoil is a state of the art propeller airfoil[26] that is able to achieve high lift to drag ratios. CLARK Y is an airfoil type used in historical propeller aircraft[27, 28] and on which a lot of data is available. The NACA0012 is symmetric airfoil and is not efficient to be used in a propeller but is added to the database as a reference point. The NACA4415 is an airfoil generally used on wind turbines, not on propellers, however is analysed to be used in the validation. The airfoils are shown in fig. 3.3. The XFOIL polar results are validated in section 4.1.

In order to effectively use XFOIL and generate consistent and accurate results some of the base settings of

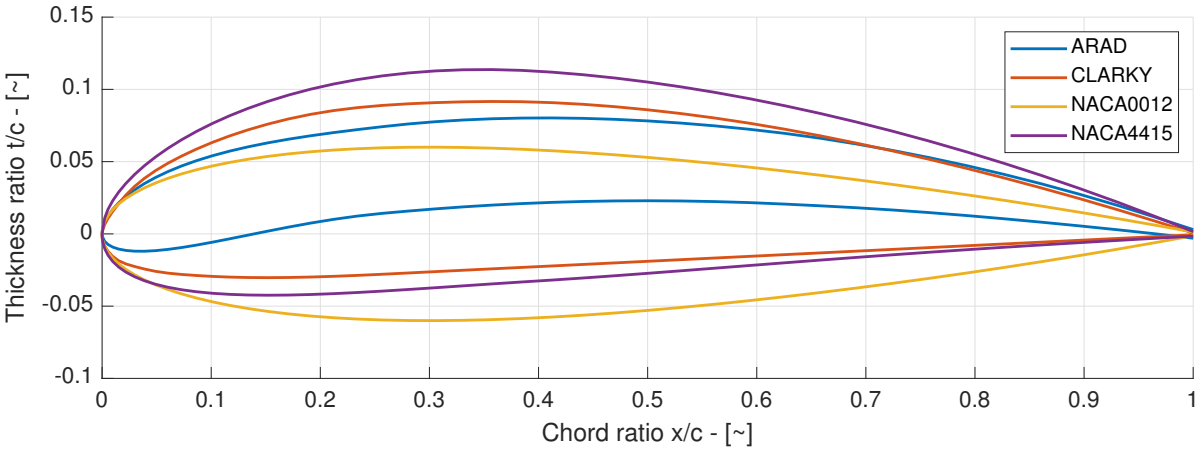

Figure 3.3: A geometry comparison of the ARA-D, CLARK Y, NACA0012 and NACA4415 airfoils

XFOIL have been altered. The parameters have mainly been altered to ensure calculation convergence at high angles of attack, where the airflow over the airfoil separates due to adverse pressure gradients.

First of all, the angle of attack step size that is used is set to 0.1°. Using such a small step size ensures convergence in the solution of the boundary layer during the analysis up to heavily stalled angles of attack of 35°.

Furthermore, the XFOIL uses the e^n method to predict the position of transition on an airfoil.[29] This method uses a a measure of the free flow turbulance, N_{crit}, to simulate the transition location. Typical values of N_{crit} used are in the range of 6-12[29, 30], where 9 is the standard value used for the average wind tunnel. The N_{crit} value to be best used for stable and accurate airfoil polar results is discussed in section 4.1.

3.4. PRELIMINARY PROPELLER GEOMETRY MODULE

XROTOR[2] is another a program created by Mark Drela and is created to design and analyse propellers. The inverse propeller design sequence of XROTOR creates a propeller that satisfies the minimum induced loss conditions along the span. In TOPAS, XROTOR is used to design a propeller geometry, generating spanwise chord and twist distributions, that could be analysed in the BEM propeller analysis. XROTOR is unable to converge at low advance ratio's, including static conditions. Therefore, the inverse design sequence to create a minimum induced loss propeller is performed in cruise conditions. Moreover, in cruise conditions it is possible to predict the required propeller thrust due to the equilibrium flight condition, deriving required thrust from the cruise drag.

XROTOR is able to calculate the Using the airfoil data from XFOIL, a selected number of blades, root and tip diameter, cruise velocity, rpm, cruise thrust and design lift coefficient a minimum induced loss propeller is created. The design lift coefficient used is the lift coefficient of maximum L/D, $C_{L_{LDmax}}$, of the selected airfoil.

It was found that since the propeller is created to match the thrust in cruise conditions, in most cases it does not provide enough thrust to perform the takeoff within the required takeoff distance. Therefore, the chord ratio factor CRf is introduced. The chord ratio factor is multiplied with the output chord lengths from XROTOR and consequently increases the possible takeoff thrust the propeller is able to provide.

An example of the propeller geometry output of XROTOR is shown in fig. 3.4. It could be seen that in this case the twist angle at 75% span is equal to 52.5°, which is this propellers pitch angle achieving $T = D$ in cruise conditions. Furthermore, it could be seen that this propeller chord distribution is shaped for aerodynamic performance. The largest chord lengths are situated around 75% span, where the most efficient lift, thus thrust, generation takes place. This propeller shape would be structurally difficult, thus heavy, to create, since the small root section has to be strong enough to withstand the large bending moment created by the propeller.

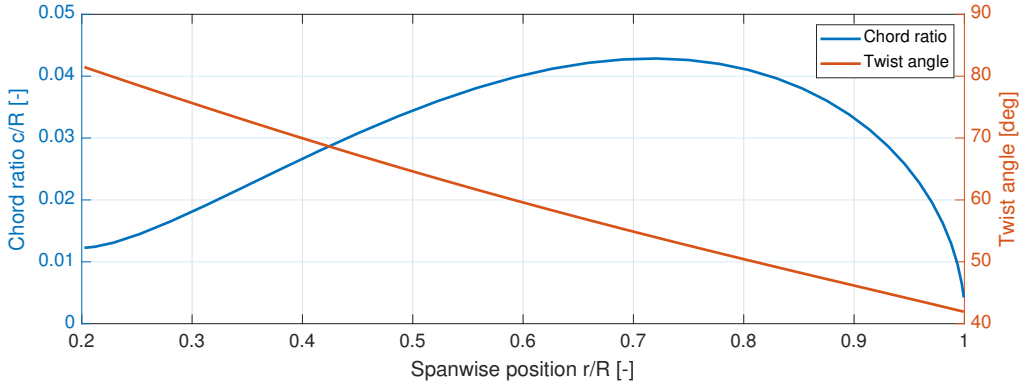

Figure 3.4: Example XROTOR propeller geometry output

3.5. 2D TO 3D AIRFOIL CORRECTIONS

The airfoil polars calculated by XFOIL are the basis for the airfoil polars to be used in the BEM propeller performance analysis. However, before airfoil polars could be used in the BEM they should be corrected in order to be able to represent the conditions encountered during takeoff, as discussed in section 2.2.2. Firstly, the post-stall correction is discussed in section 3.5.1. Secondly, the 3D rotation correction is discussed in section 3.5.2. Finally, in section 3.5.3 the extension of the polars to 360°is discussed. The corrections used will be verified and validated in section 4.1.2 and section 4.3.

3.5.1. POST-STALL CORRECTION

XFOIL is used to calculate the polars up to an angle of attack of 35°, however in propeller during takeoff it is possible for much larger angles of attack to occur. The Traub[19] correction is used to match the 2D polars to their predicted post-stall values at angles of attack up to 90°. The effects of the Traub correction were previously discussed in section 2.2.2 and it's effects shown in fig. 4.4 and fig. 4.5.

Traub uses the fact that at high angles of attack the airfoil polar could be simplified to the polar of a flat plate. From the lowest point of lift beyond $C_{L_{max}}$, the lift polar is merged with the flat plate lift and drag polar. The method requires the detailed information on the airfoil lift and drag polar characteristics.

The flow regimes to be modelled are those of fully and partially attached as well as massively separated flow. To correct the initial input airfoil polars to extend to 90°angle of attack Traub uses the lift polar from zero lift up to the onset of post-stall lift recovery[19], which is defined as α_V in fig. 3.5. The extensive set of equations used to correct both lift and drag polars is presented in a paper by Traub[19].

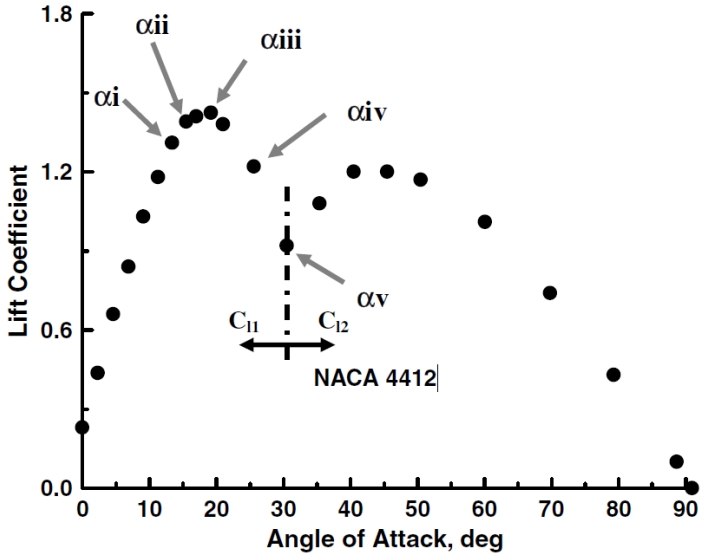

Figure 3.5: Prediction method point locations for definition of the stall location [19]

3.5.2. 3D ROTATION CORRECTION

During experiments it was noticed that on a rotating blade the lift coefficients would go as high as three near the hub. The results of research conducted to investigate this phenomenon is elaborated on in section 2.2.2. It was found that stall behaviour of an airfoil changes when an airfoil is rotating, most dominantly on hub sections of highly loaded rotors.[6, 20] The propeller blade rotation induces additional negative pressure on the airfoil surface which delay the effect stalls. This results in different airfoil polars on a rotating blade, 3D airfoil polars, than resulting polars of an airfoil experiencing 2D flow, an example is shown in fig. 3.6.

During takeoff, the free stream velocities in which the propeller operates are relatively low, up to zero at standstill. The low inflow velocity of air results in large angles of attack differences along the blade span. A large portion of the inner blade is likely to stall. Consequently, in takeoff it is especially important to take into account the post-stall and rotation effects on the propeller blades.

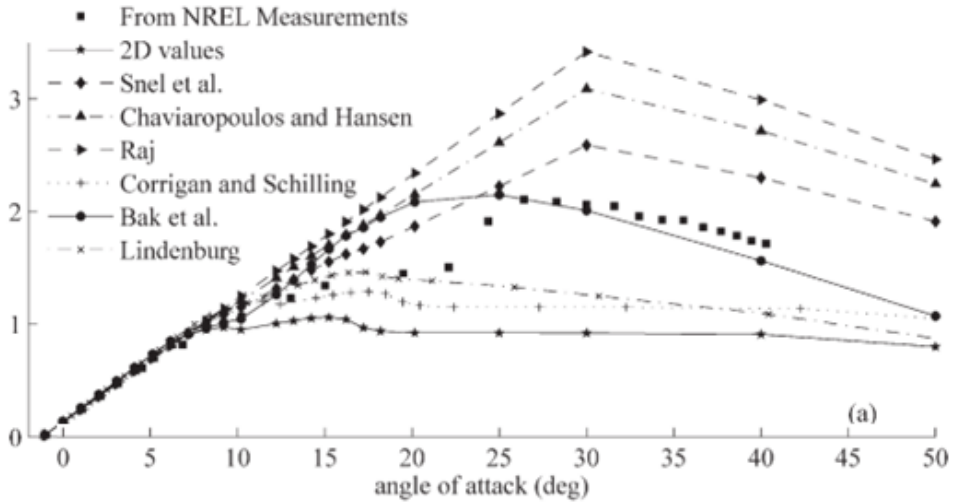

Figure 3.6: Lift coefficient as a function of angle of attack corrected by different stall delay models at 30% blade span[5]

The rotation corrections that are being investigated are the corrections by Corrigan & Schillings[4, 5] and Snel[4, 5]. Both propose a correction to the lift coefficient based on the radial chord distribution c/r and the potential lift coefficient $C_{L,pot}$. No correction to the drag is suggested. The equations used to correct for the 3D rotation effects of Corrigan & Schillings are shown in eqs. (3.1) to (3.3). Subsequently, the equations used in Snels method are shown in eq. (3.4).

Corrigan & Schillings correction is a bit more elaborate and requiring the calculation of K, the linear adverse velocity gradient, and the stall delay angle of attack, $\Delta\alpha$. Where n is a constant related to the intensity of the rotational effects which is suggested to be used as $n = 1$.[5, 24] Both calculate the 3D lift coefficient in a similar fashion, based on the 2D lift coefficient,$C_{L,2D}$, in addition to the difference between the potential lift coefficient, $C_{L,pot}$, and the 2D lift coefficient multiplied by a factor.

$$K = \frac{c/r}{0.1517}^{\frac{1}{-1.084}} \tag{3.1}$$

$$\Delta\alpha = (\alpha_{C_{L,max}} - \alpha_0)\left[\left(\frac{Kc/r}{0.136}\right)^n - 1\right] \tag{3.2}$$

$$C_{L,3D}(\alpha + \Delta\alpha) = C_{L,2D}(\alpha) + \Delta\alpha \cdot \frac{(C_{L,pot} - C_{L,2D})}{\alpha} \tag{3.3}$$

$$C_{L,3D} = C_{L,2D} + 3.1 \cdot (c/r)^2 \cdot (C_{L,pot} - C_{L,2D}) \tag{3.4}$$

The correction by Corrigan and Schillings is based on the pressure gradients in the boundary layer and results in an increase of CL_{max} and $\alpha_{CL_{max}}$ in line with the lift slope. Snel's correction increases the lift coefficient up to 50° angle of attack relative to the lift slope and thus mainly increases the post stall lift peak. Both corrections are found to be valid up to a span ratio of $0.75r/R$, consequently above the span ratio of 0.75 the 2D airfoils are used. The impact of both corrections is dependent of the propeller geometry, an example on the

changes of both methods on the airfoil lift polar could be seen in fig. 3.6.

3.5.3. 360°AIRFOIL POLAR

Finally, a last correction is performed to increase the angle of attack range up to a full 360° polar. The flat plat lift and drag polars are extended and mirrored at the 90° and -90° point up to positive/negative 180°, as discussed in section 2.2.2 and shown in fig. 2.7. The airfoil polars from -180°to 180°cover the complete 360°angle of attack range.

3.6. PROPELLER PERFORMANCE ANALYSIS MODULE

From the propeller performance analysis methods discussed in section 2.2.3, it was chosen to use the Blade Element Momentum method (BEM) in TOPAS. The BEM method is very computationally efficient, accurate and only requires airfoil polars and the propeller geometry in the form of spanwise chord and twist distribution. The BEM model used is based on the model created by Veldhuis[31]. However, the model was found to have difficulty with analysing propeller performance in static conditions. Therefore, the model was adapted to better fit the needs of analysing a propeller in takeoff conditions.

Most significantly, the induced velocity and loading calculation was changed according to Gur et al.[32]. Resulting in the equations for the thrust and torque loading components as well as axial and tangential axial velocities, respectively shown in eq. (3.5), eq. (3.6), eq. (3.7) and eq. (3.8). In these equations the w represents the total velocity at the blade section, B is the number of blades, $\frac{c}{R}$ is the chord ratio, R_p the propeller radius, r the sectional blade radius, F the factor of the Prandtl hub and tip correction, ϕ the local inflow angle and V_∞ the freestream air velocity.

$$dtdr = 0.5\rho w^2 B \frac{c}{R} R_p \left(C_l F cos(\phi) - C_{dr} F sin(\phi)\right) \tag{3.5}$$

$$dqdr = 0.5\rho w^2 B \frac{c}{R} R_p r \left(C_l F sin(\phi) + C_{dr} F cos(\phi)\right) \tag{3.6}$$

$$v_{a,new} = \frac{dtdr}{4\pi\rho r(V_\infty + v_a)} \tag{3.7}$$

$$v_{t,new} = \frac{dqdr}{4\pi\rho r^2(V_\infty + v_{a,new})} \tag{3.8}$$

Furthermore, the Prandtl tip correction was extended to also apply at the blade root. An initial axial induced velocity was implemented in cases of low (or zero) free stream velocity. The initial velocity was set such that the iteration starting combination of axial induced velocity and free stream velocity was at least 20m/s.

The BEM is run over a range of pitch angles and free stream velocities to generate a propeller performance map. An effort was made to minimise the required computational cost. Firstly, the calculated pitch step size was set to 5°and the calculated pitch range was limited. The maximum calculated pitch angle is set to be around the 75% span pitch angle resulting from the XROTOR geometry. The minimum pitch angle should be at least $\alpha_{C_{L/D,max}}$ to have that angle of attack at the 75% span position with 0 induced axial velocity. Also, the propeller always induces a certain velocity creating an induced angle of attack, which showed to also be around $\alpha_{C_{L,max}}$. The minimum pitch angle, β_{min}, is calculated using eq. (3.9). Resulting in a minimum pitch angle depending on the airfoil and used corrections of 15-30°.

$$\beta_{min} = \alpha_{C_{L,max}} + \alpha_{L/D,max} \tag{3.9}$$

Furthermore, the amount of velocity steps taken was set to 10. The velocity range is changed for each pitch angle according to the equation for the angle of the resulting flow[21], using eq. (3.10) and it's derivative eq. (3.11). Where it was found that using the constant 2.5 resulted in the maximum advance ratio at which the propeller produced thrust to be within J_{max}. This makes sure that at low pitch angles, the maximum velocity at which the propeller performance is calculated is within the range the propeller produces lift. Subsequently, increasing the calculated velocity density in the low pitch/advance ratio ranges.

$$\alpha_\infty = tan^{-1}(J) \tag{3.10}$$

$$J_{max} = 2.5tan(\beta) \tag{3.11}$$

The BEM output that is used in the takeoff analysis thrust, power and pitch angle at each velocity. The pitch has been scheduled such that the propeller always operates at maximum thrust coefficient. An example of this could be seen in fig. 3.7. It could be seen that the thrust coefficient shows are fairly stable small increase in thrust coefficient with velocity. The power coefficient shows clear jumps when a switch is made to another pitch angle. The slope of power increase, increases with higher pitch angle and velocities.

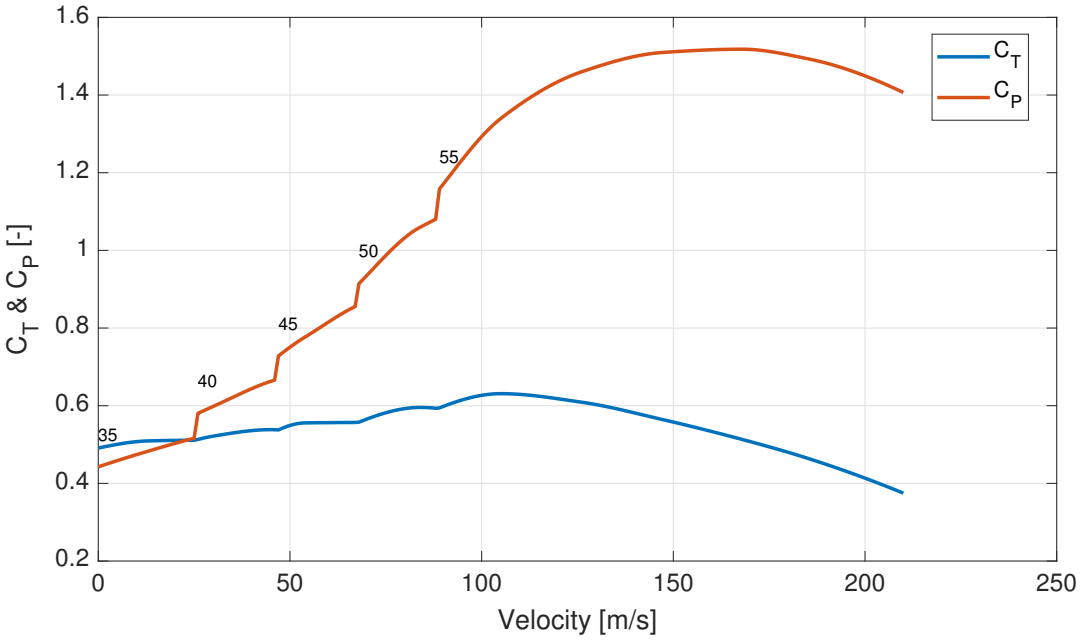

Figure 3.7: Example of pitch scheduling for maximum thrust at all velocities

3.7. TAKEOFF ANALYSIS MODULE

The takeoff analysis module (TOM) is used to calculate the aircraft minimum required takeoff distance. Firstly, the numerical method used to analyse the aircraft performance during takeoff is discussed in section 3.7.1. Subsequently, in section 3.7.2 the takeoff procedures stipulated by the EASA CS25 large aircraft regulations[33] are described. Finally, in the preliminary aircraft sizing phase various important aircraft parameters required to analyse the takeoff performance are not yet known. Therefore, a number of engineering equations have been used to determine such parameters, which is discussed in section 3.7.3. The takeoff module will be verified and validated in section 4.4.

3.7.1. TAKEOFF NUMERICAL METHOD

The takeoff procedure of an aircraft could be modelled numerically in order to determine the required takeoff length of an aircraft. An aircraft is basically a mass that is accelerated until the lift force is large enough such that the aircraft is able to lift-off. In the book of Phillips the basics of the method are described which is used in the research of Teeuwen and Zhu [13, 34, 35]. Applying Newton's second law, one could solve the equations of motion during the takeoff procedure over time to get an accurate prediction of the takeoff length. The takeoff run is once more split in three sections, the ground roll, the ground roll during rotation and the airborne section.

The equation used during the ground roll in the axial direction is given by eq. (3.12). Where T is the thrust, D the aerodynamic drag and F_r the rolling friction. These parameters are all dependent on the airspeed and thus change over time. The thrust lapse of propellers will be investigated in this thesis, on the other hand, definitions for aerodynamic drag and rolling friction are readily available. Combining this results in the extended equation given by eq. (3.13). Where μ_r is the rolling friction coefficient, $T(V)$ the thrust lapse with respect to

velocity. The resulting equations will be solved through numerical integration to get the acceleration, velocity and distance covered over time.

$$T - D - F_r = \frac{W}{G}\frac{dV}{dt} \tag{3.12}$$

$$T(V) - \left[\frac{1}{2}\rho V^2 S\left(C_{D_0} + \frac{{C_L}^2}{\pi A e}\right)\right] - \mu_r\left(W - \frac{1}{2}\rho V^2 S C_L\right) = \frac{W}{G}\frac{dV}{dt} \tag{3.13}$$

During the ground roll section the distance is mainly dependent on the aircraft design parameters. The rotation distance, on the other hand, is mostly dependent on pilot performance. Namely, how well the pilot sets the rate of rotation, at what velocity the pilot initiates rotation and the flight path angle the pilot sets. All affecting the time a pilot takes to perform the rotation manoeuvre. Therefore, a number of assumptions have to be taken into consideration to account for the nominal pilot performance.

During the ground run the aircraft moves purely horizontally and any angles that are present could be neglected with a small angle assumption. During the rotation phase and the airborne phase this is no longer the case, yielding updated equations in both horizontal and vertical directions as indicated by eq. (3.14).

$$T(V)\cos(\gamma+\alpha) - \frac{1}{2}\rho V^2 S\left(C_D\cos(\gamma) + C_L\sin(\gamma)\right) - \mu_r\left(W - \frac{1}{2}\rho V^2 S C_L\right) = \frac{W}{G}\frac{dV_x}{dt} \tag{3.14}$$

$$T(V)\sin(\gamma+\alpha) + \frac{1}{2}\rho V^2 S\left(C_L\cos(\gamma) - C_D\sin(\gamma)\right) - W = \frac{W}{G}\frac{dV_y}{dt} \tag{3.15}$$

During the airborne phase the aircraft tries to climb as quickly as possible to get over the required screen height. Consequently, the aircraft will fly at an angle of attack for the takeoff lift coefficient. The takeoff lift coefficient is correlated to the maximum lift coefficient by the correlation of stall speed (V_S) and V_2 resulting in $C_{L_2} = 0.786 C_{L_{max}}$.[17]

Using the previously mentioned equations, eq. (3.13), eq. (3.14) and eq. (3.15) for the ground run, rotation and airborne phase and integrating them over time, the takeoff distance is calculated.

3.7.2. TAKEOFF REGULATIONS

The takeoff phase is the flight phase where an aircraft accelerates from standstill up to the point where an aircraft lifts off and clears an obstacle of a certain height. This obstacle height is specified in the takeoff regulations of EASA and the FAA as 10.7m (35ft) for large aircraft as categorised by EASA C25[33]. The takeoff procedure could be split in 3 phases, the ground roll, the ground roll during rotation phase and the airborne phase. During these phases the speed of the aircraft is important, a number of speeds have been identified that are important for safety reasons and these speeds have requirements attached to them.

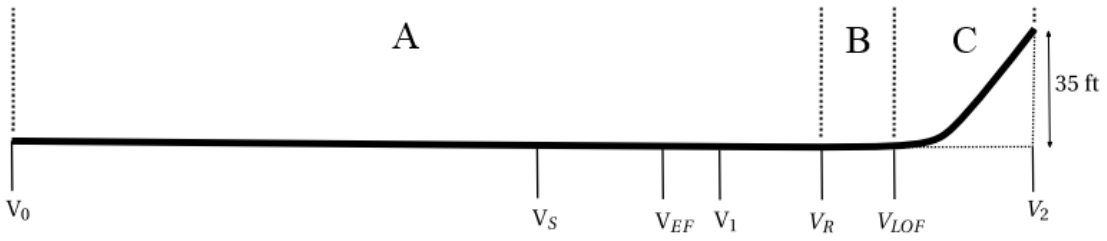

Figure 3.8: A schematic showing the safety speeds and takeoff phases. A: the ground roll, B: the ground roll during rotation, C: airborne

Figure 3.8 shows a schematic of the phases during takeoff and the important speeds that have to be taken into account. The speeds indicated in the figure are: the stall speed V_S, the engine failure speed V_{EF}, the decision speed V_1, the rotation speed V_R, the lift-off speed V_{LOF} and the takeoff safety speed, the speed when the aircraft cleared the required obstacle height, V_2. The different V-speeds are regulated in relation to other V-speeds as described in the CS-25 Certification Specifications[33], the most important relations are shown in eqs. (3.16) to (3.19). V_{MC} and V_{MU} are the minimum airborne control speed and minimum unstick speed,

respectively. While V_{MC} and V_{MU} are important speeds for aircraft handling, at the preliminary design stage not enough of the aircraft is known to use these speeds.

$$V_1 \leq V_R \tag{3.16}$$
$$V_R \geq 1.05 V_{MC} \tag{3.17}$$

$$V_{LOF} \geq 1.1 V_{MU} \ (AEI) \qquad V_{LOF} \geq 1.05 V_{MU} \ (OEI) \tag{3.18}$$
$$V_2 \geq 1.1 V_{MC} \qquad V_2 \geq 1.2 V_S \tag{3.19}$$

The decision speed V_1 is the speed at which the distance to stop after an engine failure exactly equals the distance to continue the takeoff on the remaining engines.[9] Effectively, it is the speed before which the pilot should decide whether the takeoff is continued or will be aborted, in case of, for example, an engine failure. If the takeoff is aborted the aircraft brakes until it comes to a complete stop. If an engine fails after V_1 is reached, it is to late to abort the takeoff and the aircraft has to takeoff in the so called one engine inoperative (OEI) condition. The distance in case of a rejected takeoff is called the accelerate-stop distance which is also certified by CS-25. The decision speed V_1 for the different takeoff conditions will be equal.

The takeoff distance that an aircraft will be certified for is the largest of the four conditions found below. The corresponding takeoff distance is called the balanced field length (BFL).

- 115% of takeoff distance with all engines operating (AEO TO)
- Takeoff distance with one engine inoperative (OEI TO)
- Accelerated-stop distance without engine failure (AEO AS)
- Accelerated-stop distance with engine failure (OEI AS)

The one engine inoperative (OEI) condition is often the dominant requirement for deriving the installed takeoff thrust. This is mostly the case for twin-engine aircraft since failure of an engine causes the thrust to be reduced by 50%. However, large multi-engine airplanes have a long takeoff run compared to the air distance and the 15% takeoff distance reserve for the AEO condition may well exceed the effect of the thrust loss due to failure of one engine.[17]

3.7.3. DETERMINING AIRCRAFT TAKEOFF PARAMETERS

To perform the takeoff analysis of an aircraft a significant number of parameters should be known, unfortunately these are not readily available in the preliminary design stage. Nonetheless, engineering equations and prediction methods have been used to determine the important parameters. The main parameters that had to be determined were the various drag components, aircraft braking capability, aircraft manoeuvrability (pilot performance) and reaction times in case of engine failure.

The drag components that had to be determined were the landing gear, flap, prpoeller windmilling and propeller feathering drag, as well as the runway friction. Which have been determined using methods from Torenbeek[10], Roskam[36] and the Royal Aeronautical Society[37, 38].

The braking on a currently designed CS25 certified aircraft was assumed to be done by automatic braking systems that were recently developed. The runway surface on a larger airport has been assumed to be heavily textured concrete or harsh asphalt, which is input for the wheel braking calculation of The Royal Aeronautical Society[38]. A concrete runway is assumed to have a ground friction coefficient of 0.025[36].

Typical values for the rate of rotation for large transport aircraft are 3-4 degrees per second.[10] Which is verified by a NASA studies by Hall[39], analysing takeoff distances for a supersonic transport configuration. Consequently, the aircraft rate of rotation is assumed to be 3°per second.

The pilot reaction times in case of an engine failure are provided by [40]. The pilot recognition delay in case of engine failure and the typical interval between deceleration devices is assumed to be 2 seconds. Also, activation times of brakes, spoilers and feathering of the propeller has been taken into account to become into use linearly over time instead of abruptly.

3.8. ANALYTICAL CONSTRAINT GENERATION

The output of the TOPAS sequence contains the wing loading and power loading data points and corresponding propeller design solutions for a selection of blade numbers. These data points and propeller design solutions are used to create the cruise speed and takeoff distance constraint curves. It is relatively computationally expensive to run the whole TOPAS sequence, therefore the sequence is only ran a limited number of times. At minimum four data points are required to fit a curve. However, which points should be selected.

Two things are known. Firstly, the wing loading is an input into TOPAS, and the power loading is the output. Secondly, the design condition to be satisfied is the maximum wing loading condition, which is always sized by the powered stall speed constraint. The powered stall speed constraint is a vertical line in the wing and power loading diagram for a single value of wing loading. Therefore, the wing loading value that matches the powered stall speed constraint should always be evaluated. Consequently, in order to create a constraint curve the wing loading data points should be spread around the wing loading value of the powered stall speed constraint.

The constraint curves data points are calculated at 5 wing loading values at different ratio's of the stall speed constraint wing loading value. Namely, at ratios of 9/8, 8/8, 7/8, 6/8, 5/8 the stall speed W/S. These ratios ensure a good selection of data points on, lower and higher than the selected base W/S through which a curve could be fitted.

The fitting functions to fit the cruise speed and takeoff distance constraints are selected to match the shapes of the empirical constraints. The takeoff constraint is fitted by a power series ax^b, which matches the empirical curves very well. The cruise constraint curve is more difficult since at first it looks like a power series, however, the cruise curve in some situations also decreases at high wing loading. Ultimately, the cruise constraint curve represents something between a polynomial, square root curve and power series and therefore the best fitting function is found to be $ax^2 + bx + cx^{0.5}$.

4

Verification and Validation

This chapter will discuss the verification and, where possible, validation, of the modules described in chapter 3. First of all, the XFOIL 2D airfoil analysis results as well as the impact of the airfoil post-stall correction will be compared to experimental data in section 4.1. Subsequently, section 4.2 describes the verification and validation of the used Blade Element Method. The impact of the 3D airfoil corrections is shown through the results of the BEM in section 4.3. Finally, in section 4.4 the used takeoff model is verified with the EASA regulations and validated with a 737 takeoff simulation.

4.1. 2D Airfoil Analysis

The airfoils that have been used for the verification and validation, shown in fig. 4.1, are the NACA0012 symmetric airfoil [41], the NACA4415 airfoil [42] used on wind turbines and the CLARK Y airfoil [27, 43] used in both aircraft and propellers. These airfoils have been chosen taking into account availability of data in both the linear as well as post-stall angle of attack range and use of the airfoil in a rotating frame of reference (wind turbine/propeller).

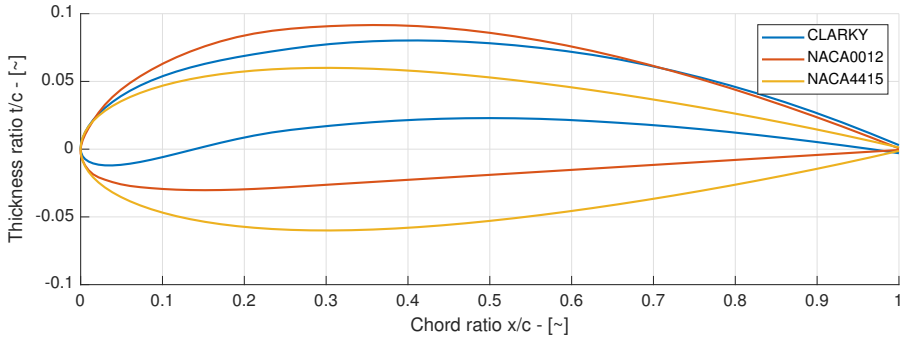

Figure 4.1: Airfoils profiles used in verification and validation

Most of the experimental airfoil data is obtained from polar graphs by semi-manual extrapolation of the data points. Therefore, an inherent inaccuracy in the obtained data is present. The direct measurement errors are given to be in the range of 0.1% [41]. However, for the CLARK Y airfoils it is indicated that interference effects of the struts used on the lower surface of the airfoil have quite a large effect on the drag coefficient in the region of zero lift [27]. Also, the airfoils data is corrected for wind tunnel boundary interference and for the fact that finite aspect ratio wings were used [27, 41].

4.1.1. XFOIL Airfoil Analysis

The computational airfoil analysis is performed using XFOIL[3]. Since this thesis is looking into takeoff performance where the propeller is operating at high pitch angles and thus angles of attack in the post/stall

region, the airfoils are analysed for an angle of attack range between -7 and 35 degrees. The angle of attack delta is only 0.1 in order for XFOIL to be able to calculate the viscous flow effects, and for the computation to reach continued convergence during the analysis.

XFOIL has been run with two different values of N_{crit} (0.01 and 1), which is a measure of free flow turbulence and is used to simulate the transition location. Typical values of N_{crit} used are in the range of 6-12[29, 30], where 9 is the standard value used for the average wind tunnel. Van Arnhem[44] indicates the use of N_{crit}=0.01 in XFOIL has shown to be reasonably stable and significantly higher or lower values can lead to non-converging solutions, which was found to be the case.

Figure 4.2 and fig. 4.3 show the results of a NACA0012 and CLARKY analysis with an N_{crit} of 0.01 and 1. In case of the NACA0012 the C_L and $\alpha_{C_{L,max}}$ looks to match better for N_{crit}=0.01. While the drag coefficient, and consequently the $\frac{C_L}{C_D}$, look to be matched better for N_{crit}=1 for the CLARKY airfoil. Imporantly, in case of the CLARKY with N_{crit}=1 drag coefficient, it could be noted that the curve is noisy and does not follow a clean curve. Furthermore, where in this case XFOIL managed to converge, the cases and tried N_{crit} factors that did not converge cannot be shown. N_{crit} factors in the typical range of 6-12 did either not converge or caused even noisier results as shown. In conclusion, due to the good and cleaner results airfoils analysed using N_{crit}=0.01 are to be used in the remainder of this thesis.

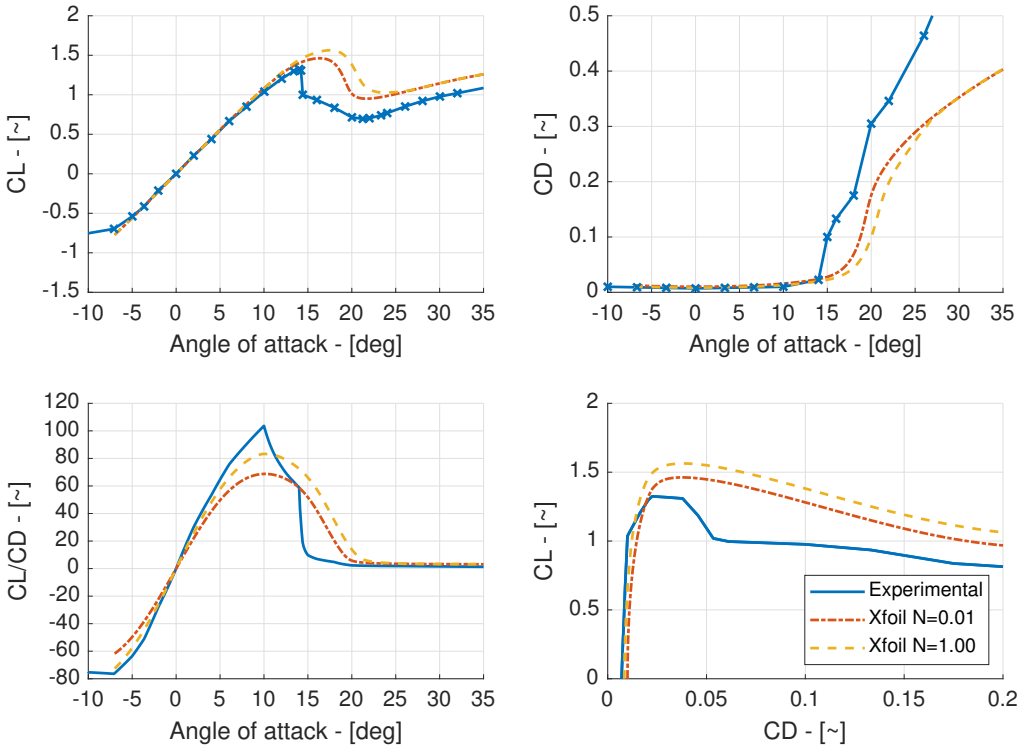

Figure 4.2: NACA0012 airfoil polars of experimental and XFOIL data, Re=1.8e6

Figure 4.2 will be used as an example for general trends that have been observed in the differences between experimental and XFOIL created data. Generally, it could be seen that the linear CL range matches very well. Discrepancies are most often seen with respect to $C_{L,max}$, $\alpha_{C_{L,max}}$, $C_{D,max}$ and L/D_{max}.

$C_{L,max}$ and $\alpha_{C_{L,max}}$ are generally higher than the experimental data. This could be due to the low N_{crit} values that are selected in order for XFOIL to be able to obtain a solution also at high (post-stall) angles of attack. The low N_{crit} values result in an early transition location of the flow which means the flow is turbulent over the whole of the blade. The turbulent flow results in more gradual loss of lift due to separation with respect to laminar flow and thus the higher values of $C_{L,max}$ and $\alpha_{C_{L,max}}$.

Estimating viscous effects and the resulting drag accurately is generally difficult. It is seen that the order of magnitude between XFOIL and the experimental data is good, however the exact values show significant differences, XFOIL predicting both higher and lower values for $C_{D,min}$. XFOIL inaccuracies are further increased by the low N_{crit} value that is used. However, the experimental data also shows inaccuracies due to wind tunnel boundary interference and use of struts on the CLARK Y airfoil experiments.

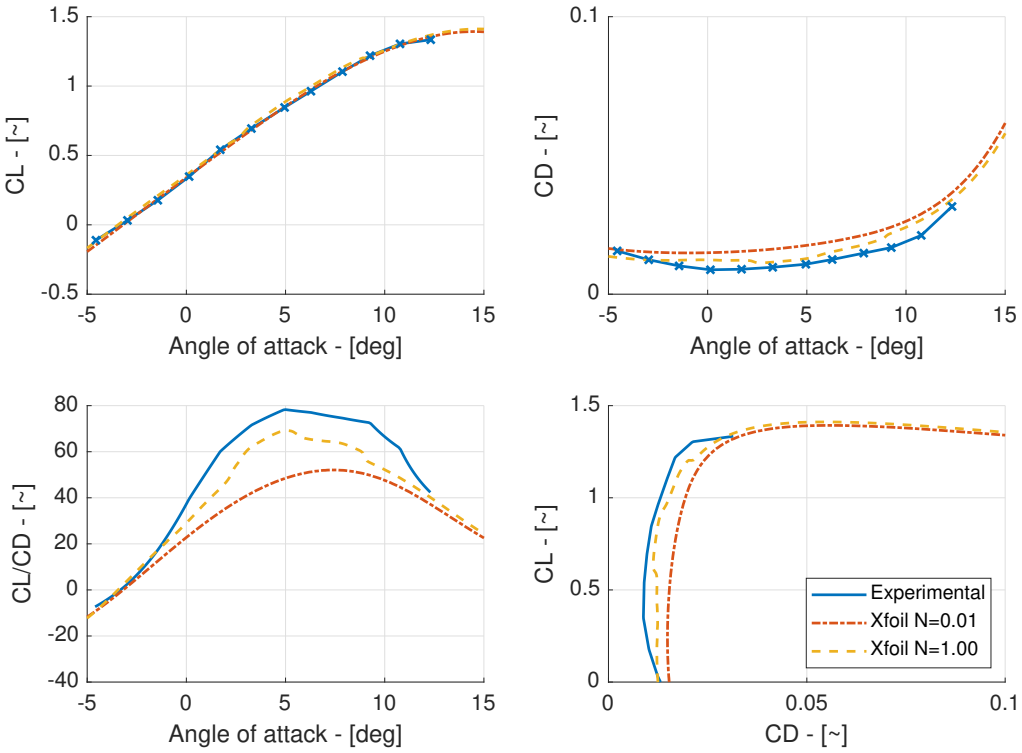

Figure 4.3: CLARKY airfoil polars of experimental and XFOIL data, Re=3.0e5

The discrepancies in L/D_{max} are a result of the combined discrepancies in C_L and C_D. The discrepancies due to their combination potentially could be very significant. However, it is seen that the order of magnitude of the L/D is generally in good correspondence.

4.1.2. POST-STALL CORRECTION

A post-stall correction is used to correct 2D airfoil lift and drag polars in the post-stall angle of attack range. XFOIL is used to calculate the polars up to an angle of attack of 35°, the region in which stall would occur, and the angle of attack range up to 90° is corrected for. The post-stall, or high incidence, correction that is used is developed by Traub[19] and is discussed in detail in section 3.5.1.

An example of the Traub correction applied to NACA0012 airfoil polars could be seen in fig. 4.4. The main discrepancies are found in the transition period between attached and separated flow, which is to be expected since the inputs for the Traub correction, $C_{L,max}$, $\alpha_{C_{L,max}}$, CL_V, α_{CLV} and $C_{D,min}$, show individual discrepancies as well. Moreover, the Traub correction matches the post-stall lift and drag very well.

The Traub correction applied to the experimental NACA0012 polars results in slightly higher values for the lift and drag coefficients at angles of attack above 40°. While for the XFOIL calculated polars the $C_{L,max}$, and CL_V values already were calculated different than the experimental results, the post-stall lift and drag coefficients match the experimental results very well.

Figure 4.5 shows the Traub post-stall correction applied to the NACA4415 airfoil. Different from the NACA0012 results shown previously, the NACA4415 results more clearly highlight the difference between XFOIL, the Traub correction and experimental results. Around 26° angle of attack the $C_{L,V}$ minimum C_L point after $C_{L,max}$ occurs for the XFOIL polars, where the experimental $C_{L,V}$ occurs at around 31°. The solid XFOIL C_L polar starts to increase after 26°, however, with the Traub correction applied the lift polar follows fairly the same post-stall polar as the experimental lift polar. Although, the lift dip between 25°-40° is not fully captured, the overall trend is better than only using XFOIL polars.

For the drag polar a similar improvement could be seen. Where the XFOIL polar only has a shallow increasing slope from 26° onwards, the Traub corrected polar better matches the experimental polar.

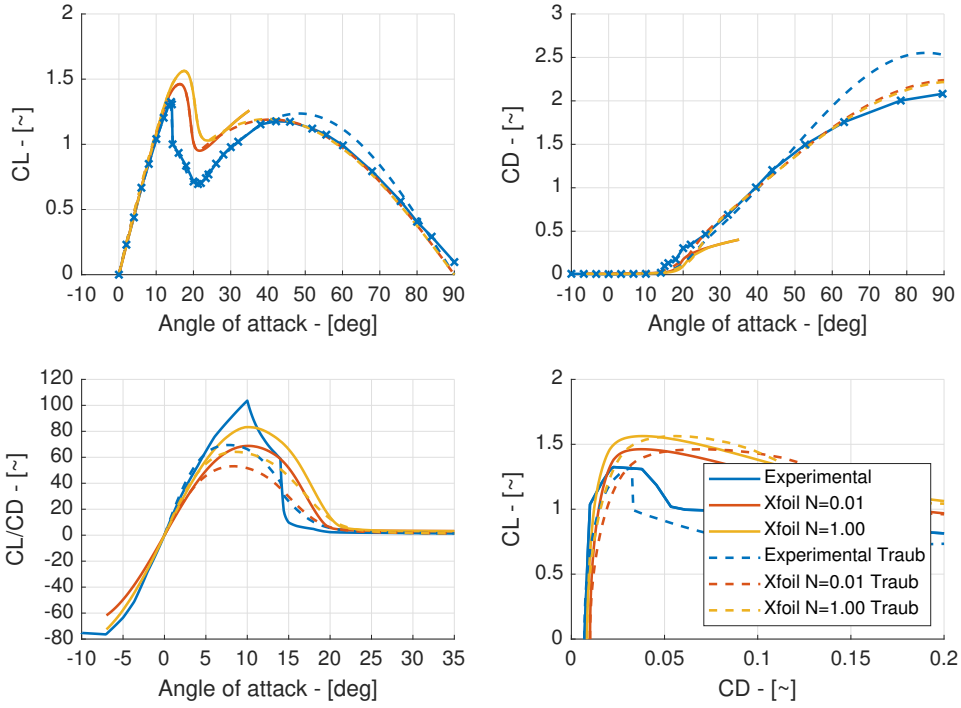

Figure 4.4: NACA0012 airfoil polars of experimental and XFOIL data both with/without the Traub correction

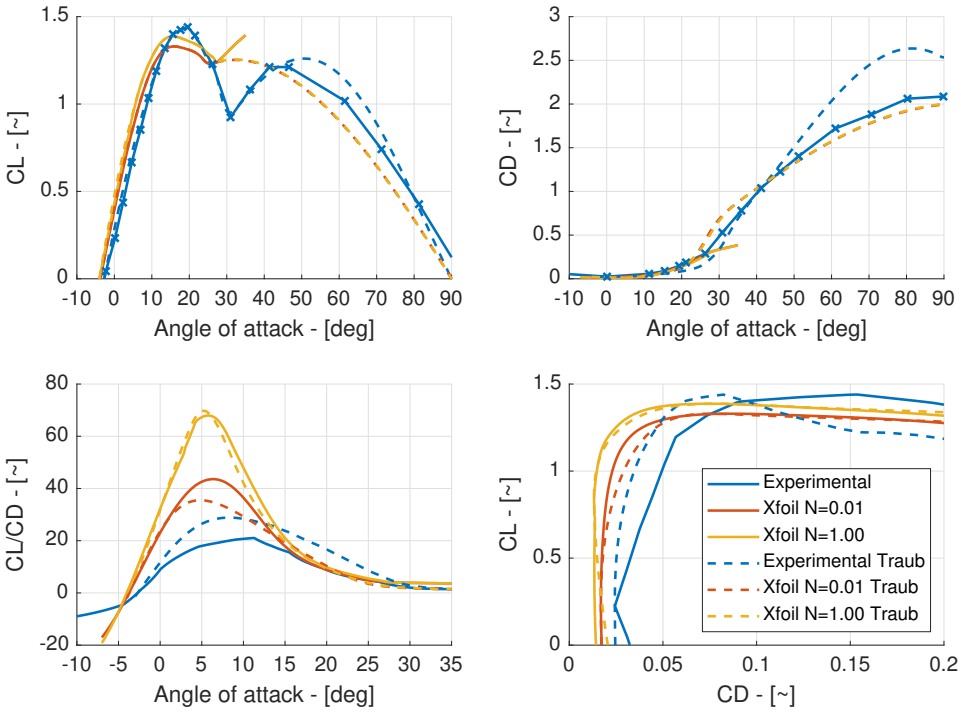

Figure 4.5: NACA4415 airfoil polars of experimental and XFOIL data both with/without the Traub correction

4.1.3. CONCLUSION AND IMPACT ON TOPAS

Simulating the airfoil polars in XFOIL is not completely accurate with experimental results. An N_{crit} factor used by XFOIL of 0.01 has been selected to generate stable results, however comes at a cost of accuracy. The linear airfoil range is simulated well, while the transition range from attached to separated flow shows the most significant discrepancies, which was expected. This means that $C_{L,max}$, $\alpha_{C_{L,max}}$, CL_V, α_{CLV} and $C_{D,min}$, show most noticeable and significant differences.

XFOIL consistently over predicts $C_{L,max}$ and $\alpha_{C_{L,max}}$, basically predicting increased linear range of the airfoil and thus a later onset of stall. Subsequently, XFOIL consistently over predicts the drag coefficient at low angles of attack and $C_{D,min}$.

The Traub correction is used to correct the airfoil polars up to angle of attack of 90°. It has been shown that correction provides good results in the post-stall airfoil range for both lift and drag coefficients. The results around $C_{L,max}$ are not improved with respect to the 2D XFOIL data since Traub's correction is heavily reliant on the XFOIL data as input. However, while the loss of lift around CL_V is fully captured, the post-stall polars show good correspondence with experimental data.

The simulated airfoil polars are good enough to be used in the subsequent BEM analysis. Although, due to L/D discrepancies the propeller would in reality most likely produce less thrust for a given power, and similarly require more power for a given thrust.

4.2. BLADE ELEMENT METHOD

The Blade Element Method (BEM) is verified and validated using data from two pre-World War II NACA reports [28, 45] and more recent data from the XPROP propeller tested within the TU Delft wind tunnel facilities. The theoretical background regarding the Blade Element Method is discussed in section 3.6. The propeller data regarding it's geometry and test conditions used in the validation could be found in table 4.1.

For the 3 NACA propellers from the 2 NACA reports[28, 45] the airfoil thickness varied over the span of the propeller. However, no accurate data is available of the airfoil shape along the span, therefore a single airfoil is used. On the other hand, detailed airfoil data of the XPROP is available, the airfoils have been analysed at 5 stations evenly spaced from root to tip and station polars in-between have subsequently been interpolated from that data. Even though detailed airfoil data of the XPROP is available, it is also investigated whether it is sufficient to use a single ARAD airfoil along the whole blade. For this the airfoil at 75% blade span has been selected which has a t/c ratio of 6%.

Table 4.1: Experimental propeller test conditions

	Airfoil	t/c [%]	Diameter [m]	RPM [-]	U_{inf} [m/s]	Pitch angles [deg]
N378	Clark Y	6%	3.048	1050	0-70	11-15-19-23-27
N658_9	Clark Y	8%	3.048	1000	0-270	15-30-45-60
N658_x2	Clark Y	8%	3.048	1000	0-270	30-45-60
XPROP	ARAD	6-35	0.3034	3400-7600	0 & 30	20-30 & 30

In verifying and validating the BEM the general performance of the results with respect to experimental data will be analysed. Furthermore, the impact of using a single airfoil over the whole blade span instead of multiple airfoils along the span will be discussed. The impact of using additional 3D corrections on the airfoil polars will be discussed in section 4.3.

4.2.1. GENERAL BEM PERFORMANCE

The performance characteristics calculated by the BEM compared to the experimental data of the N658_9[45] propeller could be seen in fig. 4.6. This figure provides the basis on which the validation comparison will be explained. The results will be discussed for the N658_9 propeller, and these results are consistent with the results of the other propellers mentioned in table 4.1.

The BEM results for the N658_9 propeller, as seen in fig. 4.6, match well at low pitch angles for C_T, C_P and efficiency. Although, the results show larger discrepancies with higher pitch angle. For higher pitch angles, results still match well for the advance ratio range from peak C_T to no thrust. However, in the advance ratio range from 0 to peak C_T, the C_T and C_P values are lower than experimental data would suggest. For high pitch angles and low advance ratios, e.g. 60°pitch and J=0, the error in C_T and C_P could be as much as 50%. Fortunately, in the peak C_T range the error in C_T is in the order of 0-5% and the error in C_P in the order of 0-15%, depending on the pitch angle.

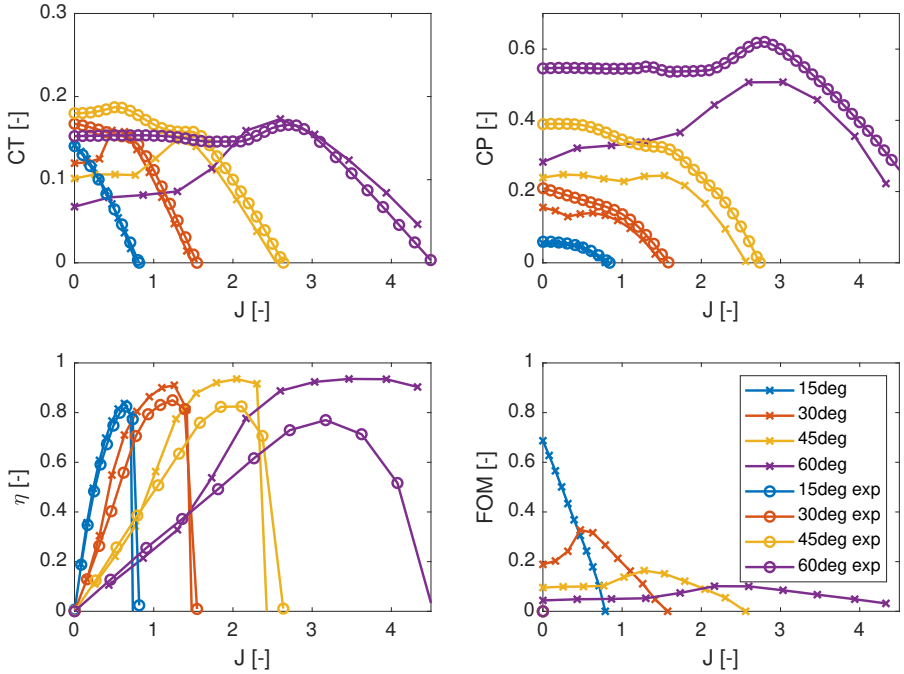

Figure 4.6: N658_9 propeller performance data using no correction

At high pitch angles and low advance ratios the mean angle angle of attack at the blade is close to the blade pitch angle and thus in the post-stall region at airfoil level. In this region the lift polars are not well known, and even using corrections the propeller performance results show significant differences. For example, the Clark Y airfoil $\alpha_{C_{L,max}}$ is around 15-20°angle of attack (for different Reynolds numbers) Thus, for blade mean angles of attack higher than 15-20°, large portions of the blade are in the post-stall regime. The 3D corrections that could be applied to better match reality are discussed in section 4.3.

Fortunately, the propeller performance matches well in the advance ratio region around peak C_T. In this advance ratio region large portions of the propeller blade operate at relatively low angles of attack. Angles of attack which correspond to the linear range of the airfoil polars. Thus, the airfoil lift and drag polars in this region are well matched to reality. Consequently, the propeller performance also matches well to reality.

The efficiency of the propeller matches well between BEM and experimental results at low pitch angles, since both C_T and C_P still match well. At higher pitch angles the propeller efficiency calculated by BEM is higher than reality. Mainly due to the discrepancy in power coefficient, which is lower than the experimental data at higher pitch angles.

The pitch angle spacing for the N658_9 propeller is rather course with a spacing of 15°. In the BEM loop within TOPAS the pitch angle spacing is 5°. This results in smaller gaps between the peak C_T advance ratio regions and thus better overlap of the regions that match well with experimental data. This could be seen in fig. 4.7, where additional results of the pitch angles 22.5°, 37.5°and 52.5°have been plotted. These curves do match the experimental results in gaps that originally existed between the pitch angles.

The experimental C_T polar at 45°pitch remains higher than the calculated BEM polars. Which could suggest that at this particular pitch angle the post-stall effects are strong, and without extra 3D corrections not fully captured. However, this high trend in C_T which is present at 45°pitch for the N658_9 propeller, is not present in the 45°pitch N658_x2 propeller results. Thus, it could also be a specific effect of the N658_9 propeller geometry.

It is possible to focus on the static propeller conditions at J=0, since the XPROP has been analysed in the windtunnel with no incoming freestream velocity. The results of the experimental data with BEM computed results could be seen in fig. 4.8. It could be seen that over the whole range of tested rpm's, the calculated thrust coefficient is higher than the experimental values. For C_T at 20°pitch angle the error remains around 9% and for an angle of 30°the error ranges between 4-10%. It is interesting to see that in this case, with the XPROP, the calculated thrust coefficient is higher than the experimental values, for both pitch angles. For

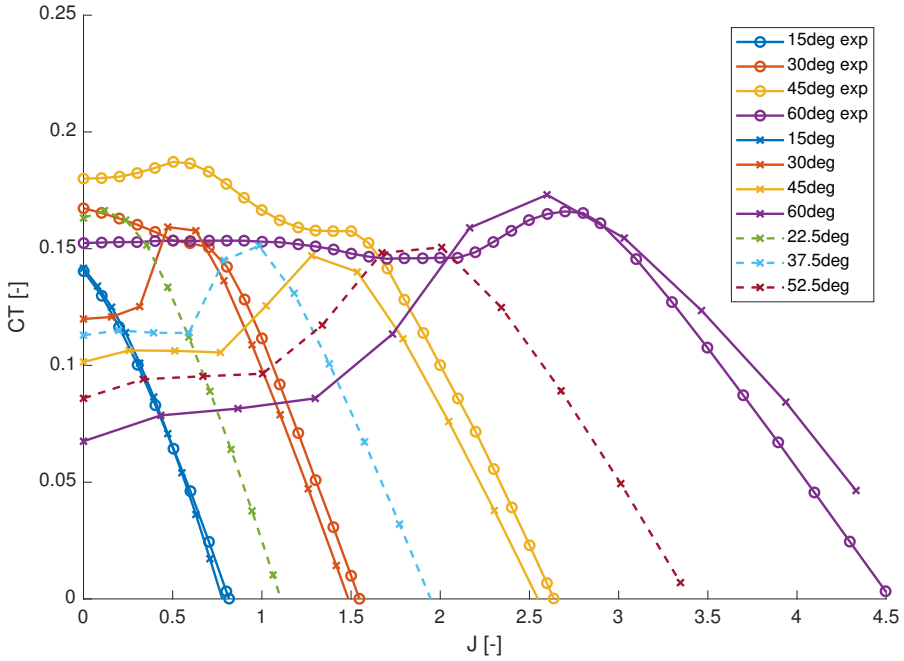

Figure 4.7: N658_9 thrust coefficient using no correction and more pitch angles

the N658_9 propeller discussed previously the calculated C_T matched well around peak C_T but was generally lower at lower than optimal advance ratios.

While the power coefficient at 20°pitch matches the experimental results almost perfectly. The C_P at 30°is between 25-28% lower than the experimental results. Which is consistent with the results previously seen for the N658_9 propeller.

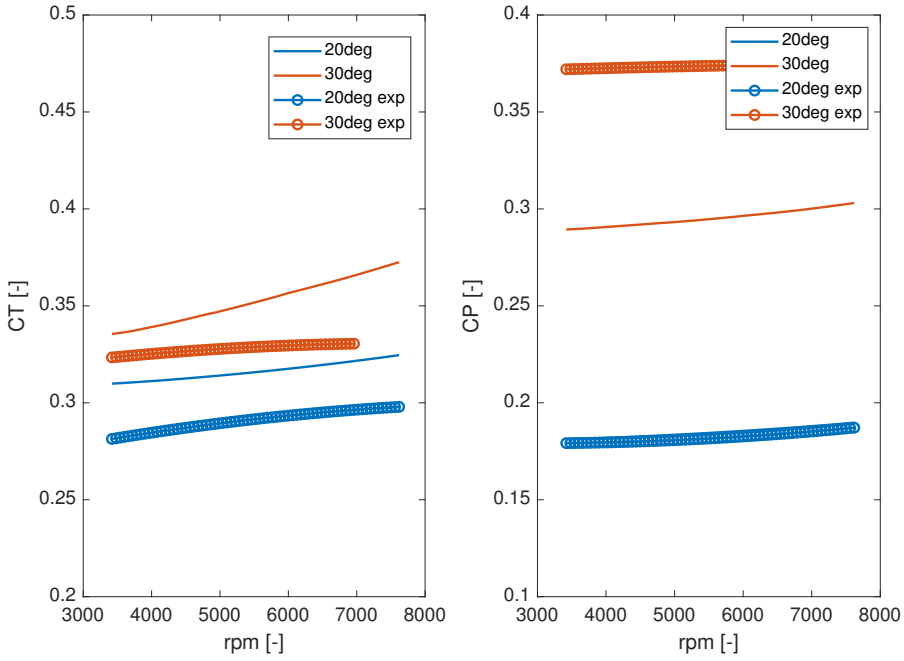

Figure 4.8: XPROP performance at J=0

In the overall TOPAS analysis it was found that the maximum advance ratio achieved during the takeoff run is in the range of 0.8-1, depending on the aircraft and propeller characteristics. Which means that during takeoff the propeller only operates in a low advance ratio regime. In this region largest possible discrepancies

due to 3D effects are possible. However, due to relatively fine pitch angle spacing in the BEM analysis the gaps between C_T peaks is small. At low advance ratios the optimal pitch angles are also low which means that the error in power coefficient, around peak C_T, is low. Where low means in the order of 0-5% error.

4.2.2. BEM USE OF MULTIPLE AIRFOILS ALONG THE SPAN

The validation of the propellers mentioned in the NACA reports[28, 45] were done using a single airfoil over the propeller blade span. For the XPROP more detailed geometric data is available and therefore it was analysed in two cases. Firstly, using only a single ARAD airfoil along the span, for which the airfoil from 75% span was used. The second with airfoils matching 5 out of 25 stations and interpolated airfoil data in-between. The airfoils are shown in fig. 4.9, where the thick dotted line airfoil is the 75% span single airfoil.

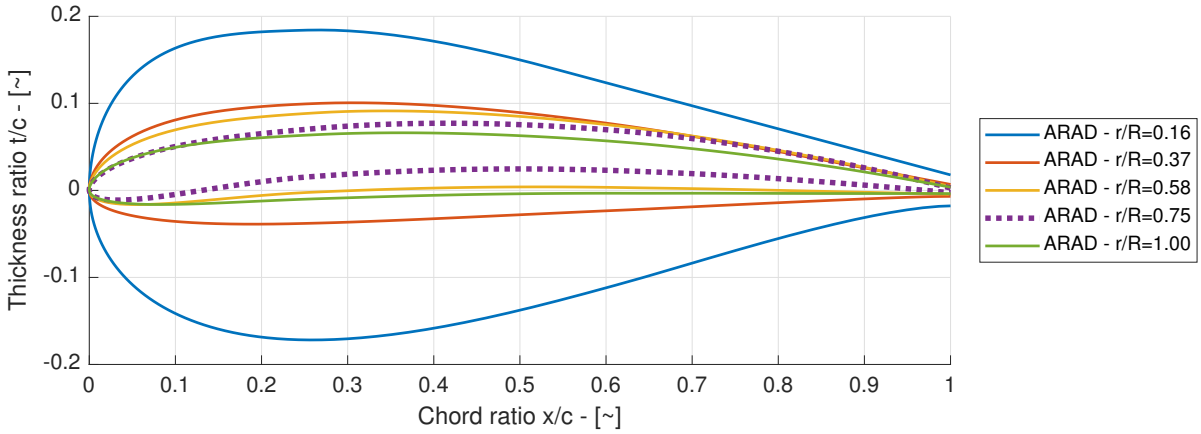

Figure 4.9: XPROP airfoils at stations from root to tip

It could be seen, in fig. 4.10, that the XPROP at V_∞=30m/s results of the BEM and experimental data match almost perfectly using matching airfoils along the span. The results of using only a single airfoil show slightly increased C_T and C_P. The coefficients increase by a fairly constant 0.01 coefficient point over the whole advance ratio range, which is around 5-15% depending on the coefficient values. Comparing it to the experimental results, making the offset of C_T larger, but decreasing the offset of C_P.

The increase in both C_T and C_P is as expected because the single airfoil is the 75% span airfoil which is fairly thin and efficient. In the case of using different airfoils at different stations along the span mainly the airfoils at the root are very different. In reality, the root airfoils are very thick, almost egg shaped, for the propeller to be structurally feasible. These thick airfoils produce less lift and even though they produce more zero lift drag, the drag rise towards high angles of attack is less steep than for thin airfoils due to their thickness. Thus, the single airfoil produces more lift and more drag along the blade span leading to increased C_T and C_P.

The results of the XPROP at V_∞=30m/s are consistent with the results of the XPROP analysed in static conditions where V_∞=0m/s, as could be seen in fig. 4.11. Using multiple airfoils along the span results in lower thrust and power coefficient than using a single airfoil. Furthermore, the results match the experimental results better when using multiple airfoils. On the other hand, the 30°pitch angle curves calculated by BEM follow a far steeper trend than experimental data. Resulting in a low error around 3500rpm and an increasing error up to 15% at 7000rpm.

4.2.3. CONCLUSION AND IMPACT ON TOPAS

The BEM propeller performance results significantly impact the results of the overall TOPAS tool since they provide the basis of the propeller performance analysis. Any errors would therefore be carried over into the final results. Due to the preliminary and off-design nature of the propeller analysis the results are not 100% accurate with respect to the experimental data. Fortunately, the results match well at pitch angles around the C_T peak advance ratio range. Below these C_T peak advance ratio ranges, where the blade airfoils encounter separation effects the results show larger discrepancies. Furthermore, the C_P for high pitch angles is lower than experimental results over the whole advance ratio range, possibly around 15% error at the C_P peak.

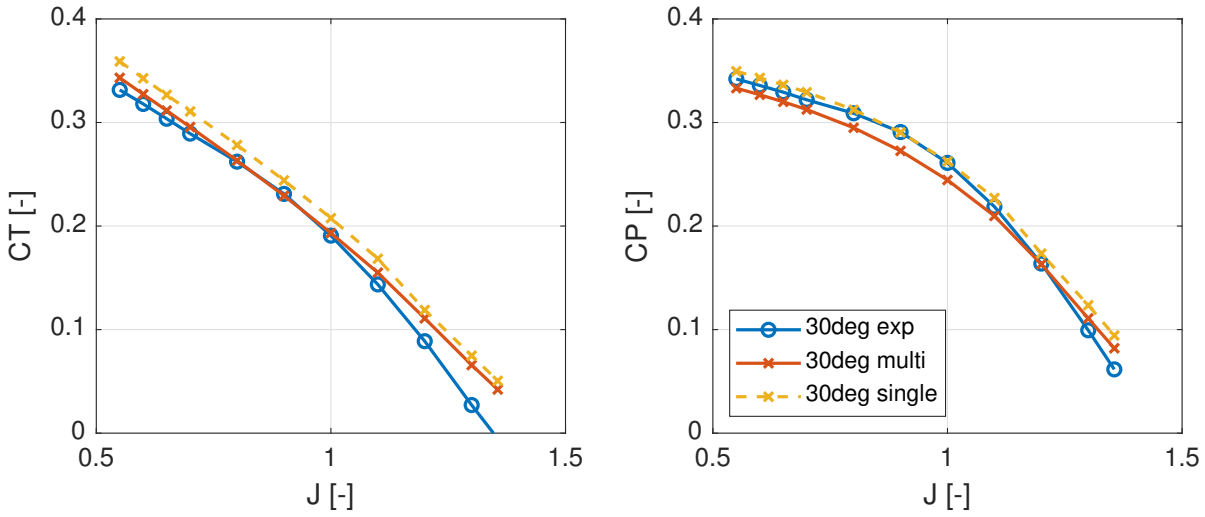

Figure 4.10: XPROP V=30m/s propeller performance with using a single airfoil or multiple airfoils along the span

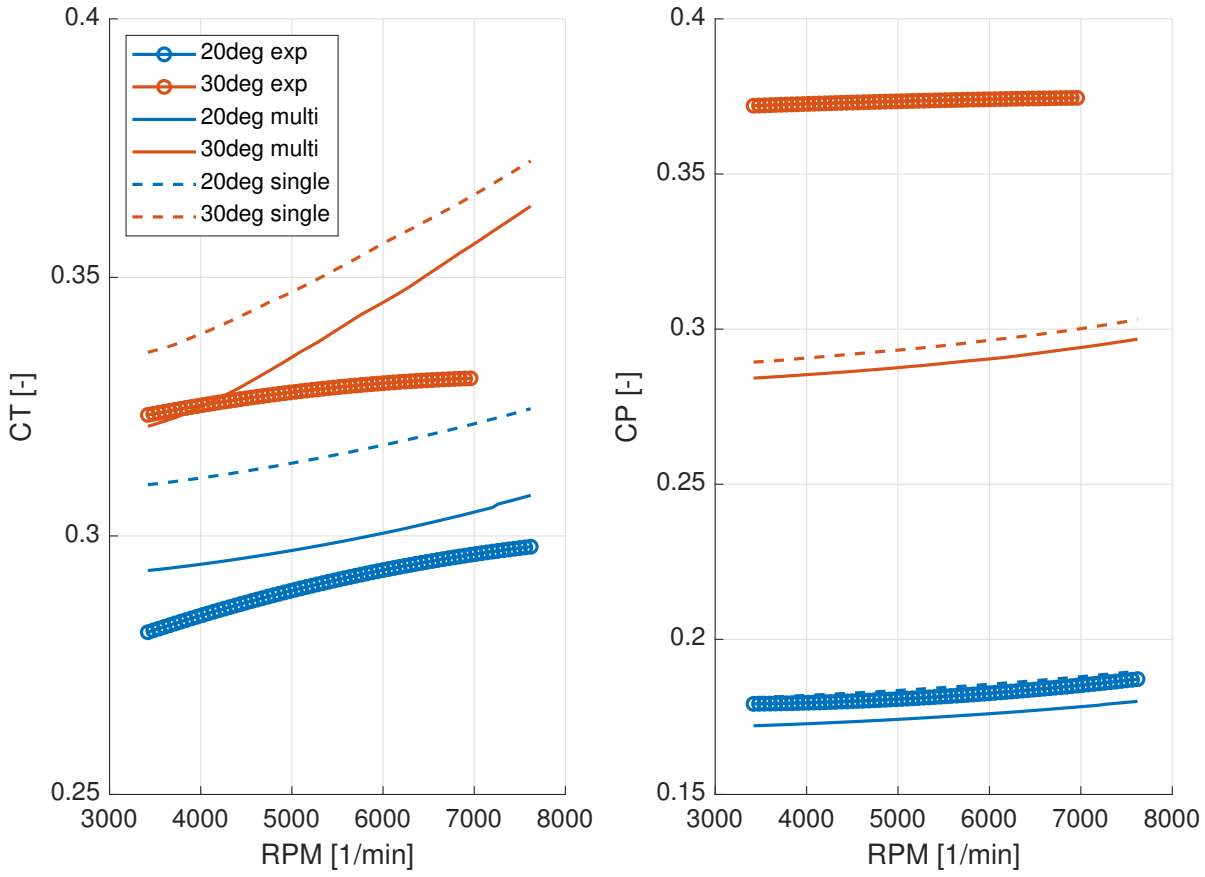

Figure 4.11: XPROP static propeller performance with using a single airfoil or multiple airfoils along the span

The discrepancies of calculated and experimental C_T values in the low advance ratio range would cause most reason for concern, because low speeds and advance ratios are the main focus of this research. However, where C_T values show large differences with respect to experimental data for individual pitch angle comparisons. When the whole maximum thrust range is concerned, thus walking across the maximum C_T peaks over a range of pitch angles, then it is seen that the maximum thrust range matches quite well. Because the C_T peaks for each pitch angle matches well, when multiple pitch angles are considered from low to high pitch angle, the discrepancies in the low advance ratio range are fairly small. Thus, the propeller thrust across the

whole advance ratio range is fairly accurate.

The overall TOPAS analysis has shown that during the takeoff procedure the maximum advance ratios are around 0.8-1. In this advance ratio range the relatively low pitch angles generally generate the highest thrust coefficient. Since for these lower pitch angles the C_P coefficient are a good match to experimental results, the estimated required propeller power should match relatively well to reality. Smaller than the maximum 15% error occurring at high pitch angles.

From the XPROP validation it could be concluded that using only one airfoil for the whole blade instead of a number of airfoils at different stations decreases the accuracy of the results. The order of magnitude of the results is still correct for both C_T and C_P when using only a single airfoil along the span instead of varying the thickness. The thrust coefficient is expected to be up to 5% larger than reality as experimental data suggests. The power coefficient looks to be becoming more accurate however it is expected that the discrepancy at high pitch angles remains. For the overall TOPAS tool it means that the propeller analysis is valid and sufficiently accurate using a single airfoil across the span, however it should be taken into account that the calculated C_T is probably slightly too high, consequently decreasing the calculated takeoff distance.

4.3. 3D CORRECTIONS

The BEM results discussed in section 4.2 show discrepancies with experimental data. Partially this could be explained by the use of only a single airfoil along the span instead of matching the airfoil geometry along the propeller blade span. On the other hand, it is likely that 3D rotation effects play a role in the discrepancies. This section discusses the impact of the 3D rotation corrections of Corrigan & Schillings[4, 5] and Snel[4, 5, 46], discussed in detail in section 3.5.2, on the 2D airfoil polars and subsequently on the BEM performance. The effect of each rotation correction could be analysed and the best matching correction with respect to reality could be selected.

4.3.1. 2D TO 3D AIRFOIL POLARS

First of all, the effect of the 3D rotation corrections on the airfoil polars is discussed and validated. The 2D airfoil polars calculated by XFOIL are corrected by Traubs post-stall correction[19] to have accurate 2D polars up to 90°angle of attack. The corrections are propeller geometry dependent and have been applied to the CLARK Y airfoil polars of the N658_9 propeller.

As explained in detail in section 3.5.2 Corrigan & Schillings' correction primarily impacts the maximum lift peak, CL_{max} and $\alpha_{C_{L,max}}$, and less strongly impacts the post-stall lift polar. No 3D correction is applied to the drag coefficient, conform the theory. These effects at various stations along the propeller blade could clearly be seen in fig. 4.12. The linear lift range is extended such that the CL_{max} increased from 1.46 to 1.74 at the root (r/R=0.2), respectively 2D and 3D corrected, which is a 20% increase. For this case, the CL_{max} at 75% span is increased by 12% to 1.64. Giving an indication of the decrease in strength of the 3D rotational effects further to the tip. The lift curves of r/R=0.8 and r/R=1 overlap with the 2D airfoil polar since above 75% span the 3D corrected stall delay effects were found to be no longer present[5].

Snels rotation correction[4, 5, 46] does impact the primary lift peak, however more strongly impacts the post-stall lift peak. No 3D correction is applied to the drag coefficient, conform the theory. The details of Snels correction are explained in section 3.5.2. Figure 4.13 shows the effects of Snels rotation correction at various stations along the propeller blade. Depending on the location of the station along the blade the linear lift range is extended, strongly near the root and less strong toward the blade tip.
indent More significant is the impact of Snels correction to the post-stall lift peak. At the root the second lift peak lift coefficient is almost double the 2D post-stall peak lift coefficient. Again, the strength of the effects is high near the root and decreases towards 75% span, from which point onwards the correction is not applied.

Comparing Corrigan & Schillings' and Snels rotation correction both clearly affect the 2D polars differently. Both corrections extend the linear lift polar range and increase CL_{max} and $\alpha_{C_{L,max}}$. Although, Corrigan & Schillings' correction impacts the linear lift range stronger than Snels correction. At the root and at 75% the $C_{L,max}$ is respectively, about 6% and 10% higher than at the same station for Snels correction. Both corrections also impact the post-stall lift peak, however the impact on this lift peak by Snels correction is much

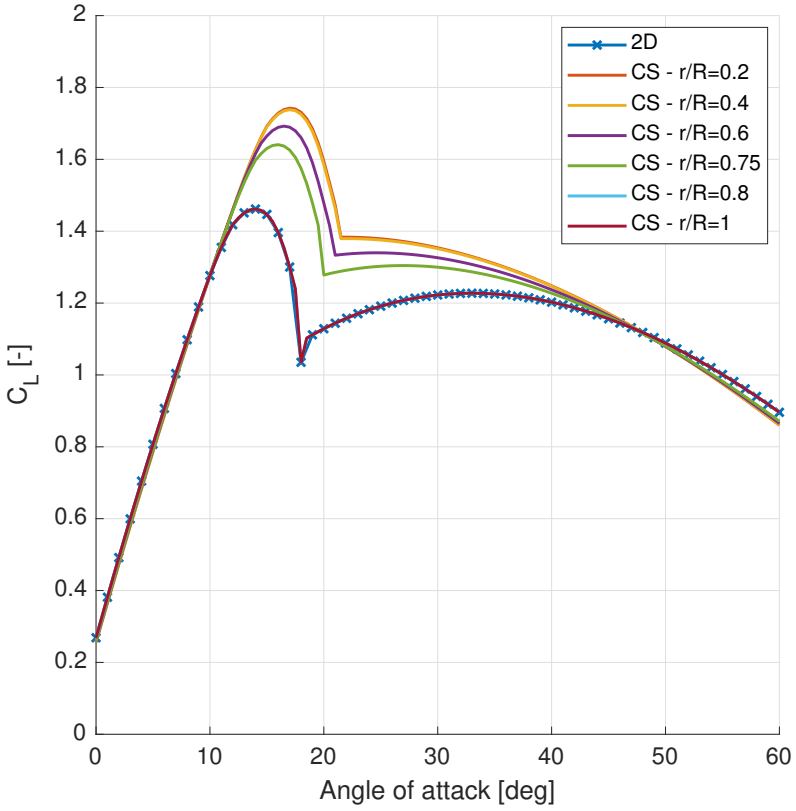

Figure 4.12: Corrigan & Schillings' rotation correction applied to CLARK Y lift polar at Re=1e6 on the N658_9 propeller

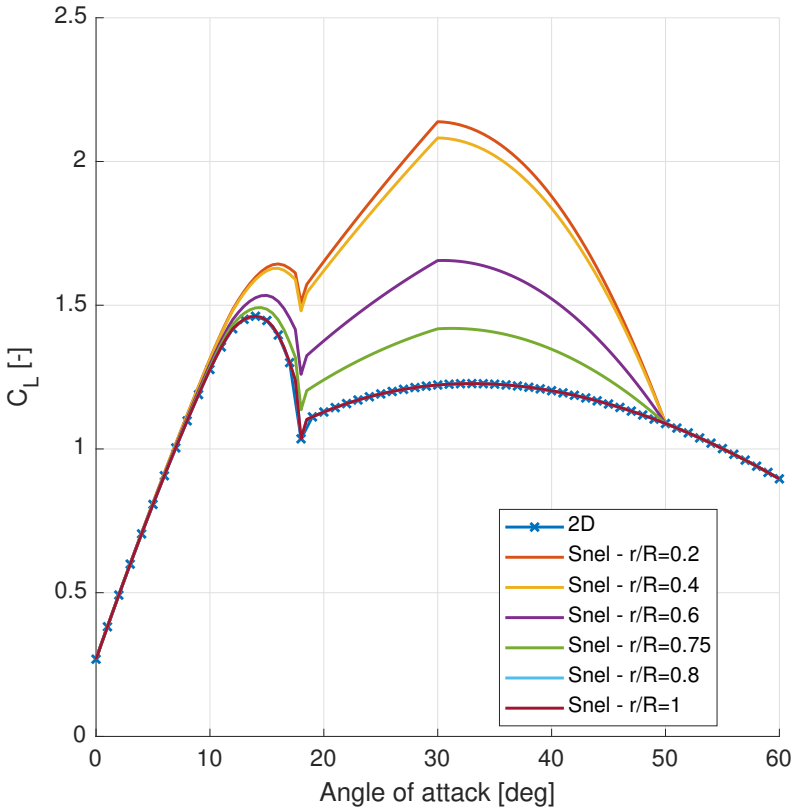

Figure 4.13: The Snel rotation correction applied to CLARK Y lift polar at Re=1e6 on the N658_9 propeller

more significant. Both corrections function as predicted by theory[4, 5] however based on impact on the 2D airfoils alone it is difficult to determine which correction results in the best approximation of reality in the BEM analysis.

4.3.2. CORRECTED BEM PERFORMANCE

It has been shown how the Corrigan & Schillings and Snel corrections impact the lift polar peak and post-stall 2D airfoil polar range. Consequently, the different airfoil polars impact the BEM performance results. The impact on the BEM propeller performance in comparison with the experimental results will be discussed.

First of all, the Corrigan & Schillings and Snel corrections are applied to the BEM analysis of the N658_9 propeller and shown in respectively fig. 4.14 and fig. 4.15. At first glance, the results don't differ much from each other or the results without any 3D correction, shown in fig. 4.6. However, subtle differences between the results are present which are more clearly visible in fig. 4.16.

From fig. 4.16, it could be clearly seen that using the 3D corrections the calculated thrust coefficients are increased, and consequently also the power coefficients. Interestingly, the C_T and C_P coefficients at advance ratios above the C_T peak for a particular pitch angle have not increased. Since at these higher advance ratios the blade angles of attack become smaller and move towards and/or along the linear lift range and the linear lift range is unaffected by the 3D corrections.

The changes are visible at the advance ratios at or lower than the C_T peak, which is logical since the corrections affect the lift peak, separation and the post-stall lift. The lower the advance ratio for a particular pitch angle, the lower the angles of attack along the blade become.

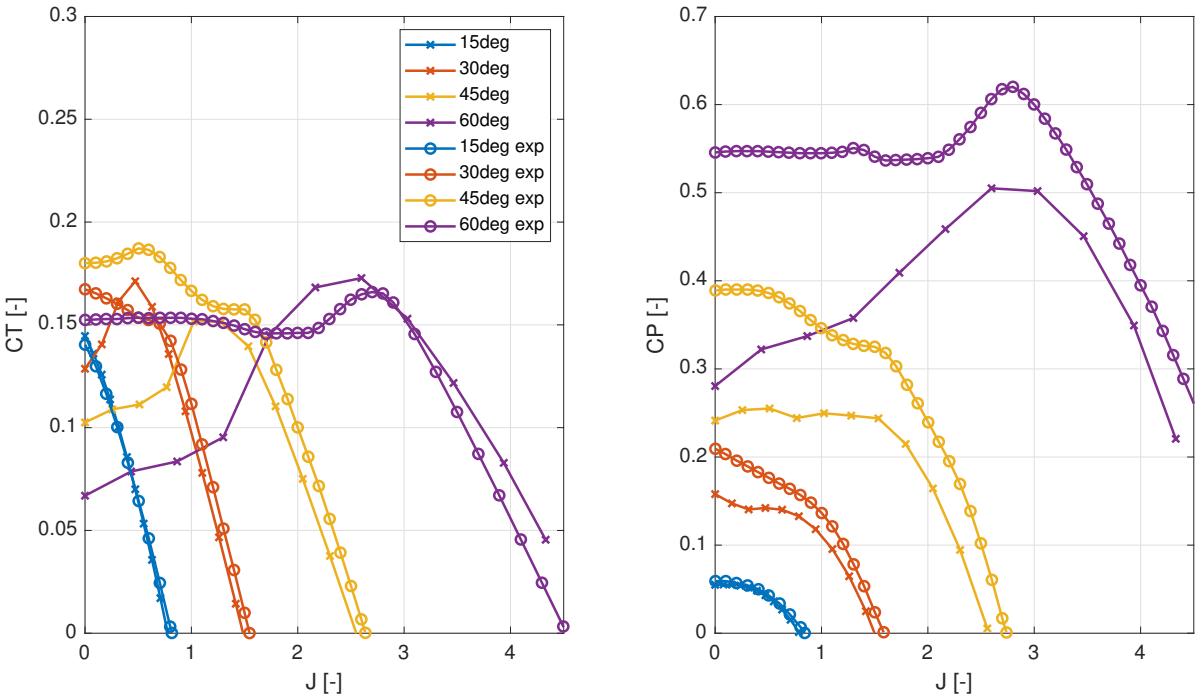

Figure 4.14: N658_9 propeller performance data using the Corrigan and Schillings correction

Snels rotation correction increases the thrust coefficient around the C_T peak, which is clear from fig. 4.16. However, the results corrected using Corrigan & Schillings method increase the C_T even more. Both not only increase the maximum C_T, they also both elongate the advance ratio range at which the C_T is at it's peak for a particular pitch angle. The cause of this is the elongated linear airfoil lift range which has increased $C_{L,max}$ at a higher $\alpha_{C_{L,max}}$, the primary lift peak of the airfoil is larger.

The significantly increased second (post-stall) airfoil lift peak which results from Snels correction method results in higher C_T coefficient at low advance ratios, as could be seen in fig. 4.15. Here it could be seen that the sharp decrease in C_T at advance ratio's lower than the C_T peak is damped. The C_T remains relatively high, higher than using Corrigan & Schillings or no correction method, up to lower advance ratios.

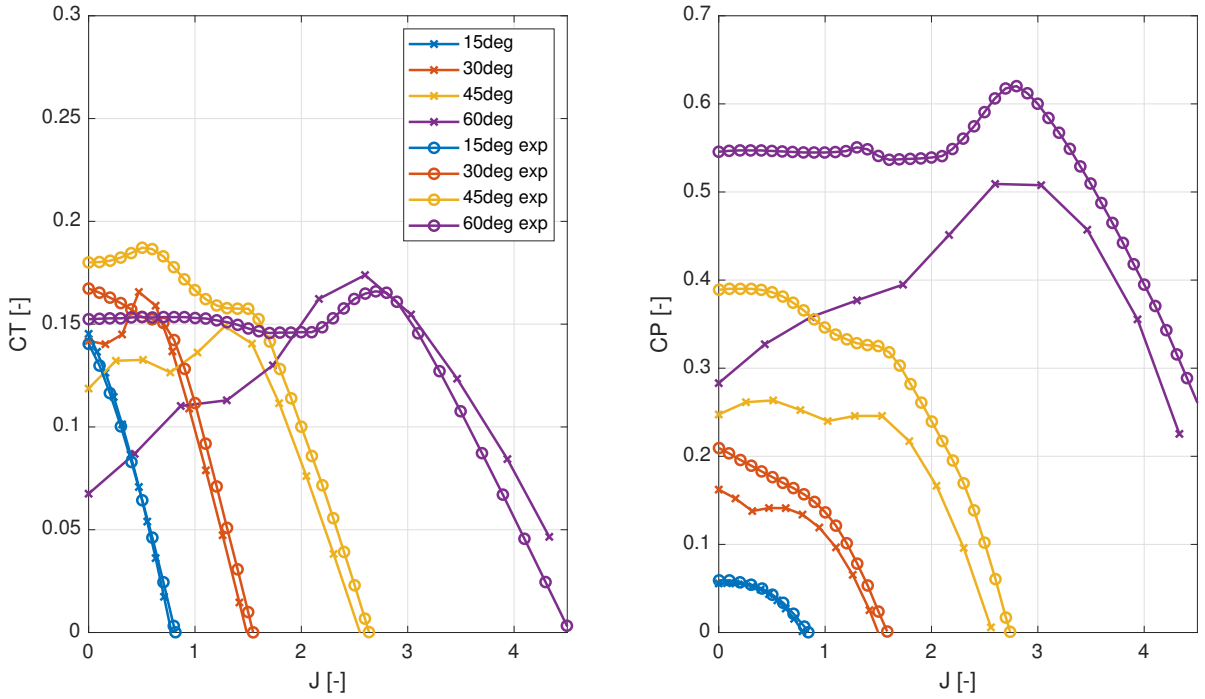

Figure 4.15: N658_9 propeller performance data using Snel's correction

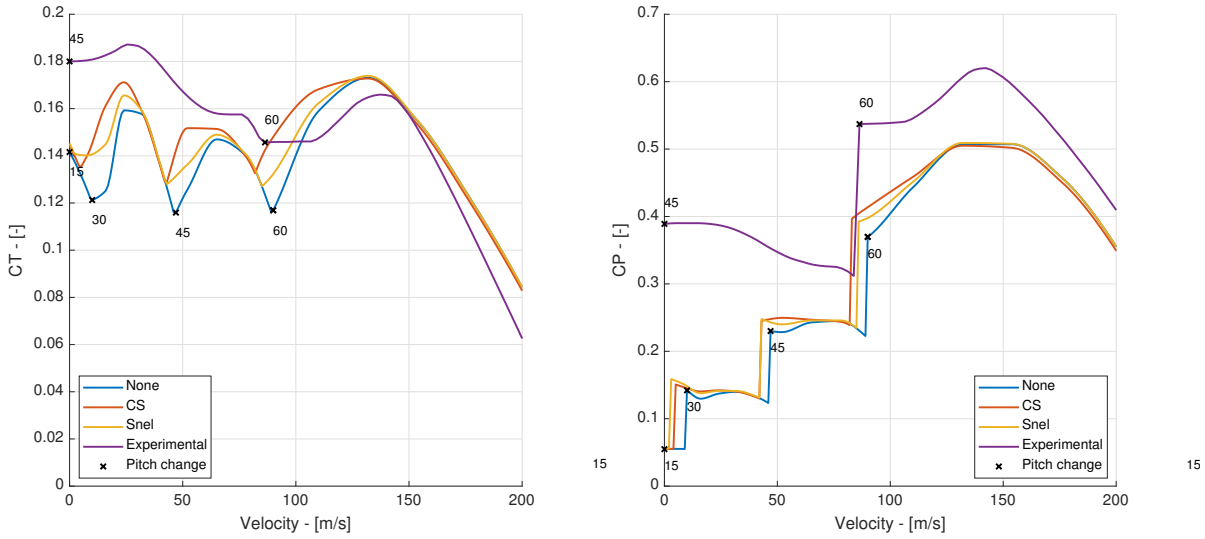

Figure 4.16: N658_9 propeller max C_T performance using 3D corrections

It remains difficult to select the best correction method with matches with the experimental results when looking only to fig. 4.16. The 45°pitch angle thrust coefficient curve lies still significantly above the BEM results, corrected or not. Corrigan & Schillings correction looks to be best when comparing to the N658_9 results because it achieves the highest corrected thrust coefficients.

However, the N658x2 propeller results, of which the maximum thrust curves for a higher number of pitch angles is shown in fig. 4.17, provide an additional point of view. From the results in this figure, the more moderate C_T increase resulting from Snels correction looks to provide a better approximation to the experimental results. Furthermore, on an airfoil level Snels correction method showed a more significant impact on the post-stall lift peak which better theoretical post-stall lift increase due to 3D rotation effects. Therefore, it was decided to use Snels correction as a basis for TOPAS.

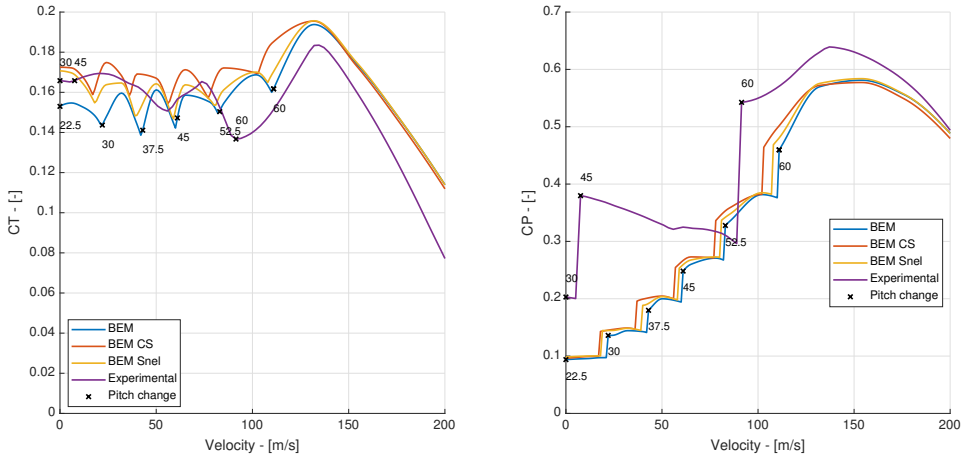

Figure 4.17: N658x2 propeller max C_T performance using 3D corrections including additional intermediate pitch angles

4.3.3. CONCLUSION AND IMPACT ON TOPAS

Verification of the 3D rotation corrections by Corrigan & Schillings and Snel on the 2D airfoil polars have shown the corrections to be in good correspondence with theory[4, 5]. Both correction methods increase the thrust coefficient of the propeller due to a higher airfoil lift peak. The power coefficient is only slightly increased due to the increased thrust coefficients. Corrigan & Schillings method increases the C_T more than Snels correction. However, using Snels method dampens the drop of C_T at advance ratios below the C_T peak.

It has been decided to use Snels 3D rotation correction method in TOPAS. On an airfoil level it had a more significant impact on the post-stall lift peak which better matched theory. Furthermore, Snels correction C_T increase shows good correspondence with experimental data.

Applying 3D rotation corrections to the 2D airfoil polars results mainly in higher C_T coefficients and only a small increase in C_P coefficient at lower advance ratios. This would mean that propellers using 3D rotation corrections would be able to provide more thrust, resulting in a lower required takeoff distance and smaller required propellers. The use of 3D rotation corrections increases the accuracy of the BEM calculation and subsequently of the TOPAS results.

4.4. TAKEOFF MODEL

A Take-Off Model (TOM) has been created on the basis of a point-mass model and the equations of motion which are solved over time using Newton's second law, which is further elaborated on in section 3.7. This section describes the verification and validation procedures of TOM. Firstly, discussing the regulations that have been followed in section 4.4.1. Section 4.4.2 elaborates on the verification of the takeoff procedure. Section 4.4.3 will discuss validation of TOM using a Boeing 737-200 aircraft. Finally, the TOM verification and validation will be concluded in section 4.4.4.

4.4.1. EASA REGULATIONS

First of all, the programmed takeoff procedures in TOM have been checked to match with current EASA takeoff regulations[33] stipulated in sections CS25.105 to CS25.113. These sections deal with takeoff conditions, takeoff speeds, the accelerate-stop distance, the takeoff path, the takeoff distance and takeoff run. The requirements stipulated in the EASA CS25 regulations have been followed and implemented in the TOM program.

4.4.2. TAKEOFF VERIFICATION

The calculated takeoff results have been verified by investigating the speed, forces and angle evolution along the takeoff path for the four different takeoff cases; All Engines Operating (AEO) takeoff and accelerated-stop and One Engine Inoperating (OEI) takeoff and accelerated-stop.

The altitude and velocity profiles with respect to the runway distance are shown in fig. 4.18. In this case OEI

takeoff case requires the longest takeoff distance. In the OEI cases it could be clearly seen that engine failure, occuring at V_EF, happens before V_1 around 1000m and V_1 is reached at the same point around 1400m. In both OEI takeoff cases in the event of engine failure the aircraft has, as stipulated by the EASA regulations, accelerated to V_1.

In case of (continued) takeoff, after V_1 the aircraft rotation occurs from V_R, the rotation speed, onwards untill the aircraft lifts off the ground at V_{LOF}. During an accelerated-stop the aircraft starts the first deceleration action after the initial reaction and recognition time at V_1[40], since in modern aircraft the wheel brakes and spoilers are applied automatically. Following the first deceleration action, the second deceleration action of feathering the propellers is performed after "the demonstrated time interval between activation of 1st and 2nd deceleration devices"[40], at $V_{feather}$.

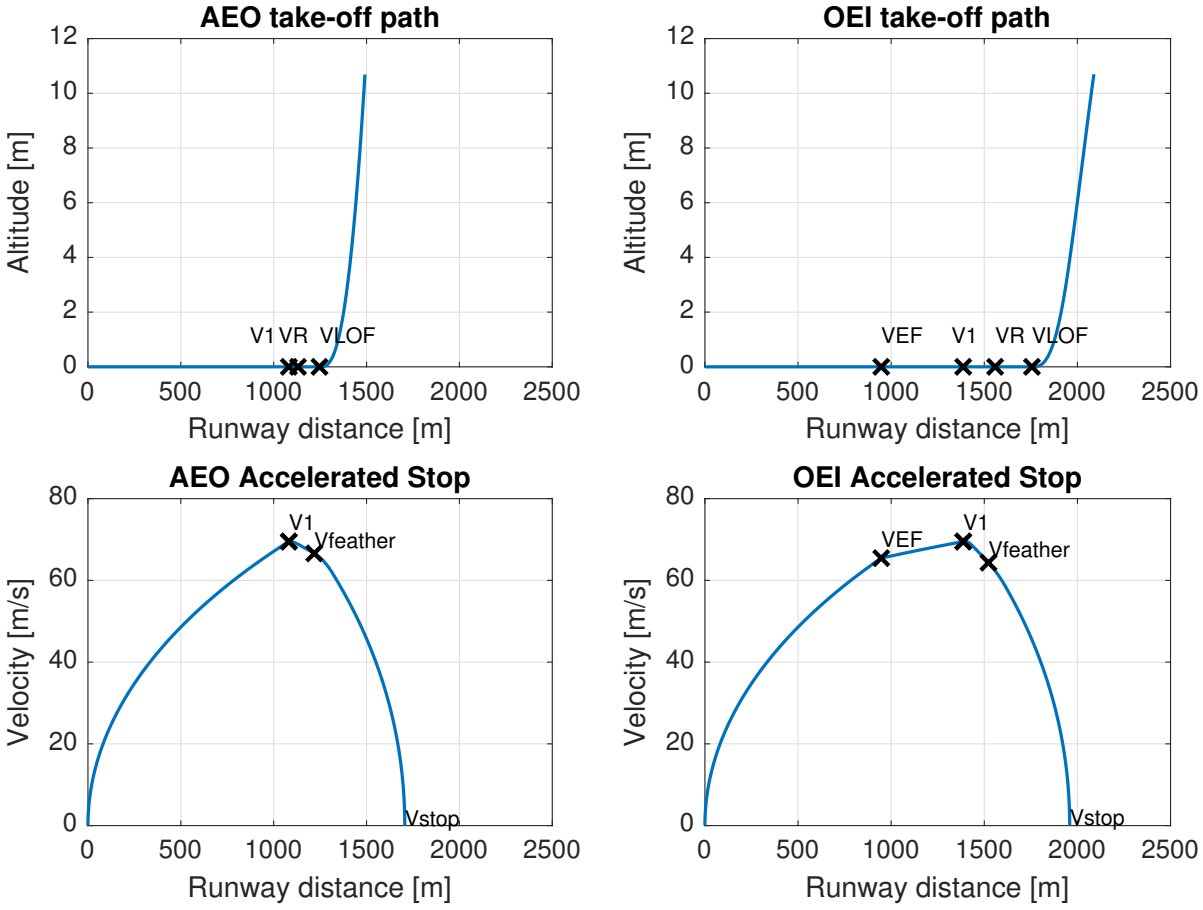

Figure 4.18: The altitude and velocity profiles of the AEO and OEI takeoff and accelerated-stop distances

Complementing the altitude and velocity profiles of fig. 4.18 are the detailed force and orientation profiles of the OEI takeoff case shown in fig. 4.19. The OEI takeoff case is most often critical and sizing for the balanced field length, besides it shows all interesting aspects of TOM verification.

The impact of the engine failure could clearly be seen, around 1000m the engine fails and the thrust force is halved and, consequently, the resultant force in horizontal x direction drops significantly. Following the engine failure and reduction in horizontal resultant force, the aircraft acceleration is decreased which dampens the trends of the velocity, lift and drag increases. Which would be also occurring in reality.

What would likely be different from reality is the aircraft handling from rotation on wards[2], occurring around 1500m. As could be seen from fig. 4.19, at V_R rotation of the aircraft is initiated with a constant pitch rate up to a point where the pitch is again decreased to stabilise the speed at V_2. In reality, the takeoff procedures are optimised such that the aircraft reaches V_2 without needing to reduce the pitch angle. However,

[2]Private interview with a Boeing 737 pilot

since TOM iterates to find the minimum BFL using the given aircraft and handling parameters, this method resulted in the lowest BFL and most stable calculation result.

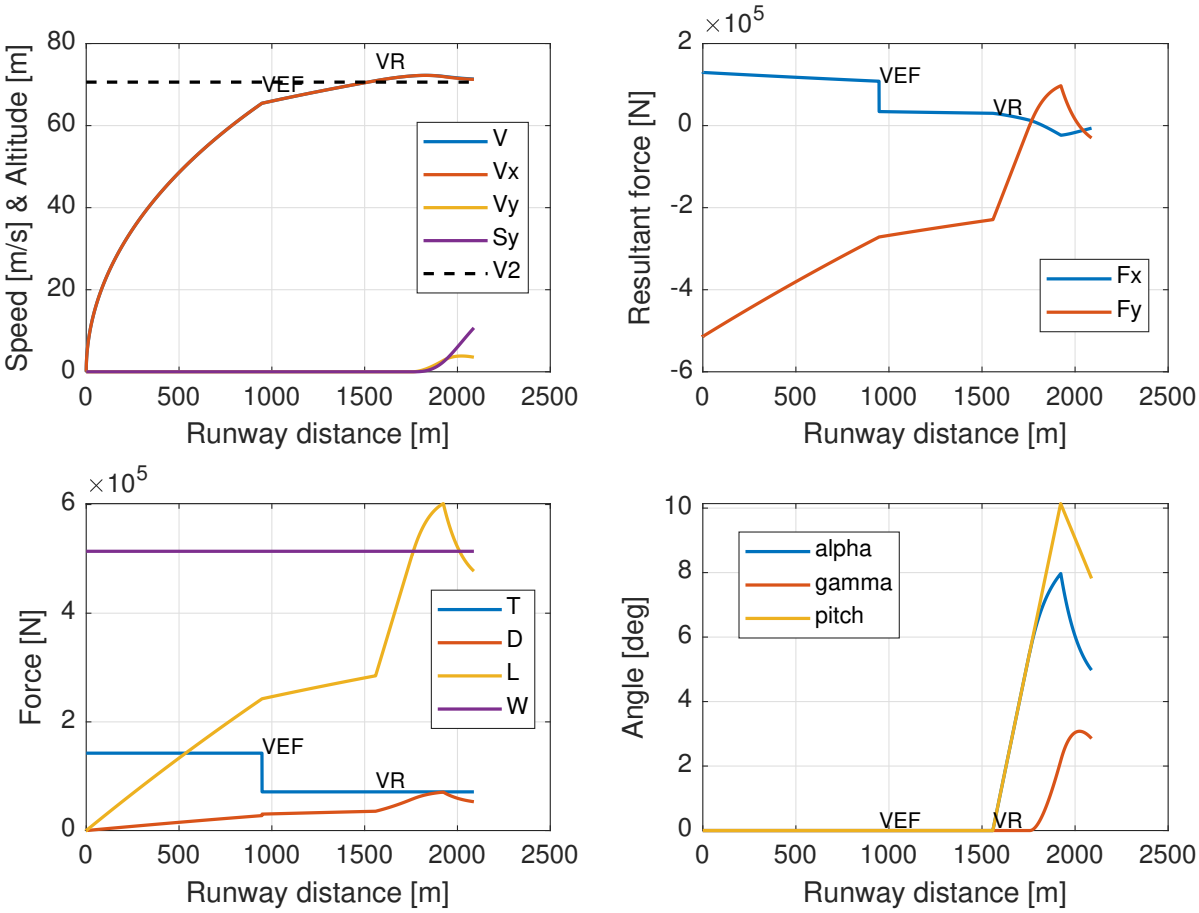

Figure 4.19: Detailed takeoff performance in case of engine failure

The takeoff model is iterating over the decision speed V_1 and a Vratio $\frac{V_1}{V_R}$, determining V_R as a function of V_1, to find the minimum BFL of the four takeoff cases. The results of such an iterative process could be seen in fig. 4.20. For the OEI takeoff case the required takeoff distance decreases with increasing V_1 and increasing Vratio, basically V_1 and V_R becoming closer together. The AEO takeoff case increases with V_1, however relatively decreasing V_R through the Vratio dampens this increase and makes it relatively stable with V_1. This follows logic, since increasing V_1 increases the aircraft acceleration that is done going straight (no rotation) on the runway and reduces the required velocity to accelerate in case of an engine failure.

In the accelerated-stop cases the aircraft does not rotate, so logically, these takeoff distance increase solely based on increasing V_1. A higher V_1 means a larger velocity from which to decelerate the aircraft back to standstill, thus a larger required runway distance.

The AEO and OEI takeoff lines are not straight, as is often seen in literature, but they zigzag. The zigzag pattern occurs due to different optimal ratio's for V1/VR for different V1 speeds up to a maximum ratio of 1 that are being tried.

As theory dictates, the smallest balanced field length is at the intersection of the takeoff and accelerated-stop cases. In this case, the intersection of OEI takeoff and accelerated-stop distance. Also, it could be seen that a step size of 0.5m/s (0.25kts) for V_1 and 0.01 for the Vratio iteration is sufficient to get accurate results while requiring relatively low computational time.

4.4.3. B737 TAKEOFF VALIDATION

TOM has been validated using the Boeing 737-200[3] as a reference case, the relevant parameters could be found in table 4.2. Subsequently, a sensitivity study has been performed with the same data. The Boeing 737-

[3]Boeing 737-200 technical specifications http://www.b737.org.uk/techspecsdetailed.htm

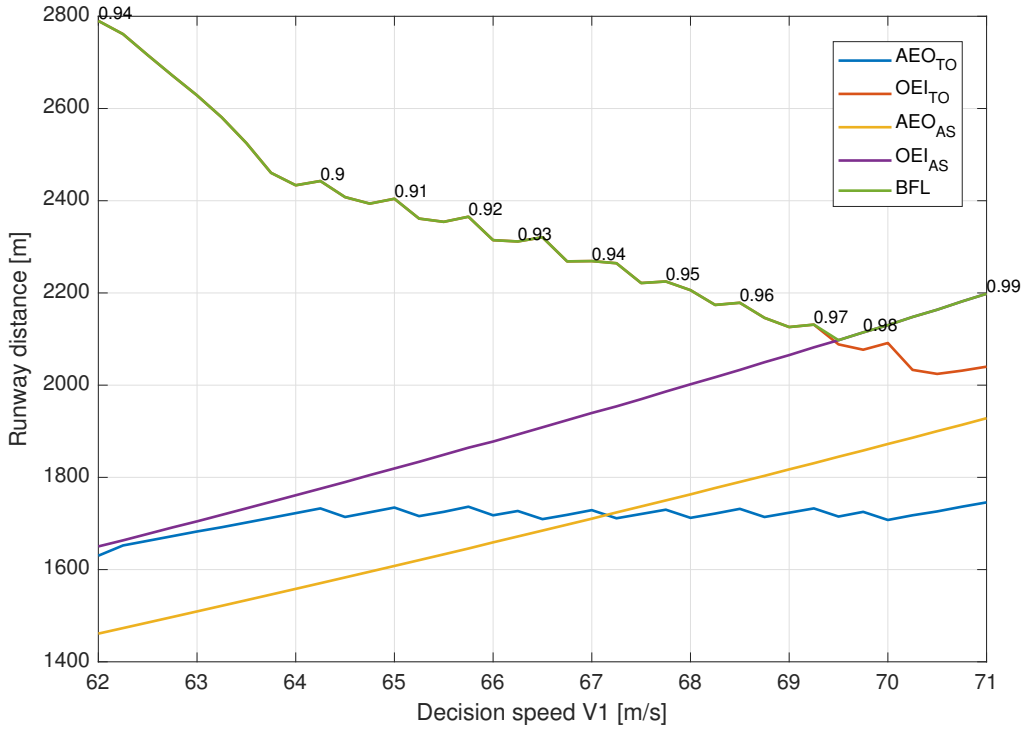

Figure 4.20: The balanced field length as a function of decision speed V1

200 has been chosen specifically due to its low bypass ratio turbofan engine which should have a low thrust lapse, thus fairly constant thrust along the takeoff path.

Table 4.2: Boeing 737-200 takeoff parameters

Variable	**Value**	**Unit**
TO distance	1990	m
Maximum Takeoff Mass	52390	kg
Number of Engines	2	-
Engine Thrust	71.2	kN
Wing surface area	102	m^2
Wing aspect ratio	8.83	-
$C_{L_{max,clean}}$	1.6	-
$dC_{L_{max,TO}}$	0.5	-
C_{D_0}	0.02	-
e_{TO}	0.9	-

Calculating the BFL of the Boeing 737-200 in TOM results in a BFL of 2097.5m, as could also be seen in fig. 4.20, which is 5.4% above the quoted takeoff distance of 1990m at ISA conditions. The calculated BFL is not identical to the quoted distance but close enough to call the results valid. It is likely that not all parameters used are identical to real conditions and thus a discrepancy is as expected.

Since a number of parameters required for the takeoff analysis are estimated based on reference data or engineering equations, for the B737 but also for TOPAS in general, as has been further elaborated on in section 3.7. A sensitivity analysis has been performed with respect to the most critical aircraft and performance parameter. The results of this sensitivity analysis of the TOM for the B737-200 is shown in table 4.3.

Differences in takeoff weight, thrust and wing surface area show the largest sensitivity, with a 10-20% difference from a 10% change in variable. However, these input parameters are also the most certain. The other variables are taken to be the values that are used in the overall TOPAS analysis and whilst being close, will likely not be identical to the B737-200.

The aircraft aerodynamic parameters $C_{L_{max,clean}}$ and α_{CLmax} most significantly impact the results, being 2-6% different from a 10% change in variable. Fortunately, in TOPAS the $C_{L_{max,clean}}$ could be picked such that the W/S matches closely between reality and TOPAS calculated aircraft. Therefore, $C_{L_{max,clean}}$ changes with reality are small and do not significantly impact the final result.

The zero lift drag coefficient, $C_{D_{0,clean}}$, has a 1-2% impact on the BFL if it is changed by 10%. The value for $C_{D_{0,clean}}$ is an estimate and could possibly be in the order of magnitude of 10% off reality. Finally, ϵ_{TO} and the pitch rate only marginally affect the calculated BFL.

Table 4.3: Sensitivity analysis results of the takeoff model

		-10% variable		+10% variable	
Variable	BFL base [m]	BFL [m]	Change [%]	BFL [m]	Change [%]
Takeoff weight	2097.5	1708.7	-18.538	2567.2	22.390
Thrust	2097.5	2391.0	13.991	1894.5	-9.678
Wing surface area	2097.5	2337.8	11.454	1916.2	-8.646
$C_{L_{max,clean}}$	2097.5	2226.0	6.123	2008.0	-4.271
$\alpha_{C_{L,max}}$	2097.5	2152.0	2.594	2066.6	-1.476
e_{TO}	2097.5	2091.0	-0.310	2118.3	0.991
$C_{D_{0,clean}}$	2097.5	2143.5	2.190	2070.8	-1.273
Pitch rate	2097.5	2101.4	0.183	2107.5	0.476

4.4.4. CONCLUSION AND IMPACT ON TOPAS

The takeoff model has been created according to the EASA CS25 regulations for takeoff and accelerated-stop procedures. The TOM has been verified by analysing the velocity, individual and resultant forces and aircraft orientation over time. The TOM shows the predicted and logical response to the different stages in the takeoff and accelerated stop procedures, such as engine failure and achieving the various V-speeds.

Inaccuracies in the TOM calculation of the balanced field length directly impact the final results of the overall TOPAS tool. The BFL calculated in the TOM for the Boeing 737-200 reference case is 5.4% off the quoted value. This is a good enough matches for the preliminary nature of this research. The results of the sensitivity analysis show that 5.4% error is very well possible with the uncertainty that exists with some of the input parameter, as well as inaccuracies with reality of the parameters determined using engineering equations.

5

RESULTS

The capability of the takeoff propeller analysis sequence (TOPAS) integration into the Preliminary Sizing Tool[1] (PST), as described in chapter 3, is demonstrated and the results are discussed in this chapter. The TOPAS functionality is shown by evaluating two reference cases of 2 different turboprop aircraft. The De Havilland Canada Dash 8 Q400 and ATR72-600, both short range turboprops designed to carry 70-90 passengers, have been selected to be used as reference cases. The evaluation setup and reference base design parameters are discussed in section 5.1. The main results that will be discussed are the effects of the created propeller sizing method on the cruise and takeoff constraints in the wing and power loading diagram, in section 5.2. Following the discussion of the wing and power loading diagram resulting from the reference cases, a sensitivity analysis with respect to a number of key input parameters will be elaborated on in section 5.3. Subsequently, in section 5.4 the propeller design solutions that satisfy the takeoff distance requirement found during the TOPAS analysis will be analysed. The aircraft design solution calculated by the Preliminary Sizing Tool is significantly different from reality due to large differences in calculated maximum takeoff weight, and will therefore not be used as comparison in this thesis. Finally, section 5.5 will discuss the validity and impact of the results.

5.1. EVALUATION SETUP

The TOPAS and PST functionally is shown with respect to the De Havilland Canada Dash 8 Q400 [4, 5] and ATR72-600 [6, 7] reference aircraft. Table 5.1 shows the relevant input parameters of the reference aircraft that could be extracted and are used by TOPAS. The table is split between the upper part which shows the reference values that are actually used as input in TOPAS and the lower part which shows data that is used as reference to the results presented in this chapter. The PST and TOPAS inputs could be found in appendix A.

It has to be noted that the $C_{L_{max,clean}}$ and propeller airfoil type are noted with an asteriks (*), these parameters are not directly given in literature and are assumed. $C_{L_{max,clean}}$ is selected such that the the reference W/S and minimum W/S resulting from PST stall speed constraint are equal. The Q400 and ATR72 are relatively modern aircraft and therefore it is assumed they have advanced airfoil sections. The ARAD airfoil is an advanced airfoil[26] and is available since it is the airfoil used on the XPROP.

5.2. WING AND POWER LOADING DIAGRAM

Using the Q400 and ATR72 reference data as input, the TOPAS+PST analysis sequence has been used to generate wing and power loading diagrams. The wing and power loading diagrams could be generated with respect to different component powers, such as gas turbine power, sea level corrected gas turbine power, shaft power and propulsive power. It has been chosen to show the wing and power loading diagrams using the sea level

[4] De Havilland Dash 8 Q400 data: https://dehavilland.com/en/dash-8-400
[5] Q400 - Janes All the World Aircraft https://customer.janes.com/JAWADevelopmentProduction/Display/JAWA0096-JAWA
[6] ATR72-600 fact sheet http://1tr779ud5r1jjgc938wedppw-wpengine.netdna-ssl.com/wp-content/uploads/2020/07/Factsheets_-_ATR_72-600.pdf
[7] ATR72-600 - Janes All the World Aircraft https://customer.janes.com/JAWADevelopmentProduction/Display/JAWA0440-JAWA

Table 5.1: Q400 and ATR72 reference data

Parameter	Q400 value	ATR72 value	Unit
TOPAS inputs			
Operative Empty Mass	17817	13311	[kg]
Payload mass	8489	7500	[kg]
Wing aspect ratio	12.8	12	[-]
Cruise altitude	7620	7620	[m]
Cruise Mach number	0.6	0.45	[-]
Takeoff distance	1425	1333	[m]
Range	2040	1527	[km]
$C_{L_{max,clean}}$ *	1.9	1.45	[-]
Engine rpm	1020	1200	[1/min]
Number of engines	2	2	[-]
Propeller airfoil type*	ARAD	ARAD	[-]
Reference values			
Maximum Takeoff Mass	29574	22800	[kg]
Wing surface area	63.08	61	[m^2]
Maximum engine power	3781	2051	[kW]
Propeller diameter	4.11	3.93	[m]
Propeller blade number	6	6	[-]
Maximum wing loading	4598.9	3667.0	[N/m^2]
Maximum power loading	0.0384	0.0553	[N/W]

corrected gas turbine power. The sea level corrected gas turbine power would be used to size the gas turbine engine and therefore best represents the engine sizing solution.

The wing and power loading diagrams resulting from the TOPAS+PST analysis of the Q400 and ATR72 reference cases could be seen in respectively fig. 5.1 and fig. 5.2. Using TOPAS, additional analytical cruise and takeoff constraints are created for propellers using different amount of blades. The complete constraint curves are fitted through the wing/power loading data points representing different propellers as a result of different input wing loading values into the TOPAS.

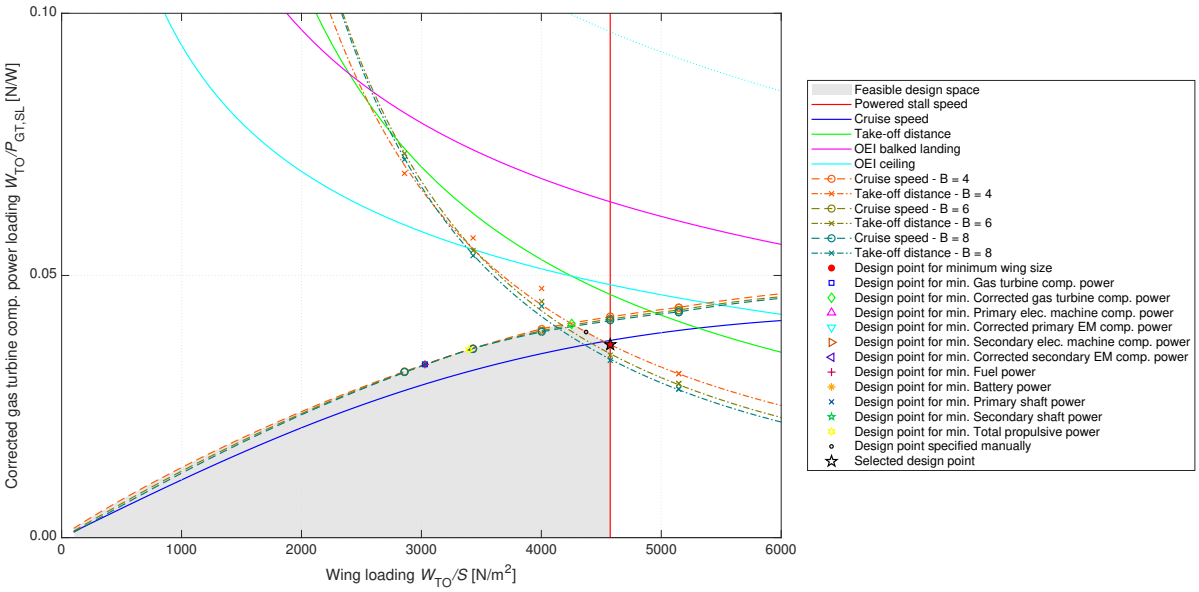

Figure 5.1: Q400 wing and power loading diagram

The TOPAS cruise constraint curve follows the same trend as the empirical cruise constraint. However, the TOPAS power loading is slightly higher than the empirical values. This discrepancy between the two is due

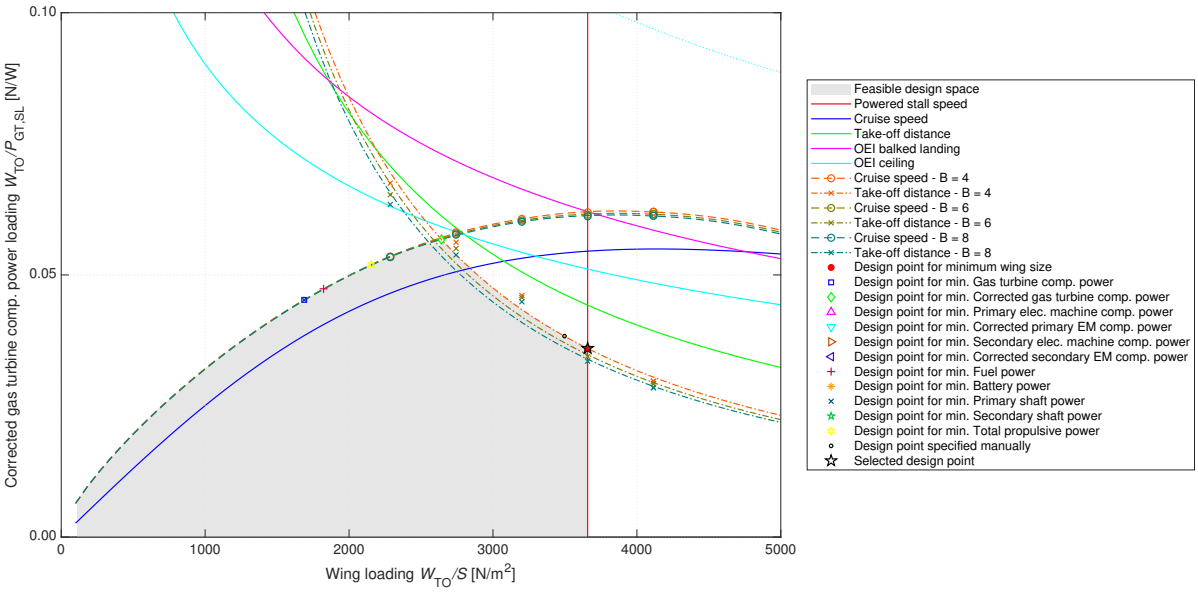

Figure 5.2: ATR72 wing and power loading diagram

to the difference in cruise propulsive efficiency. Where the efficiency in cruise as a basis in the Preliminary Sizing Tool is $\eta_{CR} = 0.8$, the calculated values for the TOPAS propeller are approximately $\eta_{CR} = 0.85 - 0.9$. Resulting in less required shaft power for the TOPAS constraint than the empirical constraint. The calculated and empirical cruise constraint curves are overlapping for propulsive power, the actual power exerted on the air by the propeller, instead of sea level corrected gas turbine power. The TOPAS curves for different number of blades lie exactly on top of each other. The number of blades has no significant on the cruise constraint power loading.

Similarly, the TOPAS takeoff constraint follows the same trend as the empirical constraint. However, in this case the TOPAS power loading is lower than the empirical values.

The actual propeller shaft power calculated by the BEM analysis is used, where the empirical power is based on the relation between thrust and power, $P = T * V$. It has been chosen to use the calculated power from the BEM since it is thought to represent reality best as it is validated in section 4.2. Even though, it was found that when using $P = T_0 * V_2$, where thrust is the static thrust and the velocity the V_2 safety speed, the takeoff curve was higher and thus lay closer to the empirical curve.

The TOPAS propeller efficiency in takeoff, taken close to V2, is around $\eta_{TO} \approx 0.6 - 0.7$, where the base value in PST is $\eta_{TO} = 0.7$. However, this is only part of the discrepancy. The propulsive power takeoff requirement curve, independent of efficiency, is also below the empirical constraint curve.

The TOPAS takeoff constraint curve does show a dependency on number of blades. Made increasingly visible due to the fitting, but even so, at each wing loading data point the different number of blades result in different required power loading values. The dependency on number of blades is interesting since during takeoff the propeller often has the highest propeller disk loading which could be relieved with having more blades.

The difference between 4 and 8 blades is around 5% difference in W/P. In both reference cases the propeller with 4 blades has the highest required power loading, requiring the least amount of power. This is an unexpected result since generally a propeller becomes more efficient with a higher number of blades[13], at the cost of additional propeller weight.

The TOPAS and PST wing and power loading results of the Q400 and ATR72 are compared to the reference values in respectively, table 5.2 and table 5.3. Due to matching of the $C_{L_{max,clean}}$ for each reference aircraft the calculated wing loading values of both PST and TOPAS are within 0.5% accurate to the reference values. For the power loading values it was already seen previously in the wing and power loading diagrams that the TOPAS calculated W/P is lower than the empirical PST value, for both reference aircraft. From the tables it could be seen that while the PST error with respect to reality is around 20%, 21% higher for the Q400 case and

-20.1% for the ATR72 case. The TOPAS difference is only 4.1% with respect to the W/P of the Q400, which is a very good result. However, this result does not translate to the ATR72, where the error is -34.9%.

Unfortunately, the small discrepancy with reality calculated for the Q400 reference case is not consistent with the results of the ATR72 reference case. In case of the ATR-72 both the empirical and TOPAS calculated wing loading prediction are significantly off. It is difficult to determine what the cause of the discrepancy is, whether it is cause by the used analysis methods, or due to the inputs that have been used. A sensitivity analysis with respect to some key input parameters is discussed in section 5.3.

Table 5.2: Wing and power loading output Q400

	Reference value	PST value	TOPAS value	Unit	PST difference	TOPAS difference
W/S	4599	4574	4574	$\frac{N}{m^2}$	-0.5%	-0.5%
W/P	0.0384	0.0464	0.0368	$\frac{N}{W}$	21.0%	-4.1%

Table 5.3: Wing and power loading output ATR72-600

	Reference value	PST value	TOPAS value	Unit	Reference value	TOPAS difference
W/S	3667	3658	3658	$\frac{N}{m^2}$	-0.2%	-0.2%
W/P	0.0553	0.0442	0.0360	$\frac{N}{W}$	-20.1%	-34.9%

5.3. WING AND POWER LOADING SENSITIVITY ANALYSIS

The wing and power loading diagrams resulting from the TOPAS analysis for the reference cases have been shown. The TOPAS results have shown to be in good correspondence to the Q400 reference data, however, the good results were not consistent in case of the ATR72-600. To try and get more insight in the impact of 7 key design decisions and inputs a sensitivity analysis has been performed. An overview of the analysed sensitivity cases is shown in table 5.4. Cases 1-6 have been performed with respect to the Q400, since this already showed the best results. Case 7, increasing the takeoff lift increment, is applied to the ATR72 to potentially get better match between calculated and reference power loading.

The chosen parameters are some of the key design decisions and inputs. The 3D rotations corrections are an important factor in development of the BEM to be able to accurately calculate the propeller performance during takeoff. The ARAD airfoil that has been used is an advanced airfoil type, however it is interesting to see how a different, in this case less advanced, airfoil type performs. It was noted that in both reference cases the propeller solution had four blades, a smaller step size could result in different results. The engine rpm is known for the reference aircraft, however it be interesting to see how a different rpm would impact the resulting power loading. Although the $C_{L_{max,clean}}$ has been selected such that it matches the reference wing loading, it is still an assumption. Together with the takeoff lift increment $dC_{L_{TO}}$, their sensitivity to the power loading would be good to know.

Table 5.4: Sensitivity analysis case parameter changes

Parameter	Base value	New Value	Case number
3D correction	Snel	CS	1
3D correction	Snel	None	2
Airfoil	ARAD	CLARK Y	3
Blade number range	[4,6,8]	[2,3,4,5,6]	4
RPM	1020	1224	5
$C_{L_{clean}}$	1.9	1.7	6
$dC_{L_{TO}}$	0.5	1	7

The results of the sensitivity analysis are shown in table 5.5. Besides the values of wing and power loading, also the resulting propeller solution parameters are shown. The propeller solution parameters give extra insight in the impact of the different changed parameters, and help track the impact on the values of wing and power loading.

First of all, the difference between the calculated power loading for using the Snel and Corrigan & Schillings

Table 5.5: Results of the Q400 sensitivity analysis cases

	Q400		Sensitivity case number and value change					
Parameter	**TOPAS value**	**Unit**	**1**	**2**	**3**	**4**	**5**	**6**
W/S	4574.3	[N/m^2]	0.00%	0.00%	0.00%	0.00%	0.00%	-6.45%
W/P	0.0368	[N/W]	-0.27%	-3.80%	1.36%	1.63%	-10.87%	-1.90%
B	4	[-]	0.00%	0.00%	0.00%	-50.00%	50.00%	0.00%
η_{CR}	0.888	[-]	0.41%	-0.95%	0.92%	3.02%	-3.09%	0.15%
η_{TO}	0.687	[-]	1.51%	-1.54%	2.71%	1.86%	-7.40%	-0.16%
T_0	34.4	[kN]	-1.52%	-3.60%	1.70%	11.83%	-4.82%	1.97%

3D rotation correction is small. Using the Corrigan & Schillings correction results in a propeller with a 1.5% higher efficiency in takeoff, however the power loading is 0.27% lower and the cruise efficiency is 1.83% lower. Using no 3D rotation correction to correct the 2D airfoil polars, results in a 3.8% lower W/P than using Snels correction. This provides a good argument for using the 3D corrections. Also, using no correction the static thrust and cruise/takeoff efficiencies are lower than using either 3D rotation correction.

The change of airfoil from ARAD to CLARK Y provided an interesting result. The resulting W/P is 1.36% higher, with a 2.71% higher takeoff efficiency and 1.7% higher static thrust. However, the cruise efficiency is lower. The result is surprising since the CLARK Y airfoil is a less advanced and less aerodynamically efficient airfoil, namely, lower $C_{L,max}$ and lower $\frac{C_L}{C_D}$. It could be that another characteristic of the CLARK Y airfoil makes it better suited in takeoff conditions, but that is currently not known.

The blade number variation from 4, 6 and 8, which was the expected optimal blade number range due to the amount of blades of the reference aircraft, has been expanded to 2-6. It was seen in section 5.2 that the propeller solution generally had 4 blades. However, using a lower range with a smaller step size it was found that the propeller solution resulted in a propeller with only 2 blades. The 2 bladed propeller solution has a higher cruise and takeoff efficiency and static thrust resulting in a power loading that is 1.6% higher than for the 4 bladed propeller solution. Thus, aerodynamically it is found to be better to have less propeller blades. Despite all this, when looking at the corresponding wing and power loading diagram, shown in fig. 5.3, the results are not so clear. The 2 bladed propeller takeoff constraint curve shows to be a poor fitted curve. Moreover, the 2 bladed propeller solution data point from TOPAS, marked by the x, is shown to be even further above the fitted curve. Consequently, drawing consistent conclusions from this result is difficult due to the poorly fitted 2 bladed propeller solution.

The engine rpm has a significant impact on the blade geometry as well as performance. Increasing the engine rpm by 20%, from 1020 to 1244 results in a propeller with a 16.7% smaller diameter and subsequently 11% lower power loading. Rpm is the most sensitive parameter of those that have been tested. Furthermore, propeller has a 5.2% lower cruise efficiency and 7.4% lower takeoff efficiency. The increased rpm resulted in a selected propeller solution that features 6 blades, instead of the 4 that was up to now found to be the chosen number of blades. However, from analysing the wing and power loading diagram it was found that the W/P results of the 4 and 6 propeller design solution were almost identical.

In sensitivity case 7 the maximum clean lift coefficient has been decreased by 10.5% from 1.9 to 1.7. This results in 6.5% lower wing loading which subsequently affects the power loading. The 6.5% decrease in wing loading decreases the power loading by 1.9%. Together resulting in a significant cost in overall aircraft weight due to requiring a larger wing and engine.

Table 5.6: Results of the ATR72 sensitivity analysis case

	Q400		**Case 7**	
Parameter	**TOPAS value**	**Unit**	**Value**	**Change**
W/S	3657.9	[N/m2]	3657.9	0.00%
W/P	0.0360	[N/W]	0.0497	38.06%
B	4	[-]	4	0.00%
eta_CR	0.909	[-]	0.915	0.72%
eta_TO	0.700	[-]	0.717	2.46%
T0	28.7	[kN]	23.7	-17.36%

The results of the sensitivity case 7, which was with respect to the ATR72-600, is shown in table 5.6. Increasing

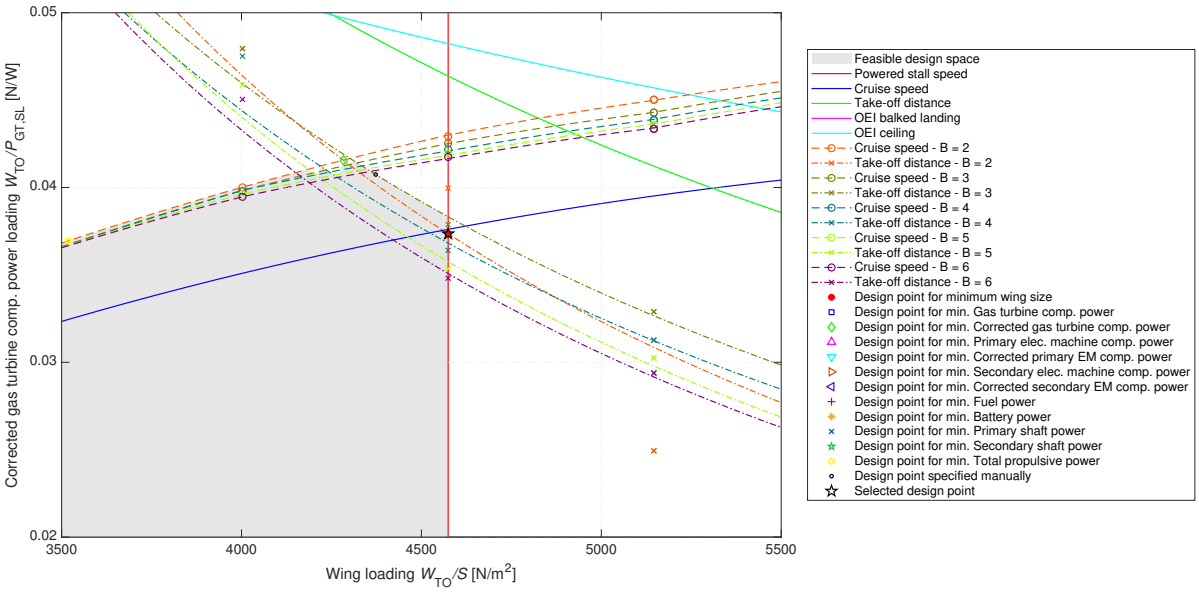

Figure 5.3: Wing and power loading diagram for the Q400 sensitivity case 4 using a lower blade number range

the takeoff lift increment $dC_{L_{TO}}$ from 0.5 to 1.0 for the ATR72 reference case results in a significant increase in power loading. The power loading increased by 38% from 0.036 to 0.050 while the wing loading, sized by the landing constraint, remains constant. Which changes the discrepancy with the ATR72 reference power loading from -34% to -10%. Clearly the different lift coefficients that have been assumed where in case of the ATR72-600 incorrect and way off reality. Moreover, the lift coefficients show significant sensitivity to the results which decreases the validity of the results since no value of the various lift coefficients is exactly known.

5.4. PROPELLER DESIGN SOLUTION

In the sensitivity analysis in the previous section some results of the propeller design solution were shown. It was seen that generally a propeller with 4 blades showed to have the highest power loading that satisfied the takeoff distance requirement. This section will look closer into the propeller design solutions of the Q400 reference case of propellers with 4 blades at different wing loading values and at the propellers of multiples blades at the design wing loading.

The propeller design solution results for a constant amount of 4 blades with varying wing loading could be seen in table 5.7. From the table it could be clearly seen that for increasing wing loading, thus a smaller wing surface area, the propeller has to provide more thrust and requires more power to achieve takeoff within the take distance requirement. Consequently, the chord ratio factor and activity factors also increase with increasing wing loading and static thrust. This is logically explained since both are a indication of propeller blade surface area and a higher blade surface area increases the possible thrust to be generated by a propeller blade.

Both the figure of merit in static conditions (FOM_{T_0}) and efficiency in takeoff remain, while being erratic, rather constant. The cruise trust is constant for the first 3 wing loading values but then decreases for both the final wing loading values. At such high wing loadings the required takeoff trust demand is very high and more significantly changes the propeller geometry originally designed for cruise conditions. Resulting in lower cruise trust efficiencies.

From the table it could be found that the relation between static trust and total activity factor (TAF) remains approximately constant over the range of wing loadings around a value of 87N. Meaning that for a propeller of 4 blades, 87N of thrust is generated for each unit of activity factor. Furthermore, the relation between maximum power required, P_{max}, and the chord ratio factor, CRf, remains approximately constant around 1250-1300 kW. Which would indicate that if the chord ratio of the propeller is increased across the whole blade span, the takeoff power required increases proportionately.

In the case of a constant wing loading and a varying number of blades, the propeller sizing results could be

Table 5.7: Propeller design solution results for a constant blade number and varying wing loading

Parameter	Value	Value	Value	Value	Value	Unit
W/S	2859.0	3430.8	4002.5	4574.3	5146.1	[-]
B	4	4	4	4	4	[-]
CRf	1.296	1.682	2.149	2.648	3.125	[-]
TAF	260.1	293.5	338.9	387.9	434.5	[-]
BAF	65.0	73.3	84.7	96.9	108.6	[-]
P_{max}	1765	2145	2580	3367	3920	[kW]
T_0	22.5	25.3	29.6	34.4	38.6	[kN]
$pitch_{T_0}$	25	25	30	30	30	[deg]
FOM_{T_0}	0.612	0.636	0.577	0.616	0.644	[-]
η_{TO}	0.717	0.690	0.713	0.687	0.699	[-]
η_{CR}	0.905	0.907	0.907	0.888	0.874	[-]
Relations						
T0/TAF	86.53	86.19	87.42	88.61	88.89	[N]
Pmax/Crf	1360	1275	1200	1271	1254	[kW]

seen in table 5.8. With a constant wing loading the propeller static thrust and power are expected to remain rather constant also, which they do. However, the maximum power required increases for increasing blade number. The opposite is true for available static trust, which decreases for an increasing number of blades, even though the total activity factor increases also. Interestingly, the 8 bladed propeller is able to satisfy the takeoff distance requirement with a lower static thrust, which would lead to believe that although the static thrust is lower, the average thrust during takeoff is comparable to lower blade numbers since the takeoff distance is equal.

With increasing blade number, the figure of merit and both the efficiency in cruise and takeoff are decreasing. The extra blades could result in extra blade interference effects which create more drag.

The constant relations between T_0/TAF and P_{max}/CRf seen for a constant number of blades is not seen when varying the amount of blades. Adding blades decreases the created static thrust per unit of activity factor. While adding blades increases the required extra power with an increase in chord length. Leading to the conclusion that having a propeller extra blades is aerodynamically less efficient.

Table 5.8: Propeller design solution results for a constant wing loading and varying number of blades

Parameters	Value	Value	Value	Unit
W/S	4574.3	4574.3	4574.3	[-]
B	4	6	8	[-]
CRf	2.6479	2.6262	2.6113	[-]
TAF	387.9	395.3	401.4	[-]
BAF	97.0	65.9	50.2	[-]
P_{max}	3367	3521	3637	[kW]
T_0	34.4	32.9	32.5	[kN]
$pitch_{T_0}$	30	30	30	[deg]
FOM_{T_0}	0.616	0.572	0.555	[-]
η_{TO}	0.686	0.670	0.659	[-]
η_{CR}	0.888	0.872	0.860	[-]
Relations				
T0/TAF	88.61	83.16	80.87	[N]
Pmax/Crf	1271	1341	1389	[kW]

5.5. DISCUSSION OF RESULTS

The Q400 and ATR72-600 propeller aircraft have been used as reference cases to run the preliminary sizing tool (PST) and additional takeoff propeller analysis sequence (TOPAS). As seen and discussed in section 5.2 the simulated results of the Q400 reference case match relatively well to reality and are closer than using the empirical constraints of PST. Despite that, the ATR72-600 calculated power loading by TOPAS is 35% off re-

ality and is worse than the PST results. This section will discuss the discrepancies in the results and some of the probable causes to these discrepancies. On the other hand, their are improvements over the empirical method, which will also be discussed.

WING AND POWER LOADING

First of all, the propeller analysis is performed in the very early stages of the design cycle and at this stage few parameters are known. Many assumptions could be made, but with these assumptions inaccuracies with respect to reality occur. An analytical calculation of the propeller and it's performance has been made, which is an improvement over no propeller calculation at all and derivation from empirical output. The propeller is initially designed to match the cruise thrust, subsequently it is adapted, mainly by increasing the blade area to provide enough thrust to be able to takeoff within the required distance.

An iterative process has been performed to match the propeller to the cruise/takeoff requirements, however no true blade optimisation has been performed. Performing such optimisation in later design stages would increase propeller performance in both stages of flight, thus extending the currently calculated wing and power loading design area. The propeller-nacelle and propeller-wing interaction have not been taken into account, these effects would likely decrease the propeller performance. On the other hand, the propeller effect on the wing would increase the energy in the flow over the wing, increasing the lift coefficient in takeoff significantly, leading to higher wing and power loadings. Furthermore, the designed propeller features straight blade and therefore has a more strict Mach limit, thus a lower rpm/Dp could be selected than might have been possible using a swept blade. Resulting in lower propeller performance than reality. The structural integrity of the propeller blade has not been taken into account. It is expected that using thick airfoil sections at the root, to ensure structural validity, would decrease the propeller performance.

Turboprops exist which boost the propeller rpm in takeoff to maximum thrust output in that stage. This while keeping the rpm in cruise moderate to be able to increase the propeller diameter and maintaining relatively low tip Mach numbers. This is not implemented in TOPAS, however could also be used to increase the power loading in takeoff.

Besides assumptions and simplifications with respect to the propeller analysis, even more so assumptions have been made regarding the overall aircraft. Already, in section 4.4 the sensitivity of the takeoff analysis was shown with respect to a number of aircraft parameters. As already mentioned the aerodynamic characteristics of the reference aircraft are not precisely known. Furthermore, assumptions have been made on pilot performance in analysing the takeoff distance such as reaction times and pitch rate. As well as relations to predict the drag of the runway friction, flaps, engine windmilling in case of engine failure, brakes and propeller feathering in the point mass takeoff analysis. These assumptions are based on statistical and empirical data and could result in large inaccuracies.

A good step toward better predicting the required power has been made by calculating the actual propeller shaft power and efficiency in takeoff. Instead of using the thrust-power relation $P = T \cdot V$ and a pre-defined value for the efficiency in cruise/takeoff which are used in the empirical calculation. Since the velocities during takeoff are relatively low and still changing rapidly this relation does not predict the power as well as during cruise. It was found that using the thrust-power relation $P = T \cdot V$ for the TOPAS data did result in high power loading values, values closer to the empirical values. However, the calculated shaft power is deemed more realistic and is thus used in the wing and power loading diagrams and to use for the results.

A sensitivity analysis has been performed looking into the sensitivity of some of the key design decisions and inputs. Firstly, it was clearly better to use a 3D rotation correction on the airfoil polars than using the 2D airfoil polars. Of which the power loading resulting from using Snels method was slightly better than the method of Corrigan & Schillings.

Changing the airfoil type and blade range had a 1.5% effect on the resulting W/P. Although it is believed that the impact of a different airfoil could be larger.

The lift coefficient proved to be an important parameter. Where decreasing the $C_{L,clean}$ by 20% resulted in a 6.5% decrease in the wing loading and a 1.9% decrease in the power loading. Since no other parameters were changed, this also means that the changing the wing loading by 6.5% has a 1.9% effect on the power loading.

Moreover on the effect of lift coefficient. In the case of increasing the takeoff lift increment from 0.5 to 1,

an increase of 100%, the power loading increased by a huge 38%, while the wing loading remained constant. High lift-devices in takeoff are shown to be very impactful, even though the added drag of larger high lift devices is not taken into account. Additionally, the sensitivity of the whole propeller sizing tool is highlighted. Since an incorrect estimate of the takeoff lift increment, which is currently assumed and taken from the PST inputs, has a very large effect on the final result.

PROPELLER SIZING SOLUTION

The propeller sizing solutions of the Q400 reference case have been discussed in section 5.4. The results show consistency with the expected behaviour of the propeller with changing values of wing loading. Increasing the wing loading requires a larger propeller to generate higher static thrust values at the cost of higher required maximum power. Interestingly, the figure of merit and efficiency in takeoff conditions remained rather constant. Although the cruise efficiency looked to remain constant also, when the propeller geometry is changed significantly to adapt for takeoff performance, the cruise efficiency decreases also.

Two relations remained constant for a constant number of blades and varying wing loading, the relation between static thrust and total activity factor (T_0/TAF) and maximum required takeoff power and chord ratio factor (P_{max}/CRf). Meaning that for propellers with an equal amount of blades, increasing the TAF would proportionally increase the static thrust and increasing the chord ratio factor proportionally increases the required maximum takeoff power.

Finally, it was shown that the propeller sizing solution for a propeller with a higher number of blades is aerodynamically less efficient in both takeoff and thrust. The propellers with more blades produced less static thrust and required more maximum power in takeoff.

6

CONCLUSION

The main objective for this thesis was to develop a propeller sizing method at takeoff conditions, taking into account the low speed aerodynamic effects and the resulting effect on the takeoff performance. This objective is met in this study.

A methodology has been developed to be able to perform propeller sizing and analysis using only data available in the preliminary design stage. The goal is to generate a analytical solution of the takeoff distance requirement in the wing and power loading diagram and consequently an analytical solution for the aircraft design point.

The aircraft preliminary sizing tool (PST) by de Vries[1] is used as a basis on which the propeller sizing tool is build. The PST performs an initial aircraft sizing, generating a preliminary aircraft sizing. Following the initial sizing by PST, a takeoff performance analysis sequence (TOPAS) is performed. Using the equilibrium flight conditions in cruise a propeller could be generated that satisfies minimum induced loss conditions in cruise flight using a inverse propeller design sequence of XROTOR[2]. It was found that the generated propeller, optimised in cruise conditions, provided too little thrust to be able to meet the takeoff constraint. A chord ratio factor was introduced to scale the propeller geometry to be able to provide higher thrust values. Thereafter, the generated propeller geometry is analysed using the Blade Element Momentum method. Using the propeller performance and the initial aircraft sizing an aircraft takeoff analysis is performed, of which the results could be compared to the takeoff distance mission requirement.

During the takeoff procedure the propeller operates at low advance ratios, resulting in large portions of the blade operating in stalled conditions.[6] It was found that the stall behaviour of an airfoil changes when an airfoil is rotating, most dominantly on hub sections of highly loaded rotors. These conditions combined significantly affect the propeller takeoff performance. Therefore, two types of corrections were used on 2D airfoil polars created by XFOIL[3]. First of all, a post-stall correction developed by Traub matching the airfoil polars at high angles of attack to flat plate polars. Secondly, two different 3D rotation corrections by Snel[4, 5] and Corrigan & Schillings[4, 5] were implemented. Combining the modules, creating the propeller sizing method, it is possible to analyse the propeller performance during takeoff. Furthermore, the aircraft and propeller are being sized by an analytical calculation process in the preliminary design phase.

The combination of 2D to 3D corrected airfoil polars and the Blade Element Moment method showed good correspondence with reality. Calculating the thrust coefficient within 5% accuracy and within 5-15% accuracy for power coefficient. The errors with respect to power were on the low end for the low advance ratios that are encountered during takeoff.

Validation of the aircraft takeoff performance using a Boeing 737-200 as reference provided good results and an error within 5%. However, it was shown that the calculation of the takeoff distance was sensitive to the input parameters, of which a number were assumed or determined using engineering equations and prediction methods.

The developed propeller sizing method is used to analyse the design solution based on the mission requirements of the De Havilland Q400 Dash 8 and the ATR72-600. The generated cruise speed and takeoff distance constraint curves in the wing and power loading diagram match the shape of the empirically calculated curves.

The wing and power loading results of the reference aircraft, of the empirical PST method and of the analytical TOPAS method are compared. The wing loading values are matched within 0.5% due to selection of

$C_{L_{max,clean}}$. More interesting are the power loadings, which show only 4% error for the TOPAS results with respect to the Q400 reference data. However, in the case of the ATR72-600 the discrepancy is a significant 35%. The TOPAS generated power loading values are consistently below the values predicted using the empirical methods.

A sensitivity analysis on the wing and power loading results is performed trying to determine the cause of the inconsistent results and the impact of some of the key design decisions. It was found that the use of 3D rotation corrections improved the power loading results. A different airfoil selection showed only a 1.4% impact on the W/P.

Most interesting was the impact of the lift coefficient on the results. Changing the $C_{L_{max,clean}}$ by 20% impacted both the wing and power loading values, respectively by 6.5% and 1.9%. Increasing the takeoff lift increment, $dC_{L_{TO}}$ from 0.5 to 1, an increase of 100%, the power loading increased by a huge 38%, while the wing loading remained constant. The lift coefficients showed to have significant sensitivity with the aircraft design point result, since the lift coefficients are estimated values they could have significant impact. Additionally, the uncertainty in a number of other parameters and used simplifications could result in relatively large inaccuracies, which are difficult to quantify using the currently available data and at this stage in the aircraft design process.

With respect to the propeller design solutions that have been generated it could be seen that the propeller designs followed expected trends. Increasing the wing loading requires a larger propeller to generate higher static thrust values at the cost of higher required maximum power. Interestingly, the figure of merit and efficiency in takeoff conditions remained rather constant. Although the cruise efficiency looked to remain constant also, when the propeller geometry is changed significantly to adapt for takeoff performance, the cruise efficiency decreases also. Furthermore, it was shown that the propeller sizing solution for a propeller with a higher number of blades is aerodynamically less efficient in both takeoff and cruise conditions.

Two relations propeller performance and propeller geometry were found. Firstly, a relation between static thrust and total activity factor (T_0/TAF) which showed to be constant for propellers with an equal amount of blades, increasing the static thrust proportional to the propeller activity factor. Secondly, the relation of maximum required takeoff power and chord ratio factor (P_{max}/CRf) showing that for propellers with an equal amount of blades, increasing the chord ratio factor proportionally increases the required maximum takeoff power.

To conclude, this study shows that it is possible to develop a propeller sizing method in the preliminary aircraft design phase which is able to analytically calculate propeller takeoff performance. However, due to contradiction results and lack of matching realistic input parameters, no conclusive verdict on the effectiveness of the developed propeller sizing method could be made.

7

RECOMMENDATIONS

In this chapter a list of recommendations is presented to further develop the work that has been done in this thesis in future studies.

- The effectiveness of the propeller sizing method should be reconsidered using realistic aircraft performance data
- In this research the propeller is analysed in. isolation. The propeller and wing interaction effects could be implemented to more accurately calculated both the produced propeller thrust as well as the takeoff lift coefficients.
- Using a range of airfoil across the propeller blade span matching realistic airfoil shapes across the blade span
- Using smaller step sizes and margins in the BEM propeller performance analysis and in the TOM takeoff analysis to achieve more accurate and more continuous results.
- The BEM method could be extended. Currently only 2D blade effects are taking into account, corrected by the Prandtl tip loss correction. Using the 3D flow components in the BEM could enable even better low advance ratio propeller performance prediction

BIBLIOGRAPHY

[1] R. D. Vries, M. Brown, and R. Vos, *A Preliminary Sizing Method for Hybrid-Electric Aircraft Including Aero-Propulsive Interaction Effects,* AIAA (2019).

[2] M. Drela, *XROTOR,* (2011).

[3] M. Drela, *XFOIL,* (2013).

[4] C. Lindenburg, *Investigation into Rotor Blade Aerodynamics,* ECN (2003).

[5] S. Breton, F. Coton, and G. Moe, *A Study on Rotational Effects and Different Stall Delay Models Using a Prescribed Wake Vortex Scheme and NREL Phase VI Experiment Data,* Wind Energy (2008).

[6] O. Gur and A. Rosen, *Propeller Performance at Low Advance Ratio,* Journal of Aircraft (2005).

[7] J. Roskam, *Airplane design - Part I: Preliminary sizing of airplanes* (Darcorporation, 1985).

[8] L. Loftin Jr., *NASA Reference Publication 1060*, Tech. Rep. (Washington D.C., 1980).

[9] D. Raymer, *Aircraft Design: A Conceptual Approach*, 2nd ed. (American Institute of Aeronautics and Astronautics, Inc., 1992).

[10] E. Torenbeek, *Synthesis of Subsonic Airplane Design* (Delft University Press, Delft, 1979).

[11] J. C. Tiemstra, *On the Conceptual Engine Design and Sizing Tool*, Master's thesis, Delft University of Technology (2017).

[12] N. Nigam, A. Tyagi, P. Chen, J. Alonso, F. Palacios, M. Ol, and J. Byrnes, *Multi-Fidelity Multi-Disciplinary Propeller/Rotor Analysis and Design,* 53rd AIAA Aerospace Sciences Meeting (2015).

[13] Y. Teeuwen, *Propeller Design for Conceptual Turboprop Aircraft*, Master's thesis, Delft University of Technology (2017).

[14] M. Cavcar and A. Cavcar, *Performance Figures of Merit for Turbojet/fan Transport Aircraft Selection and Conceptual Design,* AIAA Atmospheric Flight Mechanics Conference and Exhibit (2003).

[15] T. Mahieu, *Regional Aircraft Design Space Exploration,* Delft University of Technology (2016).

[16] M. Hoogreef, R. Vos, R. de Vries, and L. Veldhuis, *Conceptual Assessment of Hybrid Electric Aircraft with Distributed Propulsion and Boosted Turbofans*, Tech. Rep. (Technical University Delft, Delft, 2019).

[17] E. Torenbeek, *Advanced Aircraft Design* (Wiley, 2013).

[18] E. Torenbeek and H. Wittenberg, *Flight Physics* (Springer, 2009).

[19] L. Traub, *High-Incidence Airfoil Lift and Drag Estimates,* Journal of Aircraft (2012).

[20] J. Bosscher, B. Montgomerie, A. J. Brand, and R. van Rooy, *Influence of blade rotation on the sectional aerodynamics of rotational blades,* The twenty-second European Rotorcraft Forum (1996).

[21] L. Traub, *Simplified propeller analysis and design including effects of stall,* The Aeronautical Journal (2016).

[22] J. Morgado, M. A. Silvestre, and J. Páscoa, *A Comparison of Post-Stall Models Extended for Propeller Performance Prediction,* Aircraft Engineering and Aeroscience Technology (2015).

[23] J. Morgado, M. Silvestre, and J. Pascoa, *Full Range Airfoil Polars for Propeller Blade Element Momentum Analysis,* 2013 International Powered Lift Conference (2013).

[24] J. Tangler and D. Kocurek, *Wind Turbine Post-Stall Airfoil Performance Characteristics Guidelines for Blade-Element Momentum Methods,* (2004).

[25] G. van Kuik, *The Fluid Dynamic Basis for Actuator Disc and Rotor Theories* (IOS Press BV, 2018).

[26] D. Davis, *The impact of noise regulations on propeller design,* SAE Technical Papers (1979), 10.4271/790593.

[27] A. Silverstein, *Scale Effect on Clark Y Airfoil Characteristics from NACA Full-Scale Wind-Tunnel Tests,* National Advisory Committee for Aeronautics (1934).

[28] H. Freeman, *National Advisory Committee for Aeronautics,* Tech. Rep. Technical Note 378 (National Advisory Committee for Aeronautics, 1931).

[29] J. L. V. Ingen, *The e^N method for transition prediction,* 38th Fluid Dynamics Conference and Exhibit (2008).

[30] H. Youngren and M. Drela, *XFoil Manual,* (2001).

[31] L. Veldhuis, *Propeller wing aerodynamic interference,* Ph.D. thesis, Delft University of Technology (2005).

[32] O. Gur and A. Rosen, *Comparison between blade-element models of propellers,* The Aeronautical Journal (2008).

[33] European Aviation Safety Agency EASA, *CS-25 Certification Specifications and Acceptable Means of Compliance for Large Aeroplanes,* November (2018).

[34] W. Phillips, *Mechanics of Flight,* 2nd ed. (John Wiley & Sons, New Jersey, 2004).

[35] Y. Zhu, J. Wang, Y. Chen, and Y. Wu, *Calculation of Takeoff and Landing Performance Under Different Environments,* International Journal of Modern Physics: Conference Series (2016).

[36] J. Roskam and C. Lan, *Airplane Aerodynamics and Performance,* 1st ed. (Darcorporation, 1997).

[37] The Royal Aeronautical Society, *Undercarriage drag prediction methods,* ESDU 79015 (1987).

[38] The Royal Aeronautical Society, *Frictional and Retarding Forces on Aircraft Tyres,* ESDU 71026 (1995).

[39] A. Hall, *Take-Off Distances of a Supersonic Transport Configuration as Affected by Airplane Rotation During the Take-Off Run,* NASA (1961).

[40] The Royal Aeronautical Society, *Calculation of ground performance in take-off and landing,* ESDU 85029 (1985).

[41] H. Critzos, Chris and Heyson, *National Advisory Committee for Aeronautics,* Tech. Rep. (National Advisory Committee for Aeronautics, 1955).

[42] C. Ostowari and D. Naik, *Post Stall Studies of Untwisted Varying Aspect Ratio Blades with an NACA 4415 Airfoil Section,* Wind Engineering (1984).

[43] C. Lyon, A. Broeren, P. Giguere, A. Gopalarathnam, and M. Selig, *SoarTech Publications* (Virginia, 1997).

[44] N. van Arnhem, *Design and Analysis of an Installed Pusher Propeller with Boundary Layer Inflow,* Delft University of Technology (2015).

[45] D. Biermann and E. Hartman, *Tests of Two Full-Scale Propellers with Different Pitch Distributions, at Blade Angles up to 60,* Tech. Rep. (National Advisory Committee for Aeronautics, 1939).

[46] H. Snel, R. Houwink, and W. J. Piers, *Sectional Prediction of 3D Effects for Separated Flow on Rotating Blades,* (1993).

A

TOPAS AND PST INPUTS

Table A.1: Relevant base Preliminary Sizing Tool input parameters

Parameter	Value	Unit	Description
a.AR	TOPAS input	[-]	Wing aspect ratio
a.Lambda	0	[-]	Half-chord sweep angle of wing
a.TR	0.62	[-]	Taper ratio of wing
a.tc	0.18	[-]	Thickness-to-chord ratio of root section
a.nUlt	$2.5 \cdot 1.5$	[-]	Ultimate load factor
a.CD0_clean	0.02	[-]	CD0 in clean configuration (i.e. flaps retracted)
a.dCD0_TO	0.005	[-]	CD0 increase due to flaps in TO position
a.dCD0_L	0.055	[-]	CD0 increase due to flaps in landing position
a.dCD0_LG	0.01	[-]	CD0 increase due to extended landing gear
a.CL_minD_clean	0	[-]	Lift coefficient corresponding to minimum drag (CD0) in clean configuration
a.dCL_minD_TO	0	[-]	Change in minimum-drag lift coefficient with TO flaps
a.dCL_minD_L	0	[-]	Change in minimum-drag lift coefficient with landing flaps
a.e_clean	0.8	[-]	Oswald factor in clean configuration
a.de_TO	0.9	[-]	Oswald factor increase due to flaps in TO position
a.de_L	0.95	[-]	Oswald factor increase due to flaps in landing position
a.CLmax_clean	TOPAS input	[-]	CLmax in clean configuration
a.dCLmax_TO	0.5	[-]	CLmax increase due to flaps in TO position
a.dCLmax_L	1.2	[-]	CLmax increase due to flaps in landing position
p.config	'conventional'	[-]	Powertrain architecture
s.SelDes	'minWS'	[-]	Selected design condition ('minWS','minGT',... or 'manual')

Table A.2: Relevant TOPAS base input parameters

Parameters	Value	Unit	Description
Aircraft conditions			
$\alpha_{C_{L,max}}$	10	[deg]	Aircraft alpha at maximum CL
Jetpercent	15	[%]	Percentage of propeller thrust as extra turboengine jet thrust
Machbreak	0.7	[-]	Maximum allowable Mach number before drag divergence
Propeller design parameters			
Machblade	0.925	[-]	Maximum allowable Mach number of blade
Brange	4,6,8	[-]	Blade number analysis range
CRfstart	3	[-]	Chord ratio factor starting point
rRhub	0.2	[-]	Propeller hub spanwise location
XROTOR Settings			
Nradial	35	[-]	XROTOR propeller radial elements
XROTORmode	'T'		XROTOR input use cruise thrust or power as
BEM Settings			
Usteps	10	[-]	BEM number of velocity steps
Pitchstep	5	[-]	BEM pitch angle step size
Pitchschedule	'CTmax'		Pitch scheduling criteria
TOM Settings			
Screenheight	10.668	[m]	Screen height
dt	0.01	[s]	Time steps in TO distance integration
Vstep	0.25	[m/s]	Velocity intervals of V1 to determine BFL
TOPAS settings			
WSrange	$\frac{9}{8}, \frac{8}{8}, \frac{7}{8}, \frac{6}{8}, \frac{5}{8}$	[-]	WS fractions used to create TOPAS constraint curve
STOmargin	2	[%]	Allowable error margin on TO distance